National Technical University of Athens
School of Mechanical Engineering
Mechanical Design & Automatic Control Section
Laboratory of Machine Elements and Dynamics

Design of Meso-Scale Wave Surface Features to Increase the Friction Coefficient in the Brake Applications and Validation Using Numerical and Experimental Methods

Diploma Thesis

Faidon Michail Nousis

Supervisor:

Vasilios Spitas, Professor, Phd Eng. NTUA

Athens, September, 2023

(This page has been intentionally left blank)

(This page has been intentionally left blank)

Acknowledgements

I would like to express my gratitude towards certain people for their continuous support during my academic career those past few years. First of all, I would like to thank the supervisor of my thesis, Prof. V. Spitas, for the chance I was given to work along him and his team, and the valuable contribution he has offered in my engineering perspective during all those years, offering excellent level of knowledge and a sincere and kind approach. I would like to give a very warm appreciation to PhD graduate N. Rogkas, for his guidance during the past year in every aspect of this thesis at all times. I would also like to thank Prof. A. Karantonis and his laboratory for enabling me to use valuable equipment for this research from the Chemical Engineering School of NTUA. Furthermore, a big thank you is attributed to G.N. Rossopoulos, C. Papadopoulos and D. Skaltsas of the Naval engineering school for their excellent cooperation and for offering me valuable tools from their lab to conduct required measurements. Finally, I would like to thank deeply my family, my friends, and anyone who supported me during my undergraduate period, and especially my parents for always letting me choose the path I wanted to become a better citizen, a better engineer.

September 2023
Faidon Michail Nousis.

(This page has been intentionally left blank)

National Technical University of Athens
School of Mechanical Engineering
Mechanical Design & Automatic Control Section
Laboratory of Machine Elements and Dynamics

Design of meso-scale wave surface features to increase the frictional applications and validation using numerical methods and experimental and prototype tribological rigs

Thesis

Faidon Michal Nousis

Supervisor:
Vasilios Spitas, Professor, Phd Eng. NTUA

Athens, September, 2023

Abstract

An investigation into the improvement of frictional properties in braking systems by altering disc surface topology without altering geometrical volume and materials of the examined system is carried out in this thesis. The ultimate goal is proving the prescribed concept and enable motorsport applications to design systems more efficient than ever. FEA in ANSYS Mechanical is used to export initial conclusions for an equivalent simplistic model of the pad to disc contact. Actual material properties are used to simulate the difference in relative stiffness between bodies and conclude to accurate results. Findings using the model are assessed, and data acquired are indicative of the expected behavior for each design, after convergence is secured. An attempt is made to validate FEA results in the physical world using an existing high quality tribometer and different 3D printed specimens. The quantization of the features due to printing layer size is crucial, as it influences final outcome and surface quality. Post processing of the surfaces was carried out before experiments, and measurements of the physical objects were taken using an optical profilometer to observe the surface topography of the features and the manufacturing method. Specimens were tested across a range of speeds and radiuses of pin contact, and data received were processed using a custom MATLAB tool. Results of both the FEA modeling and the physical testing are presented and preliminary conclusions are drawn regarding the proof of concept, subject to future research validation. Finally, a custom disc-on-disc tribometer is designed using low-cost innovative elements. The device can be used to simulate an accurate frictional contact in braking system, while its design is efficient, lightweight and reliable.

Keywords: (Braking system, disc brake, tribology, surface topology, macroscale features, FEA model, tribometer, surface roughness, qualitative analysis)

(This page has been intentionally left blank)

Table of Contents

Table of Contents ix
List of Abbreviations xi
List of Indices xiv
List of Figures xv
List of Tables xx
Chapter 1 Introduction 1
1.1 Braking Technology, A Historical Review 2
1.1.1 Brake Drums & Brake Discs 3
1.2 State-of-the-Art Braking Systems. 9
1.3 Thesis Motivation 15
1.4 Thesis Structure 16
Chapter 2 - Literature Review 17
2.1 Design Principles 18
2.2 Analytical Tools and Mathematical Models 23
2.3 FEA & CFD Simulations 30
2.4 Wear Models 34
2.5 Scope of this Thesis According to Literature Review 35
Chapter 3 Development of the FEA model 36
3.1 Simulation Model Setup 37
3.1.1 Initial Approach 37
3.1.2 Final Model and Conversion to Symmetry Model 41
3.2 Parametric Investigation 49
3.2.1 Flat Disc 51
3.2.2 Sinusoidal Feature 51
3.2.3 Rectangular Feature 52
3.2.4 Big Fillet Feature 53
3.2.5 Ramp Feature 53
3.3 Parametric Analysis Results 55
3.3.1 Fx Reaction versus Feature Amplitude 55
3.3.2 Stress and CoF Diagrams Across Features 57
3.3.4 Further Investigation of Features 62
3.3.5 General Observations 64

Chapter 4 Experimental Investigation.....66
4.1 Specimen Fabrication.....67
4.4 Design of A Novel Low-Cost Disc-On-Disc Test Rig.....84
4.4.1 Goals and Constraints.....84
4.4.2 Range of Application – Motor Selection.....88
4.4.3 Measuring Devices.....91
4.4.4 Materials and Cost Reduction.....92
4.4.5 Tribometer Compliances and FEA Models.....93
5. Conclusions and Future Research.....95
6. Literature References.....98

List of Abbreviations

%	Percentage
3D	3 Dimensional
A	Amplitude / Surface
ABS	Anti-Lock Braking System
BBW	Brake-by-wire
CAD	Computer Aided Design
CFD	Computational Fluid Dynamics
cm	Centimeter
CMC	Ceramic Matrix Composite
CNC	Computer Numerical Control
CoF, μ	Coefficient of Friction
DC	Direct Current
DMLS	Direct Metal Laser Sintering
DoF	Degrees of Freedom
DSC	Dynamic Stability Control
E	Young's Modulus
EBD	Electronic Brake Distribution
ECU	Electronic Control Unit
EDM	Electrical Discharge Machining
EHB	Electrohydraulic Brake
EMB	Electromechanical Brake
ep	Factor Load Distribution
Eq.	Equivalent
ESP	Electronic Stability Program
et Al.	and others
EV	Electric Vehicles
F	Force (in N)
F1	Formula 1

FB	Fixed Base
FD	Fixed Disc
FEA	Finite Element Analysis
FEM	Finite Element Model
FS	Formula Student
G	Shear Modulus
GPa	Giga Pascal
gs	Gravitational Accelaration
h	Height
HCU	Hydraulic Control Unit
i.e.	Id Est (that is)
J	tortional moment of inertia
k	stiffness
K	matrices
kg	kilogram
kW	Kilo Watts
l	length
LC	Load Cell
m	Meter / Mass
M,T	Moment
MB	Main Base
ML	Main Lever
mm	Millimeter
MMC	Metal Maroix Composite
ms^{-1}	Meters per Second
N	Newtwon
NAO	Non-Asbestos Organic
NSF	Normal Stiffness Factor
OEM	Original Equipment Manufacturer
P	Pressure
p(h)	Height Distribution
PID	Porportional-Integral-Derivative Controller

PMSM	Permanent Magnet Synchronous Motor
PSM	Porsche Stability Management
PVT	Pillar Venting Technology
PWM	Pulse Width Modulation
q_0	Heat Flux
R	Radius
RD	Rotational Disc
RPM	Rads Per Minute
Sa	Arithmetical mean height
Sku	Kurtosis
SLS	Selective Laser Sintering
Sp	Maximum Height from Mean Plane
Sq	Root Mean Square Height
Ssk	Skewness
Sv	Minimum Height from Mean Plane
Sz	Maximum Height
t	time
V	Volt
v	velocity
VCU	Vehicle Control Unit
VSA	Vehicle Stability Assist
WEC	World Endurance Championship
WRC	World Rally Championship
δ, Δ	difference
θ	corner
ν	poissons ratio
π	pi
σ	Normal Distribution
τ	shear stress
φ	Brake Distribution Between axles
Ω	Rotational Speed (RPM)

List of Indices

0	Initial
d	Disc
I	Inner
a,b,c	Constants
eq	Equivalent
i	Number
nd	Second
o	Outer
st	First
x	Variable in X Dimension
y	Variable in Y Dimension
z	Variable in Z Dimension

List of Figures

Figure 1 The Brake Drum Concept. U. Left: Wooden shoe brake, U. Right: Basic elements of brake drum assemblies. Lower: Brake drum exploded view 3

Figure 2 Brake Drum and Brake disc concept in contrast 4

Figure 3 Different brake caliper designs. U. Left: AP Racing PRO 5000, U. Right: Yamaha R1 piston caliper, L. Left: Ferrari racing brake caliper by Brembo, L. Right: Bugatti 3D printed caliper 5

Figure 4 Floating 1 piston caliper 6

Figure 5 Brake Pads. U. Left: Brake pad layers and composition, L. Left: Different pad materials Right: Cooling and Dust removal features for brake pads 7

Figure 6 Bendix Hydro-Vac booster 9

Figure 7 Booster principles and example. Left: Early vacuum booster schematic with working principles. Right: Modern day hydro booster for BMW 10

Figure 8 ABS system schematic 11

Figure 9 Audi E-Tron hydro assisted braking system explanation 12

Figure 10 Electromechanical brake boost concepts. Left: Bosch 1996 concept, Right: Mando 2020 concept 13

Figure 11 EHB vs EMB concept. U. Left: Schematic comparison of the two concepts, U. Right: Pinion rack EHB concept with valve control unit. L. Left & Middle: Bosch EMB iBooster design, L. Right: Continental MK C1 EHB design 14

Figure 12 Brembo discs: 20 years of F1 braking disc evolution 18

Figure 13 Brake disc examples. Left: Yamaha YZF-R1 floating brake disc with cooling Holes, Right: Brembo Two-piece discs; line 09.C420.13 19

Figure 14 Brembo PVT internal cooling design 20

Figure 15 Ventilation concepts for braking discs. Upper: different cooling features, from left to right 1) Solid, 2) Slots, 3) Slots and drill points, 4) Holes, 5) Slots and holes. Middle: Inner cooling features, from left to right 1) Straight vanes, 2) Pillars, 3) Tangential vanes, 4) Curved vanes. L. Left: Stoptech Kangaroo Paw desing, L. Right: CFD on brake discs 21

Figure 16 U. Left: Single-DoF structural model with hysteris [3], U. Right: Cycling loading with partial slip [3] L. Left: Contact of rough surface with smooth flat [24], L. Right: Shape of bodies in contact [7] 24

Figure 17 Different friction models according to literature [2] Upper form left to right 1) Coulomb, 2) Coulomb with stiction, 3) Striberg Lower from left to right 1) Bengisu Akai, 2) Karnopp, 3) LuGre Model (Bristle model) 25

Figure 18 Models and results from literature. Upper: Asperity model with elastic-plastic modulation [16] L. Left: CoF values through time [17], L. Right: CoF values for different velocities [22] 27

Figure 19 Asperities in contact: Left: Ogilvy's model [17], Right: Contact expressed by flat and randomly (Gaussian) distributed surface [18] 28

Figure 20 Braking system FEA models from literature. U. Left: Thermomechanical analysis, U. Middle: Mesh for complete brake disc, U. Left: Mesh and stress plot for brake rotor. L. Left: Thermal flow in Disc/Pad pair, L. Middle: Heat transfer coefficient in brake disc rotor, L. Left: Brake pad stress field 31

Figure 21 Jian Yin et Al [31], equivalent moving load method application for heavy duty brake disc optimization. U. Left: FEM of internal structure, U. Right: Equivalent moving load method characterization L. Left: Density of optimized internal structure, L. Right: Optimized result 32

Figure 22 CFD Concepts and examples. Left: CFD thermal model for brake disc and bel [33], Right: Simplified example of a coupling process [29] 33

Figure 23 Cellular Automata model calculations through time [6] 34

Figure 24 Brake disc's designs and simulation model design. U. Left: Exploded view of Disc assembly, U. Right: Brake disc and caliper with 4 pistons L. Left: Prom Racing FS brake disc 2021, L. Right: Thesis ANSYS FEM model of brake disc 38

Figure 25 Input parameters for structural analysis. Upper: Initial approach, Lower, Improved model 39

Table 1 Material properties for structural analysis in ANSYS Mechanical 42

Table 2 Comparison of stiffness change for the models using 3 and 2 bodies respectively 43

Figure 26 Results of structural analysis for model with 3 and 2 bodies. U. Left: Model 3 bodies – Equivalent Stress, U. Right Model 2 bodies – Equivalent Stress L. Left: Model 3 bodies – Y Deformation, U. Right Model 2 bodies – Y Deformation 44

Figure 27 Force reaction for model with 3 and 2 bodies. Purple line represents backplate, blue the pad, and green the fixture on the disc side 44

Figure 28 Model behavior for different NSF Values. Left: Equivalent & Shear Stress vs NSF, Right: Reaction Force and Penetration vs NSF 45

Figure 29 Stress plots for different NSF Values NSF value from left to right and top to bottom: 0.5 – 1.0 – 2.0 – 2.5 – 3.5- 5.0 46

Figure 30 NSF Penetration plots for different NSF values NSF value from left to right and top to bottom: 0.5 – 1.0 – 2.0 – 2.5 – 3.5- 5.0 47

Figure 31 Reaction Force and Time convergence of the model vs Pad Element Size. 48

Figure 32 Different texture parameters to examine for Features used in simulations 49

Figure 33 Different features to be examined in simulations, exaggerated amplitude of features for reference. 50

Figure 34 Surface imperfections of 3D printing manufacturing method 52

Figure 35 Stress concentration near the free edges of the rectangular feature. Magnification x45 53

Figure 36 Extrapolation of Fx based on the FEA results U. Left: Compression 50μm, Amplitude range [0.01,0.1], U. Right: Compression 30μm, Amplitude range [0.01,0.1], L. Left: Compression 50μm, Amplitude range [0.01,0.05], L. Right: Compression 30μm, Amplitude range [0.01,0.03] 56

Figure 37 Extrapolation of Fy based on FEA results Left: Compression 50μm, Amplitude range [0.01,0.05], Right Compression 30μm, Amplitude range [0.01,0.03] 56

Figure 38 Equivalent Stress across features. Upper: Comparison for all models tested L. Left: Wavy Sinusoidal feature, L.Middle: Big Fillet 5 feature, L. Right: Rectangular feature 57

Figure 39 Equivalent Stress plot comparison for different features. From top to bottom: 1) Wavy Sinusoidal, 2) RampIn-RampOut, 3) WaveIn-RampOut5, 4) BigFillet5, 5) Rectanglular 58

Figure 40 Comparison of CoF values across features. Upper: CoF mean and extreme values for all scenarios, Lower: CoF improvement from baseline mean and extreme values for all scenarios 59

Figure 41 Extrapolation of CoF values across working range for all features 60

Figure 42 Extrapolation of Equivalent Stress values across working range for all features 61

Figure 43 Equivalent Stress values for families of features. Left: Big Fillet variations, Right: Qualitative comparison of Eq. Stress values for smooth vs sharp edged features 61

Figure 44 Coefficient of friction for families of features. Upper: WaveIn RampOut features compared to Wavy Sinusoidal and Big Fillet feature, Lower: WaveIn RampOut features compared to RampIn RampOut features 62

Figure 45 Opimization results for RampIn-RampOut feature. U. Left: Design of the feature in exaggeration, U. Right: Comparison of results with increasing grade difference, L. Left: Results for % of CoF improvement from flat design, L. Right: Results for CoF value 63

Figure 46 Interpolated disc-pad Penetration values of the FEA model across all features 64

Figure 47 Interpolated disc-pad Penetration values of the FEA model across all features focused in convergence area 65

48 Typical roughness values of various 3D printing methods 67

Figure 49 Qualitative demonstration of Sa variable 68

Figure 50 Sharpness of the asperities expressed by Sku variable 69

Figure 51 Shape of the asperities expreessed by the Ssk variable 69

Figure 52 Surface topography measurements. U. Left: BRUKER profilometer and disc specimen, U. Right: 3D representation after scanning, L. Left: 2D representation after scanning, L. Left: X and Y surface profiles compared to the reference thickness 70

Figure 53 Profilometer measurements for the flat disc, sets of 2D, 3D and scale. Upper: Measurement point 1 Middle: Measurement point 2, Lower: Measurement point 3 71

Figure 54 Profilometer measurements on the Ramp Featured disc. U. Left: 2D representation and scale (1), U. Right: 3D representation in side view, L. Left: Y profile for the points in (1), L. Right: X profile for the points in (1) 72

Figure 55 Profilometer measurements on the Wavy Featured disc. U. Left: 2D representation and scale (2), U. Right: 3D representation in side view, L. Left: Y profile for the points in (2), L. Right: X profile for the points in (2) 73

Table 3 Surface quality variables measured with profilometer. Flat disc values are the average of the total points measured. 74

Figure 56 Surface comparison of all discs with Amplitude of feature =120μm, real model and 2D representation. Left: Flat disc, Middle: Ramp featured disc, Right: Wavy featured disc 74

Figure 57 Filter application on all discs measurements at R=27.5mm. U. Left: Cases shown, U. Right: filter 18, L. Left: filter 58, L. Right: filter 38 75

Figure 58 Filtering process on the Fillet featured disc, at R = 27.5mm. Upper: filter 5, Middle: filter 25, Lower: filter 55 76

Figure 59 Data for flat disc - all cases. Upper: Speed = 25RPM, Middle: Speed = 100RPM, Lower: Speed = 50 RPM 78

Figure 60 Data for all Cases, same feature per plot. Upper: Flat disc, Middle: Fillet featured disc, Lower: Ramp featured disc 79

Figure 61 CoF data for all cases, grouped per feature and radius 80

Figure 62 CoF data for all cases, grouped per speed and radius 80

Figure 63 CoF data for all cases, grouped per radius. Upper: R = 12.5mm, Middle: R = 20mm, Lower: R = 27.5mm 81

Figure 64 CoF for all cases, quantitative comparison near expected physical vaues 82

Figure 65 Anton Paar TRB3 Pin-on-Disc Tribometer 85

Figure 66 Complete custom tribometer design, Side & Isometric Views 86

Figure 67 Fixed base and load cell attachment for custom tribometer, Side and Top Views 86

Figure 68 Main Base and Main Lever for custom tribometer, Isometric Views 87

Figure 69 Alternative motor selection. Left: JGB37-3530, Middle: RS PRO 834-7663, Right: RS PRO 834-7672 90

Figure 70 Motor mounting method for custom tribometer, Isometric and Side cross section Views 90

Figure 71 Left: Load Cell used for custom tribometer Load Cell OEM for custom tribometer, Right: Load Cell electrical working principle 91

Figure 72 Magtrol transducer TM 304 mechanical drawing 92

List of Tables

Table 1 Material properties for structural analysis in ANSYS Mechanical..... 42

Table 2 Comparison of stiffness change for the models using 3 and 2 bodies respectively 43

Table 3 Surface quality variables measured with profilometer. Flat disc values are the average of the total points measured..... 74

(This page has been intentionally left blank)

Chapter 1 Introduction

The braking of a vehicle is the process through which it transforms its kinetic energy into other forms by choice, without the aid of any gravitational field, accompanied by velocity loss towards or up to a complete stop. Every moving vehicle features a braking system for performance, comfort, and safety reasons. When examining braking systems, in every application from bicycles to airplanes the goal is to provide the ability to either completely stop the vehicle or lower its speed depending on the requirements. Mainly used in ground vehicles, the frictional mechanism is based on the act of forces produced by the contact of a spinning system and a built-in mechanism that acts as the stationary body. Given its remarkable success, this format has been employed for over two centuries - The rising popularity of electric vehicles meant that the field of braking is once again yielding cutting-edge solutions which are often entirely or partially independent of friction and contact. These options include the use of pneumatic air or regenerative braking, which converts kinetic energy into electricity.

A variety of characteristics are associated with the braking phenomena in general. Frictional braking is caused by the contact of two rough faces or many sets of rough faces moving relatively in opposite directions. Tribology is the field of studies that focuses on systems where friction is present. Depending on the size of the area of contact under the study, friction is categorized into macro, meso, and micro scales in research. Apart from the size, local roughness, temperature, humidity and time of contact also influence the nature of each system. Since the variations in attributes and conditions have a significant impact on each system's final behavior, there are multiple friction models that describe the processes occurring during frictional contact. These representations frequently depend on particular events. Aside from friction creation, the contact of the two bodies in friction causes other effects such as vibrations and noise emission. The latter, referred to as judder [53,57], has been found to be mitigated by greater manufacturing precision and smart component design. The choice of materials for braking surfaces is crucial since it affects the Coefficient of Friction (CoF), body wear and assembly cost.

A brake system is deemed efficient if it has increased CoF, reduced wear and judder, and reliability. The highest temperature reached during repetitive or forceful braking is another important aspect in system function. Temperature restrictions are crucial for material selection since component design may grow bulkier to handle thermal pressures. This can have an impact on how well a vehicle performs overall, especially in automotive applications where the braking system is mounted on the unsprung part of the suspension, decreasing efficiency for larger and heavier components. As a result, engineers are continuously looking for novel materials and creative designs that enable simpler braking systems and take into account all of the other factors and specifications of the vehicle. To end this brief introduction, it is necessary to emphasize from an environmental perspective, the non-exhaust particles which are also released into the atmosphere during each braking event, contributing to pollution. The brake system's designs and the materials used are selected to reduce harmful emissions and lessen the influence of any wear-related particulates.

1.1 Braking Technology, A Historical Review

The history of braking in automotive applications goes back to the time when carriages were used, before any sort of car was invented. Horse-drawn carriages used to brake using wooden blocks coated with leather, steel, or other durable materials. Each block was pressed via a lever against one of the wheels, reducing the rotation ability partially or completely. Preliminary designs gave little to no consideration to brakes. Briefly after the first car was invented, manufacturers changed their focus on braking improvement in parallel with engine performance. As cars got faster, braking could no longer be based on the running engine, making the design of brake systems mandatory, and the friction in the drivetrain was an additional tool. The steel wheels were changed to lightweight rims with attached rubber tires to improve vehicle efficiency across different terrains. At this point, the block braking method was proven ineffective against rubber, as vibrations and extreme wear were present.

Louis Renault fully developed the first drum brake system in 1902, which was previously invented by Gottlieb Daimler in 1899. Daimler's idea was based on wrapping a cable around a drum fixed to the chassis. When in motion, the cable tightened, allowing the driver to pull a lever, which actuated a wooden block at the time. This system lacked a form of casing, allowing dust and water to intrude on the contact area of friction. The friction shoes used were placed inside the drum brake and were activated by a rotating cam. Soon enough, the cam was replaced by a hydraulic circuit acting on two pistons. Hydraulic brakes were introduced in 1918 and have completely replaced mechanical brakes to this day. This change of concept multiplied the force applied to the drum, making braking systems more efficient. Malcolm Loughead's patent was first used on the Duesenberg and was adopted by nearly every vehicle during the 1920s. Simultaneously with the design of L. Renault, the Englishman Frederick W. Lanchester invented the brake disc system, like today's applications, but the system was yet to be used until 1952's Jaguar C-Type, as the reliability of brake drums was satisfactory for the period before. Brake Disc Systems incorporate a rotating disc fixed to the wheel shaft. A caliper containing a piston is attached to the chassis, or to the fixed part of the suspension, and applies pressure to a friction pad that comes in contact with the disc, producing friction forces that ultimately stop the vehicle.

Following this juncture, advancements in vehicular braking capacity entered a phase of heightened activity and scrutiny. Mechanical brake boosters were introduced to mitigate the force applied by the driver, enabling less tiring actuation. Predecessors of the Anti-Lock Braking System (ABS) were showcased in 1965, and the first electronically controlled ABS system was invented in 1971 by the Fiat Research Center, based on the 1960s designs for the Concorde aircraft. Brake boosting (power braking) is now a standard feature in most cars, allowing the driver to apply less force for a comfortable ride. Sophisticated systems exist that use tiny pumps to compress air, which is then released with solenoid valves to increase the pressure applied to the brake fluid. Nowadays, braking systems also use electronic devices controlled by the Electronic Control Unit (ECU) that distribute brake pressure to each wheel according to the demands of the car without notifying the driver. ESP systems are used to minimize excessive yaw rotation in cases of hazardous events, but this is yet the most extraordinary event. By using electrical motors, hybrid or pure electric cars switch from traditional hydraulic brakes to electromagnetically actuated solutions. Moreover, certain designs abandon completely the friction of materials used for over two centuries and rely only on copper coils to produce the required braking force.

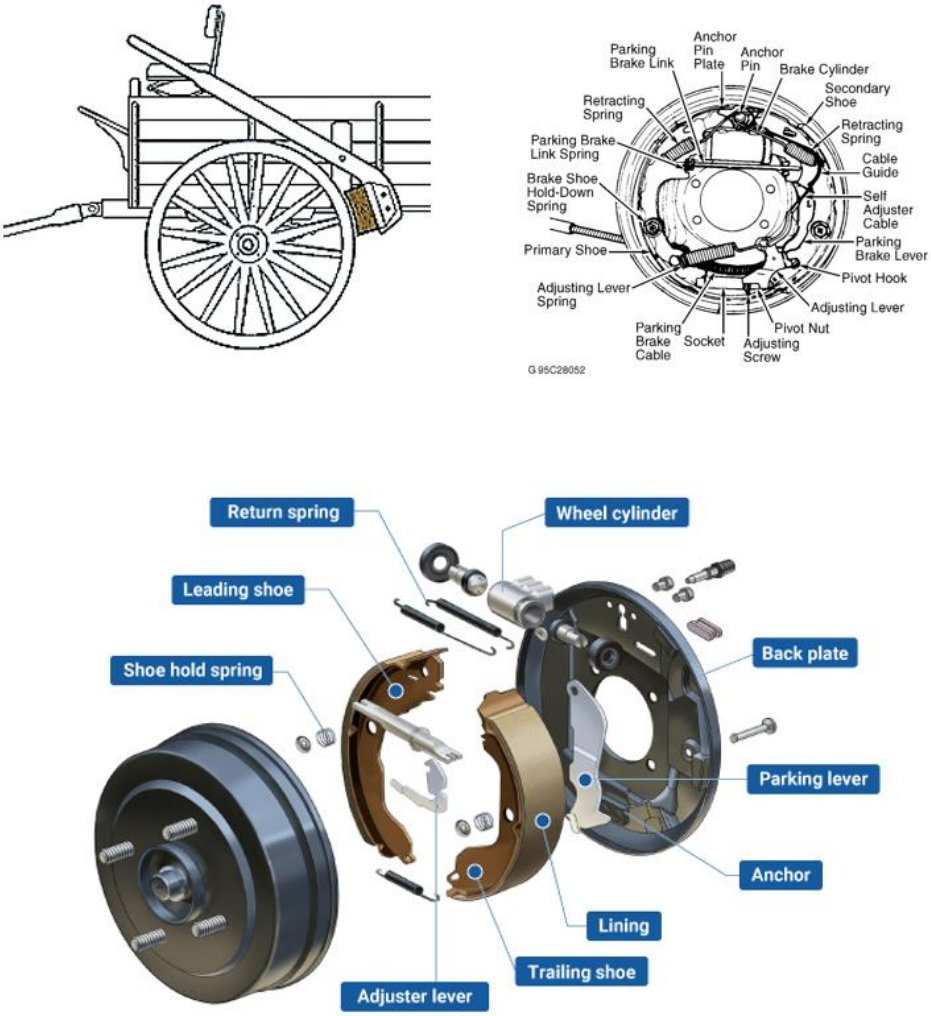

Figure 1 The Brake Drum Concept. U. Left: Wooden shoe brake, U. Right: Basic elements of brake drum assemblies. Lower: Brake drum exploded view. Source: www.quora.com

1.1.1 Brake Drums & Brake Discs

Although the introduction of electric devices for pure breaking is now being researched to some extent, the probability of abandoning traditional breaking elements is minimal to zero. Companies like Tesla, LightYear and Bosch Automotive focus their manpower on improving this concept. Yet, safety concerns arise for vehicles controlled solely by ECUs. In the event of an unexpected malfunction of this subsystem, the vehicle is subjected to external parameters, and its velocity cannot be reduced by user input. To avoid fatal accidents, traditional brakes are used as a backup for almost every production vehicle. Consequently, the utilization of brake drums and brake discs does not appear to be imperiled in the immediate foreseeable future. Their development is still a valuable topic while innovative systems and improvements on existing designs are still currently being released as showcased in the following entities. These working principles will be explained in detail in this chapter.

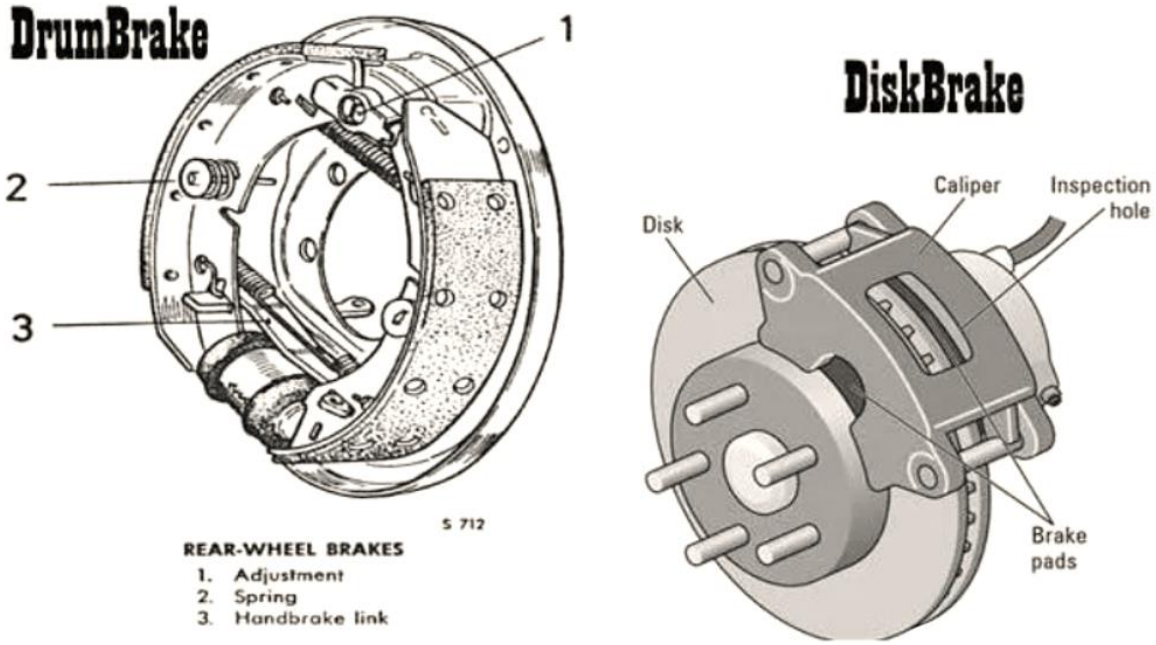

Figure 2 Brake Drum and Brake disc concept in contrast. Source: www.reviewtalks.com

Starting with the brake drums, which originated from L. Renault's patent in 1902, the idea behind the concept is rather simple. Rubber tires at the time did not provide an adequate surface to produce the desired friction force, and the materials used did not suit contact with the rubber tire as they used to with steel wheels. Renault overcame this problem by fitting a rotating drum to the wheel rim and a fixed mechanism on the chassis side. Inside the drum, friction shoes were placed, which, after activation, contacted the rotating drum, reducing its angular velocity. The shoes were activated by a cam connected to a lever available to the driver, and the cam was later replaced by a hydraulic barrel containing two pistons, which pushed the brake pads outward. This increased the total braking force and allowed for the installation of brake booster mechanisms. As the shoes wore thinner due to usage, the system required frequent adjustments until the invention of a self-aligning mechanism based on springs in the 1950s. Brake drums also fit the separate handbrake mechanism, also based on springs, in a compact assembly. Although brake drums have proven quite cost-effective and provide big braking forces, due to their large contact area, they are prone to some disadvantages. By their nature, brake drums cannot disperse heat and maintain their reliability. When exposed to heat, the drums expand away from the pads, reducing the pressure achieved, and water cannot be expelled from the system as efficiently as in a brake disc system. Consequently, brake drums do not exist in motorsport applications but are still found in small commercial vehicles and large trucks due to their low installation and maintenance costs.

Brake discs, on the other hand, have seen relatively slow usage in their early life, which was followed by a drastic market expansion in the last 40 years to date. This system contains a rotating disc, usually made of cast iron, attached to the axle of the wheel. A fixed caliper on the chassis side contains the brake pads, which are actuated by hydraulic pistons. In contrast with the drum assembly, the disc is flat, as are the pads, which are placed parallel to the disc. Every caliper is equipped with brake pads in sets, one on either side of the disc, and multiple sets of pads and/or pistons may exist in one caliper to introduce greater or variable

perpendicular force across the disc. When the brake pedal is applied, hydraulic pressure acts on the pistons, which move the pads against the disc, reducing its rotational speed. During repetitive or hard braking, the disc expands towards the pads, so brake-fade is much lower. Brake discs are often designed with additional cooling features such as vanes and drilled holes to minimize thermal stress.

Figure 3 Different brake caliper designs. U. Left: AP Racing PRO 5000, U. Right: Yamaha R1 piston caliper, L. Left: Ferrari racing brake caliper by Brembo, L. Right: Bugatti 3D printed caliper

Furthermore, channels may be engraved on the disc to disperse dust and water collected during working conditions. Although discs are usually made out of cast iron steel alloys to reduce cost, recent studies have focused on reducing disc weight to improve the efficiency of the car. Lighter alloys based on aluminum can reduce the overall disc weight and also minimize corrosion resistance and brake judder. The consistency of the braking is also improved using aluminum alloys, as studies show constant values of CoF. The main disadvantage of aluminum discs is their low thermal capacity and low melting point, as they cannot withstand temperatures greater than 400°C. To benefit from the lightweight approach, high-performance racecars and road hypercars often use Ceramic Matrix Composite (CMC) brake discs made from carbon fiber and matrices of silicon carbide. In 1974, the first Formula 1 racecars with carbon fiber composite brake discs were introduced. They are lightweight, improve overall friction generation, reduce corrosion, and are suitable for extreme temperatures. Those high-quality components are expensive to fit on everyday cars, and their design is based on the development of each vehicle to maximize its braking capacity. One drawback with CMCs is their lower volumetric heat capacity, which is compensated for by slightly larger and wider discs, but this is a minor disadvantage compared to the vast improvement in road cars' applications.

The brake disc concept has found many applications through the years, as new concepts arise for the improvement of their efficiency for each application. The two main types of discs are floating and fixed. In fixed assemblies, the disc is bolted to the axle of the wheel, providing great reliability, and this type is found in most applications, especially on high-performance vehicles. The disc is a single-piece cylinder designed with cooling features, mounted on a bell or directly onto the wheel axle. To reduce weight, the bell is often

manufactured from aluminum alloys. The floating concept, on the other hand, introduces a sliding brake disc mounted on floating pins with suitable stoppers to prevent excessive axial movement. The disc can move in the direction of the wheel axle, which improves cooling performance but introduces vibrations. Floating discs are also vulnerable to the penetration of external substances into the sliding pin surface, increasing the sliding resistance of the disc. Calipers may also be fixed or floating, depending on the volumetric capacity of the wheel assembly. A fixed assembly uses pistons on both sides, and the hydraulic circuit is common for every piston used. The symmetry provides a smoother and stronger braking process with more power. Floating calipers, on the other hand, use sliding bearings and pistons on one side of the disc and are designed to contract in size during brake application. They reduce the overall volume of the caliper as they only use pistons on one side; they are cheaper, require fewer parts, and are lighter compared to fixed ones. On some occasions, calipers use pistons on one side, and the brake pads on the other side are fixed, so that friction force gradually increases during the start of the braking as the total area of contact is doubled from the start of the piston movement up to full braking.

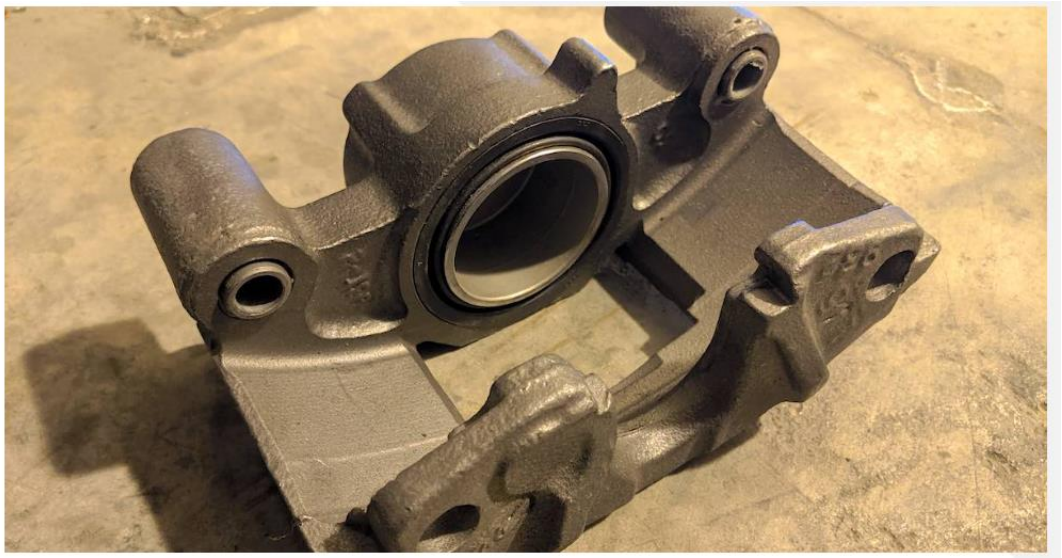

Figure 4 Floating 1 piston caliper. Source: https://knowhow.napaonline.com/

Both systems rely on pressing a braking pad against the rotating surface. Pads are consisted of a friction material that is bonded to a stiff back plate which is usually made from steel. This plate must be stiff enough to maintain the flat shape of the pad and receive vibrations during the braking event, as brake pads are subjected to harsh conditions with extreme requirements. Materials used for pads must have a high CoF and be stable during working cycles. It is critical that they showcase a low wear rate and long life combined with low wear interaction with the disc material. They must be environmentally and human-friendly, as particles are emitted during their usage and they should provide smooth braking without vibrations or squeals. To achieve all of the above, pad materials are composite structures that often combine over 15 different substances. To improve the behavior of the pad, free edges are chamfered, and slots are carved to reduce noise, improve cooling, avoid cracks, and clean any collected dust between the disc and the surface of the pad. Additional improvement is observed by inserting a third layer between the pad and backplate to reduce vibrations. Pads exhibit a learning curve in their coefficient of friction, and friction gradually increases during initial pad use, which is attributed to the flattening of the composite rough surface of the pad. This phenomenon is further explained in Chapter 2.

Given the extreme requirements of the brake pads, enormous research has been done to improve their mechanical properties [54-56,58]. Early attempts were based on asbestos, a natural mineral resistant to high temperatures. Asbestos wear-out particles in chrysotile were later proven to be related to cancer incidents, so manufacturers changed to semi-metallic and cerametallic friction composites after the ban of asbestos-based materials by the Environment Protection Agency in 1986. Other pad materials include Non-Asbestos Organic, Metal Matrix Composite (MMC), and Carbon-Carbon Composite. Metallic and semi-metallic pads (i.e., with an increased percentage of metallic fibers) are used for heavy-duty applications. They are based on iron, copper, brass, and tin and are usually made by casting or sintering, with the latter improving overall properties. MMC pads were used as a replacement for asbestos-based ones for heavy-duty applications. Boron carbide-reinforced aluminum matrix was fabricated by Chapman et al., who observed high wear resistance and zero fading behavior in high temperatures. Other manufacturers produce copper matrix composite pads reinforced with graphite, iron, and other substances for railway applications. Ceramic and carbon-carbon brake pads are also used for heavy-duty aviation and railway applications due to their high thermal and wear resistance. Additionally, the CoF of these materials is increased, requiring a lower braking force. Investigations show that the efficiency of carbon-based pads against steel rotors is reduced by nearly 30% in wet conditions.

Non-Asbestos Organic (NAO) is the most commonly used type for automotive applications. They are often reinforced by metallic fibers (ex. steel, copper, brass, bronze, and aluminum) and glass fibers to improve wear and strength as well as thermal properties. The resin is usually phenolic, and an improvement to this is heat-resistant resin, which also reduces particle emission, and rubber can be added to increase damping properties. Graphite and copper are also used to increase thermal conductivity, and the former also reduces wear rates. Metal fibers are mixed in the tangential and radial directions but not in the axial direction to avoid heat transfer directly to the brake fluid. During the wear of the pad, particles are emitted to the environment, and as asbestos, copper, zinc, lead, and antimonial emissions are related to health issues, eco-friendly NAO pads using natural fibers and substances are used. The use of fillers such as dust, mica, and barium sulfate improves manufacturability, while lubricants are also added to stabilize the friction coefficient across the working range. Abrasives increase CoF, but they also increase the wear rate of the disc as they remove iron oxides and protective surface films. For motorsport applications, this can be neglected, as efficiency is the goal, sacrificing sustainability. Finally, NAO pads are extremely sensitive to wet conditions, so they are designed to remove water from the contact area.

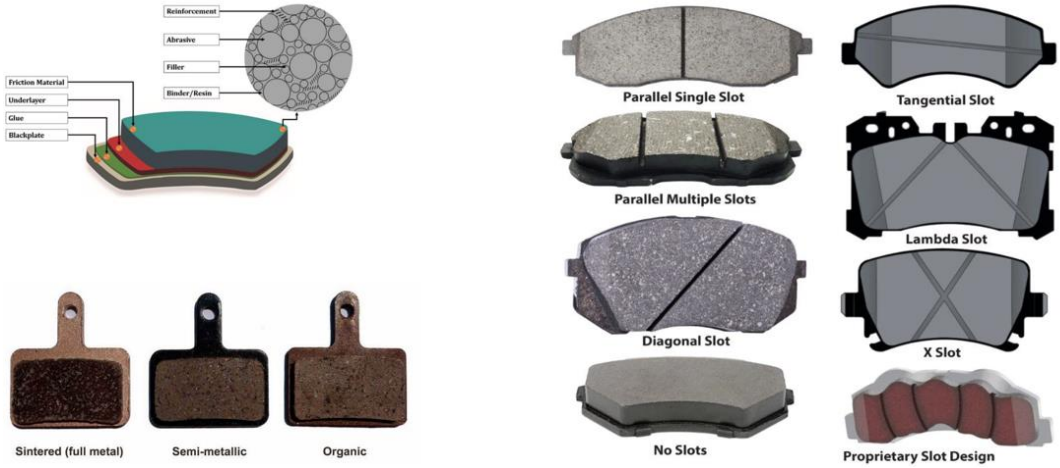

Figure 5 Brake Pads. U. Left: Brake pad layers and composition (A. Purna Irawan), L. Left: Different pad materials, Right: Cooling and Dust removal features for brake pads (Rick Muscoplat)

Every friction material differs in constitution in relation to others. Composite pads are the pinnacle of braking engineering for friction-based systems. Their constant improvement allows for lower wear rates, reliable systems and reduction of vibrations and squeal. During the last decades, the aim was to decrease harmful particle emissions, and now it is focusing on sustainability and recyclability of the materials. The overall performance of a braking system always depends on the disc-pad pairing, the heat transfer properties, and the contact parameters introduced by the used materials. Since pad materials can be customized, research is guided towards improving all of the other parameters, especially wear and CoF values, considering the pads' composition is already satisfactory.

1.2 State-of-the-Art Braking Systems.

Automotive and transport engineering applications and concepts are continuously evolving in every aspect. In this sense, brake systems have seen great improvements through the years, either small advances in pre-existing concepts or revolutionary breakthroughs. Regardless of the braking mechanism, the first breakthrough in brake history was the introduction of hydraulic actuation of the brakes. By applying the same pressure through different diameters, the brake force was multiplied, reducing the human effort. Every other innovation in the brake field has either been focused on increasing the braking force or improving the brake force distribution for the driver without any additional action other than the pedal press. Of course, material selection and research improve the CoF and thus the specific braking capacity of each system, but this section focuses only on design innovations and upgrades, as pads were examined in Section 1.1.

Pierce-Arrow added vacuum assist to the hydraulic brake system in the 1920s, which was described under the term ‘power braking", related to the additional braking force those systems introduced. The first actual commercial attempt at power braking was the Hydrovac system, used in the early 1940s. This system was based on a series of valves to improve overall brake pressure. During application, a threshold was determined above which a sliding valve pushed a triangular arm to open the vacuum valve and close the atmospheric valve, previously acting on the free side of the cylinder. The vacuum air available in a chamber is used to push a bellow against the valve in the slave cylinder, increasing the available fluid pressure. The more input pressure applied to the braking system by the driver, the greater the vacuum air supply to the system by the vacuum valve. In a similar way, during the disengagement of the brake pads, the braking assistance gradually drops as the valves close and atmospheric pressure is restored. The vacuum is generated by the piston-cylinder arrangement of the engine, making the Hydro-Vac efficient.

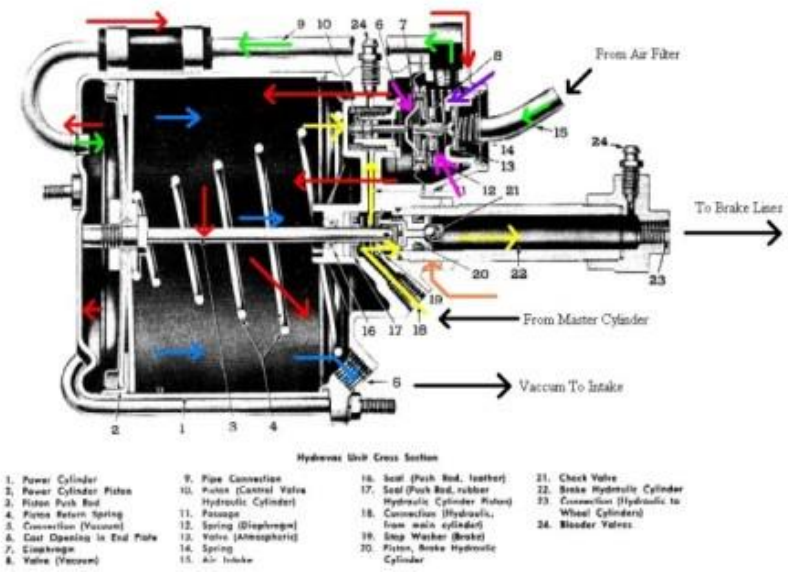

Figure 6 Bendix Hydro-Vac booster. Source: http://dave78chieftain.com/

Hydro-Vac was the inspiration for future projects, such as the Hydroboost and the Vacuum Boost systems. Hydroboost works on the same basis, except for the fact that it uses power generated by the power steering pump without any vacuum. Other designs now use electric motors to increase the pressure on the brakes.

Pressure is increased as a port in the master cylinder allows the higher pressure of the power steering system to flow, aiding the brakes. For this reason, Hydroboost produces significantly greater forces than Hydro-Vac and is simultaneously more compact and efficient for installation. One other concept, Vacuum boost, is the descendant of the original idea. The additional pressure is added by the intake manifold vacuum or, in certain engines, by a belt-driven pump. The essential improvements to other designs have been the reduction in size and cost. Moreover, both systems can be further controlled by the ECU to provide the appropriate volumetric flow in every situation.

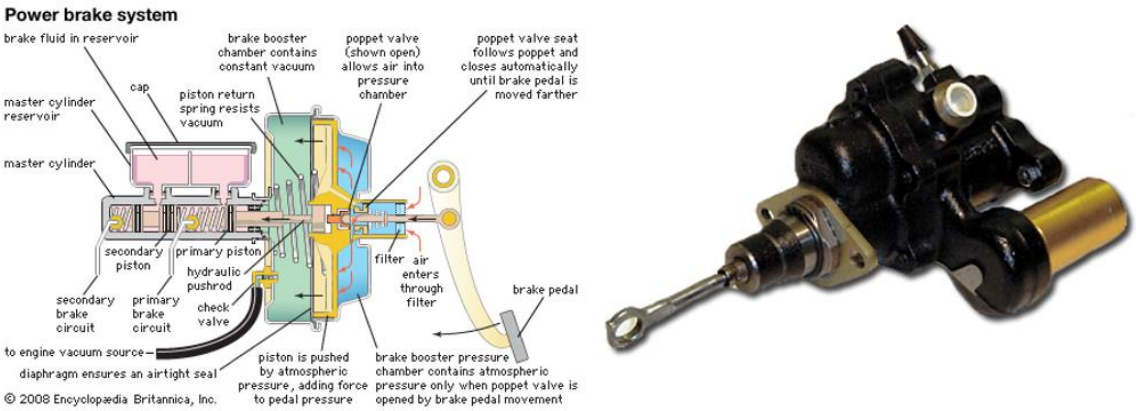

Figure 7 Booster principles and example. Left: Early vacuum booster schematic with working principles. Source: https://www.workshopservicerepair.com/. Right: Modern day hydro booster for BMW

In this paragraph, some other innovative systems used in modern cars to improve the general behavior of the braking system are introduced. The most notable system in brake applications is the ABS, or Anti-Lock Braking System. This system is installed in every modern-day vehicle and found great appreciation upon its first introduction. ABS is responsible for correcting braking torque distribution during hard braking events and providing adequate braking in low-friction terrain. Essentially, the vehicle is equipped with speed sensors that trigger a signal to close a system of valves when wheel speed is reduced abruptly. In this way, the wheel is subjected to lower resistance and rolls again until the valves are released and braking is reactivated. This phenomenon happens faster than the driver's reaction and has saved passengers in millions of situations. The next great invention in vehicle control was ESP, or Electronic Stability Program, originally introduced in Mercedes-Benz vehicles in 1995 in cooperation with Bosch Mobility. This system utilizes various sensors to compare the yaw inertia with the expected trajectory input calculated from the throttle and steering sensors. If those are not compatible, ESP actuates the brake system, distributing brake pressure and producing a rotating torque to counteract the loss of trajectory. ESP is also known under a lot of different names, mainly for marketing reasons, such as DSC for BMW, VSA for Honda, and PSM for Porsche. ESP systems have been proven so useful that from 2011 until 2014, Canada, the USA, and the European Union issued laws that required mandatory installation in all new cars produced. Furthermore, Electronic Brake Distribution (EBD) is currently used to distribute brake pressure on each wheel or on each axle, depending on the situation, to increase the efficiency of the brake systems. Those systems divide the braking capacity of the vehicle based on the demands of each wheel. The demand is the product of weight transfer during braking and cornering as well as deviation from the desirable trajectory calculated by the ECU.

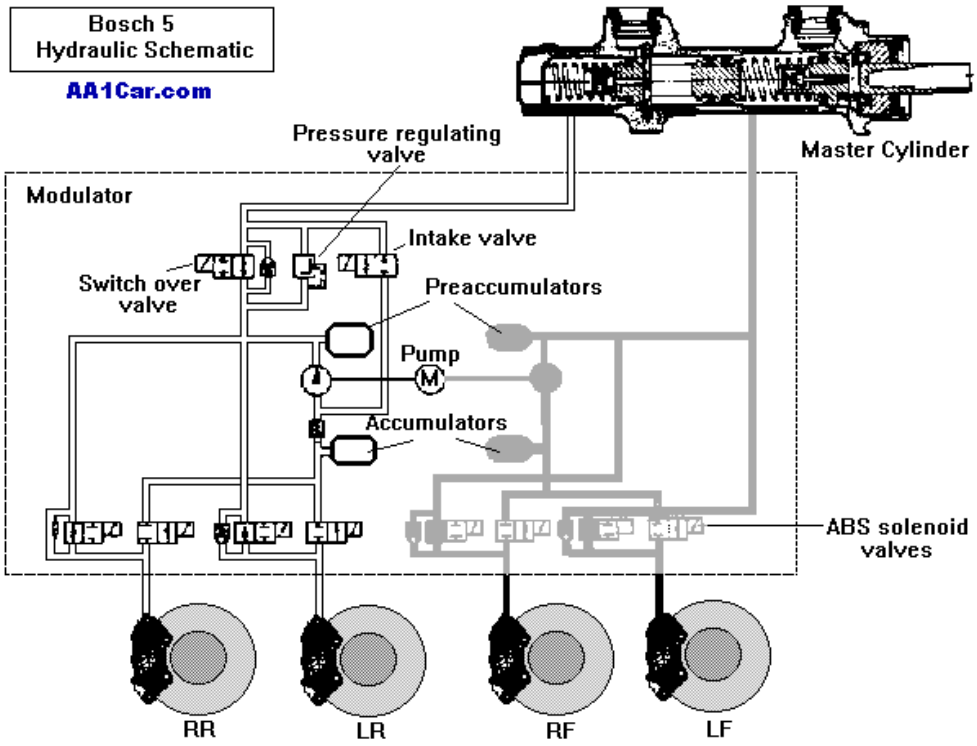

Figure 8 ABS system schematic

Back on brake boosting and increasing the efficiency of the system, manufacturers switched their interest from traditional braking to new methods over the last thirty years. Braking-by-wire (BBW) is braking actuation based on electric systems alone, either by exploiting hydraulic components or discarding them at all. In its purest form, BBW doesn't even involve brake pads of any kind, as the braking achieved is purely by electrical components. With the evolution of electronics and control units, mechanical boosting has been replaced with electrically actuated systems either acting through a hydraulic system (Electro Hydraulic Boost) or using an electrical motor mechanically connected to the pistons actuating on the pads (Electro Mechanical Boost).

Electrohydraulic systems (EHB) use motors to move a pump that increases the brake fluid pressure based on the driver's input to the brake pedal. The brake pedal is not directly connected to the pad, acting solely on a master cylinder connected to the pedal feel simulator, which transfers a smooth and comfortable pedal feel to the driver's leg. On the other side of the system, the pump is responsible for heavy-duty action on the pistons to increase braking power. Continental has experimented greatly with their MK C# systems, currently installed in road cars. The braking power is controlled by the Hydraulic Control Unit (HCU), which is a level lower than the main VCU board. To avoid hazardous events, manufacturers often connect this system in parallel with a failsafe fluid line directly connected to the brake pedal in case the control of the HCU fails.

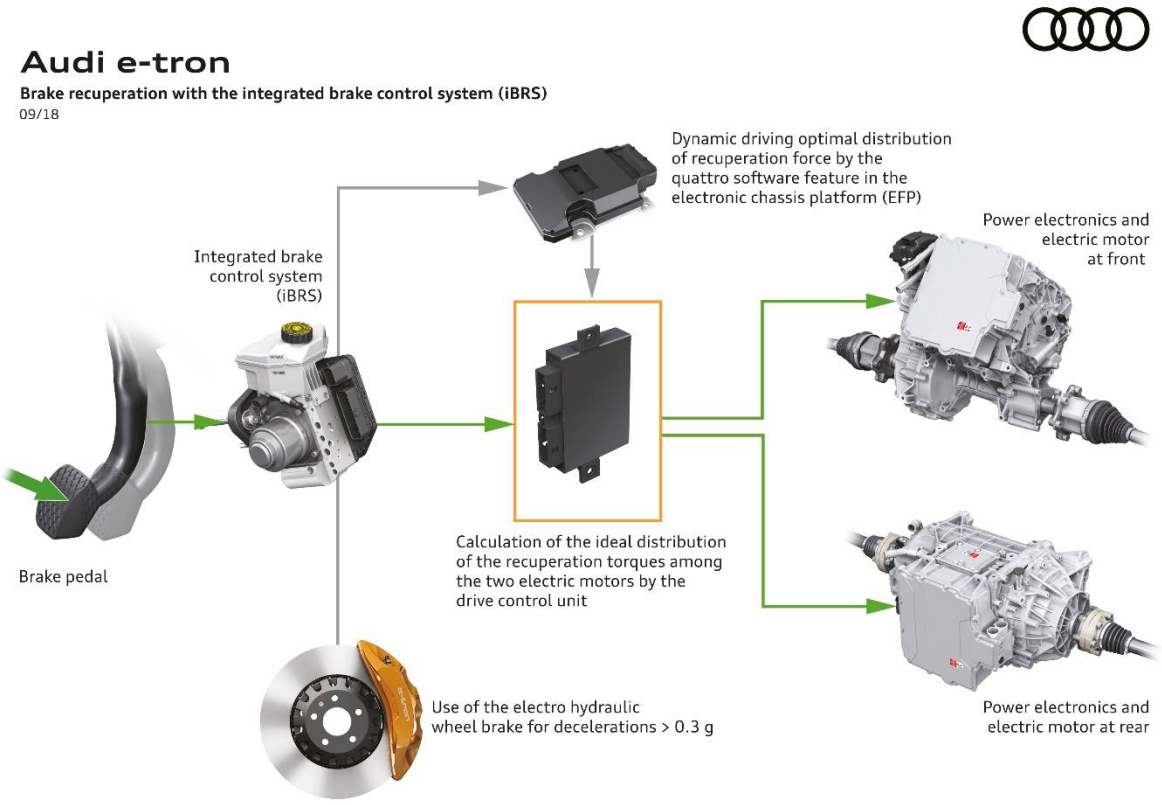

Figure 9 Audi E-Tron hydro assisted braking system explanation

Electromechanical systems (EMB), on the other hand, are systems directly actuated by a motor connected to the brake pads. Hydraulic fluid is absent in those systems, but the pedal feel simulator is still present, sometimes electrically controlled. The advantages of the EMB systems include reduced volume and weight, convenient installation, and a lack of fluid leakage and relevant pollution. Other key features include faster response (as solids are involved rather than liquids) and zero residual drag torque. Continental, Bosch, and Siemens led the field in the mid-90s. Today's structures consist of a motor connected to a spindle, which transforms the rotational motion into linear motion using a ball screw mechanism. An external nut is translated towards the piston, which finally presses the brake pads to contact the disc. Given the geometrical complexity of the system, floating calipers or discs are used so that the rolling-sliding mechanism is assembled single-sided. The correct function of the system is based on the design of the reducing mechanism from the motor input to the pad output movement. Spur gear trains are mostly combined with worm gear trains of larger ratios. Other designs use planetary gear trains, increasing the cost and assembly difficulty. Motors used are either: Brushed or Brushless DC motors, PMSM or Switched reluctance motors.

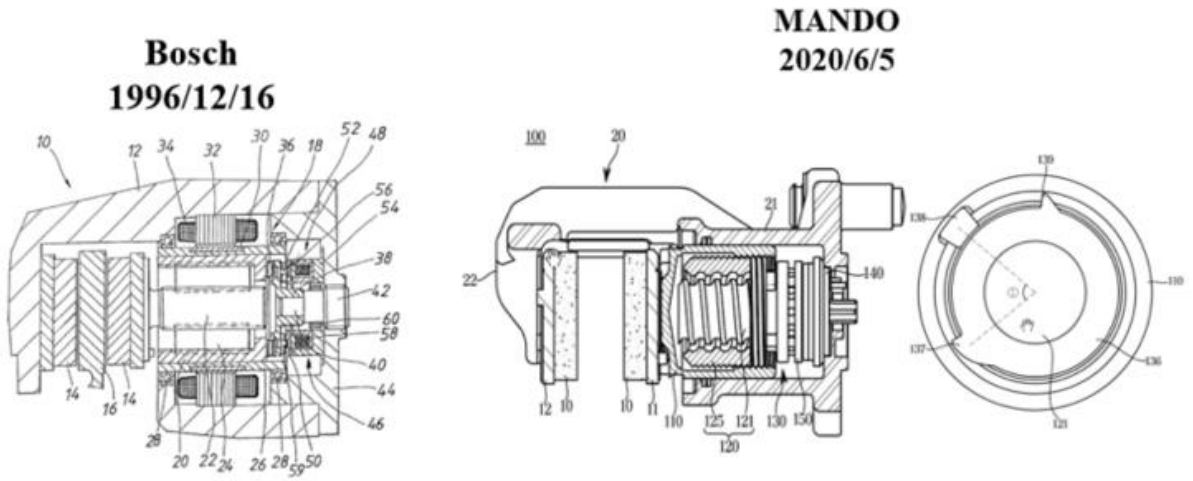

Figure 10 Electromechanical brake boost concepts. Left: Bosch 1996 concept, Right: Mando 2020 concept

Both EHB and EMB systems produce brake forces multiple times larger than those achieved previously on traditional systems in an extremely efficient way. Brake lag is non-existent, and friction hysteresis is minimized. They both rely on electronic control based on the PID method and are prone to fatal accidents in the event of a failure of the responsible control unit. Given the complexity of the EMB assemblies and the requirement of one mechanism per wheel, their usage is limited to motorsport and high-cost production cars. EHB, on the other hand, has a better installation cost and can be paired with failsafe systems as a hydraulic system is involved and connected to all wheels. Yet their efficiency is lacking in comparison to the EMB applications.

True brake-by-wire systems don’t use brake pads or friction surfaces but solely rely on electronic actuation. This is achievable in assemblies using electric motors to drive the wheels. Electric Vehicles (EVs) use motors driven by an inverter connected to the accumulator for wheel driving. The most common application is based on in-hub motors that replace the traditional axle of the wheel assembly. In this way, power is directly transferred to the wheels without energy loss. Furthermore, the constant evolution of motors for automotive applications has led to small, lightweight designs, improving the unsprang assembly weight. When a motor is not used to drive the vehicle, energy can flow in the opposite direction towards the battery, creating a regenerative effect. This effect contributes to the car's braking and can produce up to 600 kW of breaking power, based on the observations on the DS E-Tense, a car without mechanical brakes. Regenerative braking has been used in Formula 1 for 15 years and also finds applications in Formula E and other forms of motorsports such as WEC cars, prototype Formula Student cars, and many hypercars of the modern era. With the constant increase of EVs available on the road and the pressure of the engineering world towards sustainable driving and hybrid cars, regenerative braking is the way of the future. Electric braking is used mainly on the rear axle, where friction power needs are reduced due to weight transfer.

Although achievable, the eradication of mechanical brakes is a long way off for production cars, as Control Units are not 100% reliable and require additional mechanical backup under current laws.

The final part of this section summarizes other relevant concepts in the braking field that are considered state-of-the art. The use of various sensors, cameras, and LIDARs has helped the evolution of various safety features. The biggest automotive manufacturers add automatic breaking subsystems that sense the probability of crashing with any vehicle or object in their trajectory and urge the vehicle to halt once triggered. Autonomous cars work in a similar way by analyzing visual signals and acting on the braking system or reducing the motor's torque depending on the severity of the signal. Additionally, adaptive cruise

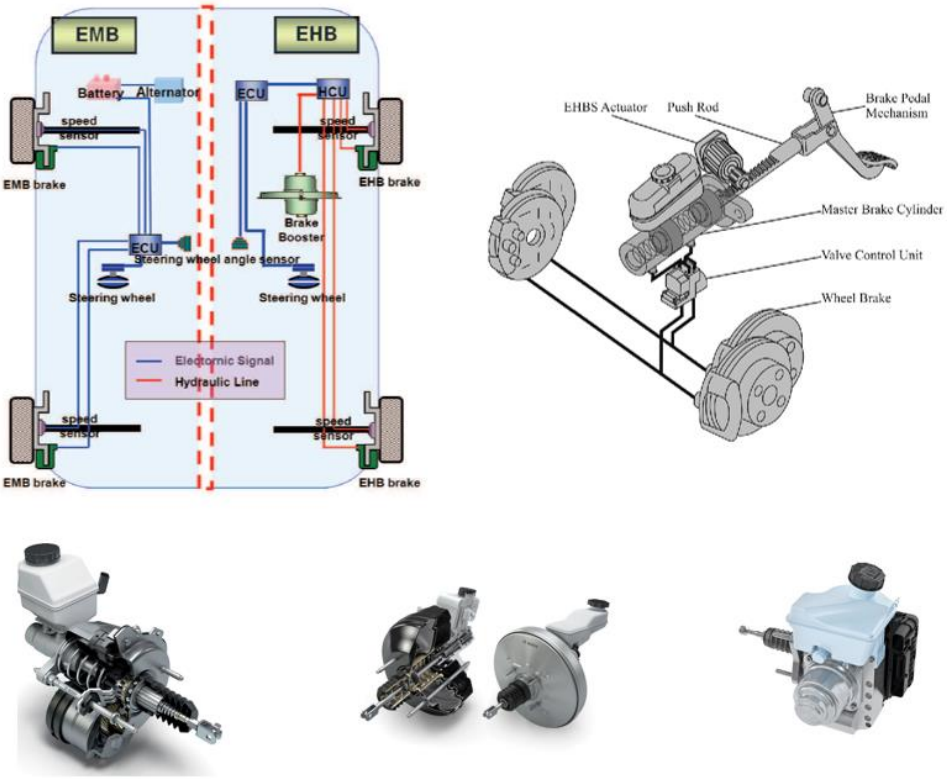

Figure 11 EHB vs EMB concept.
U. Left: Schematic comparison of the two concepts (K. Jung), U. Right: Pinion rack EHB concept with valve control unit (E. Farshizadeh). L. Left & Middle: Bosch EMB iBooster design, L. Right: Continental MK C1 EHB design

control is equipped in many vehicles in an attempt to increase active brake assist in road cars. This is more than justified given research results that indicate up to half the braking distance using those systems compared to manual, unaided driving and slow human reactions. Given the low cost of sensors, the research goes on to increase road safety and improve the overall efficiency of the braking systems. Along with material evolution, the brakes of the future will save thousands of lives and reduce environmental impact, contributing to a more sustainable future.

1.3 Thesis Motivation

As seen from the brief introduction to the history of braking evolution and the state-of-the-art systems, brake discs will not be replaced in the near future. Although regenerative electrical systems are already used in mass production, companies are still searching for advancements in the braking disc concept. This thesis focuses on the validation of a new concept to improve breaking efficiency related to performance in motorsport environments where the goal is reduced braking time and reduced distance. Racing conditions are different than those met on commercial cars, i.e., components are designed based on weight-to-stiffness criteria and last specific races or kilometers, often replaced by next generations of upgrades or spare parts. Pad wear is not an issue unless the vehicle cannot compete successfully in each specific race. The "race" distance varies from a few kilometers in small categories up to 13,500 kilometers in the famous "Le Mans" 24-hour race. The main focus is the increase of CoF and the reduction of braking lag and hysteresis, which can be achieved by improving the material composite matrix of the pads and of the discs or by defining a better actuation mechanism.

The motivation behind this thesis was the improvement of the braking system of Formula Student vehicles. Formula Student is an international engineering competition where replicas of Formula One cars on a smaller scale are designed, manufactured, tested, and raced completely by engineering students. The vehicles are approximately 3 meters in length, yet the complexity and engineering concepts applied by the top contenders are similar to those seen in Formula 1. Given the size limitations of the wheel assembly and the low market availability, universities do not have a wide variety of material selections to further improve their designs. Experimenting with new composite pads is not feasible due to time limitations and the extremely advanced chemical engineering and material science knowledge base required. In order to improve efficiency, teams reduce the total weight of braking discs to improve the rotational inertia of the unsprung assemblies and choose the correct calipers to avoid unnecessary weight.

This thesis searches beyond the spectrum of material selection and simple 3D design in an attempt to further improve already chosen specifications in a new way, becoming the new state-of-the-art technique. The idea is to improve the CoF without altering the disc and pads' size or material by using geometrical features that introduce bending phenomena, which will in turn add tangential forces opposite to the disc movement. In standard brake discs, the CoF is determined by the asperities of the surfaces coming into contact. During braking contact, shear and bending stresses are produced at the microscale, which sum over the total contact area to produce the desired force. In macroscale, the surfaces are considered flat; thus, only shear stress exists, and the question of improving CoF still exists. A simple answer would be to increase the total number of large asperities, which has already been achieved by the introduction of abrasive elements into the pads and has reached its peak. Beyond a certain volumetric percentage, those elements introduce vibrations, and stress passes the critical limit of the disc material. In this thesis, the introduction of a bending mechanism to the meso and macro scales of the disc using specific features over the surface of the disc to improve the desired friction values is examined. Similar studies have already been conducted in clutch applications to increase the power transferred. By their nature, clutches are formed by irregular surfaces that come into contact, and features are used by researchers to improve the engagement. The aim of this study is an investigation of the implication of surface features on the CoF in brake disc braking without acting on the contact material properties. The study is initially qualitative and later on experimental to verify the proof of concept of the basic idea already existing in clutch systems but in the braking environment.

1.4 Thesis Structure

The first chapter serves as an introduction to the field of braking, tracing the development of related ideas throughout the history of vehicle braking. Breakthroughs in the development of the basic idea are presented, together with state-of-the-art concepts and predictions for the future of braking, from the first introduction of brakes to the systems used currently. The rationale for the research and writing, as well as a quick explanation of the thesis framework, are also covered in this chapter. An overview of simulation techniques applied to braking systems is presented in Chapter 2. It demonstrates how a design can be confirmed using mathematical models starting from basic design concepts and variants. Additionally, methods of data validation are defined and shown in the actual world. The development of FEA models to examine the behavior of surface features through parametric qualitative research is the subject of our own work, which is presented in Chapter 3. The application of the model is thoroughly explained, several ideas are looked at, and then outcomes are produced for the supplied inputs. The findings of our study, which are applied to the real world through experiments, form the basis of Chapter 4. A tribometer that satisfies industry requirements is used to create special specimens to test the simulations' accuracy. Last but not least, with future research in mind, a revolutionary low-cost disc-on-disc test setup is constructed and presented, taking future simulations for wet clutch systems into consideration. Chapter 5 discusses the link between theoretical and experimental data. Finally, conclusions are provided in chapter 6 along with citations of potential future research subjects for the reader.

Chapter 2 - Literature Review

In order to get a deeper grasp of the brake disc concept and the design and validation methods in the actual world, in this chapter, the engineering work already completed in this chapter will be examined. This chapter overlooks all boosting techniques in favor of emphasizing the friction process. The disc geometry and the validation models of the friction phenomenon are the area of focus while the actuation of the brake pedal up to the piston is thought of as a "black box." This chapter's primary topic involves stress analysis, which, when combined with experimental or real-time data, offers insightful conclusions. A good analysis model may have a substantial impact on the development process and greatly enhance the behavior of the produced processes as a whole. Thermal strains, vibrations, and wear are evident due to the sudden encounter of high grades of kinetic energy reduction. It is exceedingly difficult to combine all of the aforementioned factors in an accurate model, making the process for generating accurate results both crucial and challenging to complete. Furthermore, a large number of influencing parameters may lengthen computation time, making it undesirable. Given this, simplifications are frequently taken into account in simulations in order to obtain worthwhile findings faster. In an ongoing effort to streamline their model and fit the tribology qualities to their specific applications, numerous writers have studied this subject from a variety of approaches. While some models employ the same ideas, others offer more advanced or creative methods. This chapter establishes the minimum levels for understanding related literature reviews; however, the reader can consult Chapter 7 to find the associated references.

Literature review is divided into four main categories.

1. Design principles
2. Mathematical models and analysis
3. FEA models and analysis
4. Experimental approaches.

Each of the four categories aids in the development of new ideas from different perspective of view. Whereas experimental efforts calibrate the models utilized, models for stress or vibration analysis can validate the designs. New 3D ideas alter the way things are considered, and real-world applications have an impact on future shape or material advances. With the use of an accurate model, designs can be improved, redundant disc material can be eliminated, the system's inertia can be reduced, better load transmission can be achieved, and stresses may be minimized. No matter the application, all of the already mentioned characteristics of the brake system design are desirable. Since neither of the four categories appears more or less useful than the others, they will be covered. Yet it is important to highlight the importance of a good mathematical and/or FEA model in the design optimization process for top-level applications such as motorsport and aviation.

FEA models are mostly used in literature to acquire a vague image of the temperature and stress fields of the disc. Additionally, they are often compared to experimental applications in an attempt to validate the model. They are mostly composed of structural and CFD simulations, which are simplified to aid computational time. Analytical models, on the other hand, focus on a mathematical approach for the contact phenomena, sometimes introducing thermal effects, to approximate the situation in a lightweight code that can easily be run. Those models focus on the contact area, while CFDs try to extract the whole computational domain around the disc and caliper, or even the entire wheel. Hence, it is rational to divide in our minds the analytical models as the "focused" ones and the FEA models as the "global" ones.

2.1 Design Principles

When it comes to designing a brake disc system, most of the time brake calipers are defined as purchased components with interchangeable pads. Apart from the pad selection, the brake caliper also defines the width of the disc for smooth operation without lateral contact in a relaxed state. Relaxed is the state in which no brake input is given by the driver. The wheel rim defines the maximum diameter of the disc, while the axle or hub of the wheel defines the minimum inner diameter along with the attachment points. The attachment point style can also defer, as seen in Chapter 1, from floating to fixed design depending on the requirements of the system. Apart from the above, the design of individual features aims to improve overall braking performance, whether that is reduction of vibrations, improved braking force, particle removal, and so on.

An efficient brake design is reliable with minimal vibration and can dissipate heat at the maximum possible rate while producing satisfactory friction force. The rate of deceleration is proportional to the heat produced; hence, for heavy-weight applications, ventilation is introduced to improve cooling effects. Heavy weight is a loose term since it is not connected with an absolute value of friction but with the ability to produce emergency stops. For example, small Formula Student cars weighing around 175kg can produce heavy weight braking of up to 2.4 gs, and the road-legal Porsche 911 GT3 RS also produces heavy weight braking of up to 1.24gs while weighing merely 1600kg. Of course, the energy dissipated in the later event is much higher, although the deceleration is approximately half. In fact, manufacturers currently use cooling features on almost all production cars in an effort to improve weight and performance. Of course, as mass and deceleration increase, parallel discs increase in width, diameter, or complexity of cooling features, if not all together. For reference, Scuderia Ferrari F1 used a design with 1400 micro holes along the circumference of the teaching disc in 2018 in an attempt to improve energy release in braking events of up to 5.5gs.

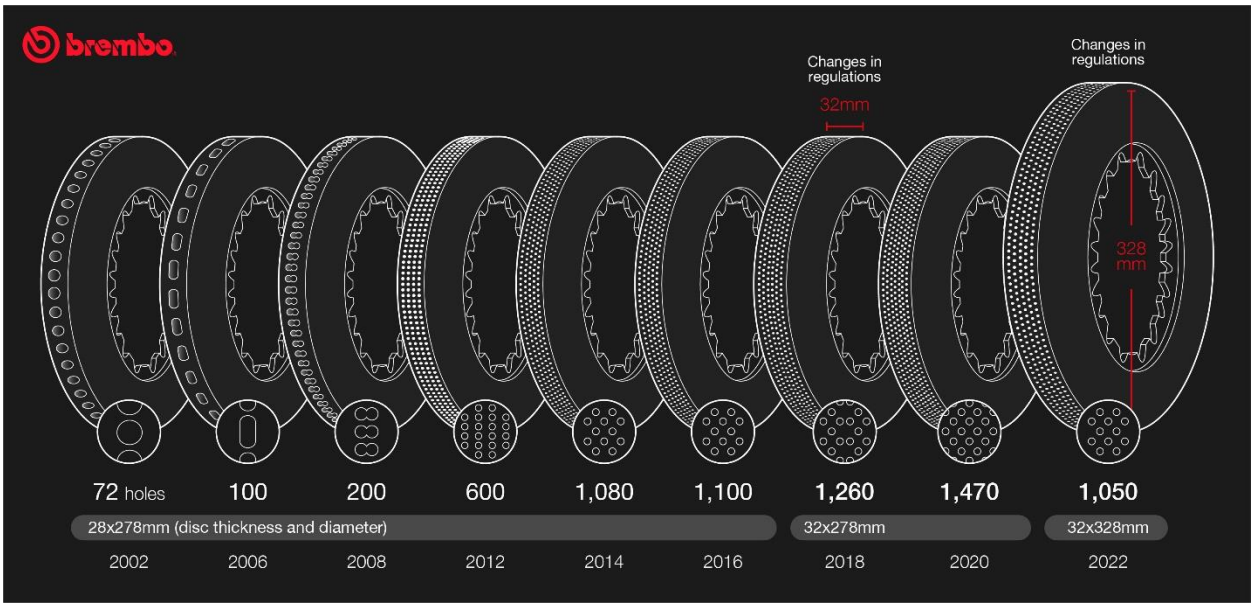

Figure 12 Brembo discs: 20 years of F1 braking disc evolution

Discs can be divided into two main categories: Solid discs and ventilated discs. The solid brake disc consists of a single solid disc, while in a ventilated disc, two separate discs are connected using pillars. Although more complex from a manufacturing perspective, ventilated discs allow airflow on the inside of the disc, massively improving cooling. Solid discs are usually used in light vehicles due to their inability to receive high thermal stress and mechanical forces. They are infrequently employed in automotive applications because their smaller cross sections result in higher stresses because the overall transversal area of force application is smaller. Due to their lower overall weight compared to cars, motorcycles and bicycles nearly exclusively use solid disc brakes. As shown later on, Formula Student vehicles also employ solid discs for the same reasons, frequently with extreme cooling designs to further decrease weight. Solid discs are usually casted and further milled to shape to reduce lead time. On specific high-end applications, they are made using turning and further milling, usually with intermediate heat treatments to improve mechanical properties. Although their manufacturing is easier than that of ventilated brake discs, their performance and cooling properties are by far inferior.

Figure 13 Brake disc examples.
Left: Yamaha YZF-R1 floating brake disc with cooling Holes, Right: Brembo Two-piece discs; line 09.C420.13

By their definition, ventilated discs provide at least double the surface area for cooling compared to solid ones since they use one flat disc on either side. Additionally, to support the two discs, vanes are connecting them, creating airflow passage from the inner to the outer diameter through the inner side of the discs. Since the assembly is rotating, they also accelerate air mass further by their shape to promote the cooling effect. Based on thermodynamics, by maximizing the available free surface of the disc body, the maximum temperature is lower. This is why, on high-end applications, hundreds of small holes are drilled on the disc to improve disc and air contact. Holes are also drilled on the flat surface of most discs, especially in solid applications, to increase the area. The density and pattern of the holes are related to the maximum stress on the disc rather than the friction ability. The friction force is mainly influenced by the pads' size and dimension and their relative position relative to the center of the disc. The pattern is also decided based on the required weight loss requirements and the need for improved cooling. On some occasions, manufacturers prefer angular slots on the radial dimension of the disc rather than holes, with the same effect. Finally, radial grooves in the disc with a sparse pattern in comparison to the holes are also met oftenly. Grooves are used to improve contact by removing moisture and foreign particles trapped on the disc's surface. Lower CoF values are produced as a result of those particles, which also lessen the total area of contact or interfere with the hard materials of the pad and the disc. Although discs typically have grooves

running the entire radial length of the disc, there are times when half-grooves are added to the design to improve contact on the outside portion of the surface. It goes without saying that more advanced designs may use both holes and grooves on the disc's surface to enhance every aspect and also add those features to a vented disc, as seen in figure 13.

After discussing surface designs for better cooling, it is time to look at vented disc concepts, which are typically used in automotive applications because heavier vehicles typically have drum brakes. Inner ventilation is achieved by removing material from the volume between the side faces of the disc. Various configurations of vanes, holes and pillars are used to achieve this, each providing unique airflow characteristics and improvements. No solution is directly better than the others, as the outcome depends on the working conditions and the specification of the vehicles. The intake of the airflow is typically shown on the inner diameter, which is strongly stressed. Configurations can also be classified as symmetric or asymmetric, with the latter requiring unique discs for each side of the vehicle, which raises the cost. The primary factors affecting cooling efficiency in every concept are the amount of heat-exchangeable surface area and the rate of air circulation.

Straight Vanes: The most popular and easiest type of vane is the straightforward type. Straight vanes are used by most vehicles on the front axle due to their easy manufacturing and their symmetrical character. Their efficiency is lower than that of other designs, but the vane draft allows for easy casting. Straight vanes are also used in composite brake discs where post-milling removes material from the disc with limited flexibility in the tool’s motion, which is usually perpendicular to the vertical plane of the cut.

Curved Vanes: An improvement of the straight vane concept that uses curved vanes either in the direction of rotation or against it. The curvature and density of the vanes are chosen using CFD. Curved vanes provide substantially improved results, as shown by Belhocine [1], with results in favor of the backward curvature, although turbulence is decreased in forward vanes as the flow is subjected to a more natural trajectory.

Figure 14 Brembo PVT internal cooling design

Pillar Patterns: Pillars differ from vanes mainly due to their non-homogenous form across the surface of the disc, and their total span is significantly smaller than that of vanes. The idea behind the concept is to increase the total surface by creating complex paths for the airflow values that favor a range of working conditions. The shape of most pillars resembles diamonds and circle sections. Additional vanes are used in the inlet to guide the airflow in a more desirable direction. The size of the pillars usually varies greatly according to

the radial dimension, and larger triangle-shaped pillars are found on the outlet. Brembo has patented PVT ventilation to increase resistance to thermal cracks by introducing a middle layer of star pillars, improving weight reduction. Stoptech patented the Kangaroo Paw design to maximize mass flow and minimize brake fade. With the use of generative design, new patterns can further exploit the advantages of pillars, which are usually manufactured using casting; hence, their geometry is relatively unrestricted.

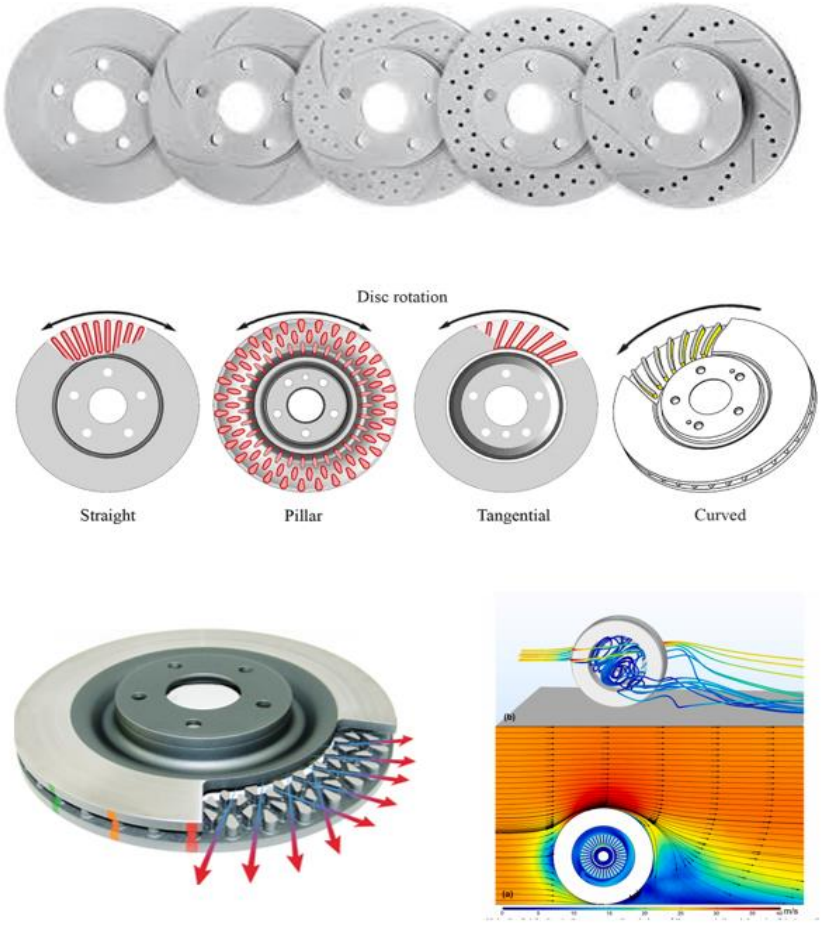

Figure 15 Ventilation concepts for braking discs. Upper: different cooling features, from left to right 1) Solid, 2) Slots, 3) Slots and drill points, 4) Holes, 5) Slots and holes. Source: https://mzwmotor.com/
Middle: Inner cooling features, from left to right 1) Straight vanes, 2) Pillars, 3) Tangential vanes, 4) Curved vanes. Source: https://mzwmotor.com/. L. Left: Stoptech Kangaroo Paw desing, L. Right: CFD on brake discs (R. Jafari).

The geometry of the disc is also determined by the available volume to construct the disc. Motorcycle brakes can be expanded in diameter since they are offset from the spokes of the rim, but this can lead to local buckling while braking. For this reason, they are directly attached to the axle of the wheel. In automotive applications, on the other hand, braking forces are multiplied, and smaller inner diameters are equivalent to increased thermal stresses. The width of the tire and rim is larger; therefore, bells are used to attach the braking disc to the hub, and the width of the brake disc is also increased to withstand the higher strain. By using bells, the inner diameter of the disc is larger and further away from the wheel bearings, which should not be thermally stressed. On motorcycles, this issue does not exist since the disc is more

exposed to the environment and the energy dissipated is less. Bells can be cast with the disc or bolted to it, with the latter providing the ability to use different materials to further reduce thermal transfer to the hub and also improve the overall stiffness while reducing weight.

It is already shown that there are many considerations taken into account when designing a brake disc. The application used has a big impact on the type of disc and the cooling requirements, which are translated into a series of features to improve thermal management. Due to weight transfer, bigger discs with complicated geometries are on the front axle while simpler and smaller ones are on the rear.

2.2 Analytical Tools and Mathematical Models

Any engineering problem can be approached and analyzed using mathematical science to produce accurate results. The models employed are increasingly complex and typically cannot be solved by hand as the complexity of the studied system rises. Moreover, extracting the optimal equations to describe those systems can be extremely time-consuming, without even adding the solving time. Such an example is the complete Navier-Stokes equation in Fluid Dynamics, which is unsolvable, and only simpler models can be solved analytically. For this reason, studies in the braking field are focusing on a specific spectrum of the total phenomenon, aiming to extract good results in a cost-effective way. Approximations are present in the models as well as simplifications to the 1^{st} or 2^{nd} order of differential equations. For example, one can study the contact effect of composite pad fibers on the steel disc in an attempt to improve a wear model, regardless of the heat generated. Other studies aim for a better understanding of the way the two bodies come into contact, focusing on the meso- and microscales of their respective surfaces.

Tribology is the study of friction, wear, and lubrication, as well as the design of bearings, or, to give a general term, the study of interacting surfaces in relative motion. In an ideal world, frictionless contact exists, though in physical applications, even the smoothest surface has a positive roughness value, so when in contact with another body in relative motion, friction is produced. Tribology encompasses a wide spectrum of engineering subjects, such as solid and fluid mechanics, material science, lubrication, heat transfer, and biology. Using tribology, the behavior of different bodies and the reaction of their contact to different working conditions, such as different external pressure or relative velocity, can be observed. This is something that can be proven extremely beneficial, as on certain occasions increased friction is desired or on others it needs to be eliminated. Wear is also a major design parameter for moving systems. By having full knowledge of the parameters involved, tribology models enable improved designs with optimized function and reduced energy loss, thus providing financial benefits as well. One example can be the study of bearings, where small reductions in the friction value can multiply the components' life and reduce the necessary service or replacement costs.

The aim of the current paper lies outside of covering a complete literature review of the tribology models used through the years, as this has already been accomplished by other respectable authors. F. Marques et al. [2] present a relatively thorough comparison of existing models to date. They conclude to the great complexity of a fully detailed modeling of the frictional phenomena and agree on trade-offs between ease of application and accuracy of the captured event. They also state that experimental characterization is mandatory on most occasions and that models cannot be 100% reliable. They conclude that static friction is easier to model, and dynamic applications, though important, are costly but mandatory when the energy dissipated is studied. E. Berger [3] also notes a wide range of studies in the tribological field, both theoretical and experimental, focusing on the role of hysteresis during the contact. From the Tribology perspective, it must be clear that none of them can be neglected.

As already stated, many engineers and scientists have dealt with the subject of frictional contacts. The need to improve existing models can be understood once one comes across the number of books solely mentioning tribology. Of course, this includes immense studies on contact mechanics, which is a wider field. Q.J. Wang et Al. [4] published the Encyclopedia of Tribology in 2013 with an astonishing number of 2161 chapters covering nearly all aspects of the domain. A.Z. Szeri [5] included the tribology field in the 2003 Encyclopedia of Physical Science and Technology, mentioning the size comparison surfaces in the interest of the field. Undoubtedly the most significant book in contact mechanics was 1985's "Contact Mechanics" by K.L. Johnson [6]. Johnson examined the contact of two bodies, mentioning the elastic half-space consideration to derive the equations described. He introduces Herzian and Non-Hertzian contact of

bodies as well as inelastic behavior throughout different situations. He also acknowledges lubrication and dynamic phenomena, as well as thermoelastic principles and observations on rough surface modeling. I. Goryacheva [7] also published a focused approach to presenting the contact mechanics concepts expressed via tribology aspects. This 1998 book targets wear models and sliding contacts and presents a rather detailed review of the frictional contact, in contrast to Johnson's general approach. Those two books are the pylons behind any other published book post-2000, as the generalized concept together with concrete foundations on the nature of the contact sum up the basic review of any application. V. Popov [8] researched further into adhesives and tried to include a variety of contact problems in his book "Contact Mechanics and Friction", and P. Wriggers [9] transferred the theoretical background into numerical simulations. Adaptive FEA, Discretization of deformation contact, and numerical thermal-mechanical elements were among those studied in this remarkable book of the early 2000s. Of course, many other books exist regarding the subject, but it is beyond the scope of this paper to present them all.

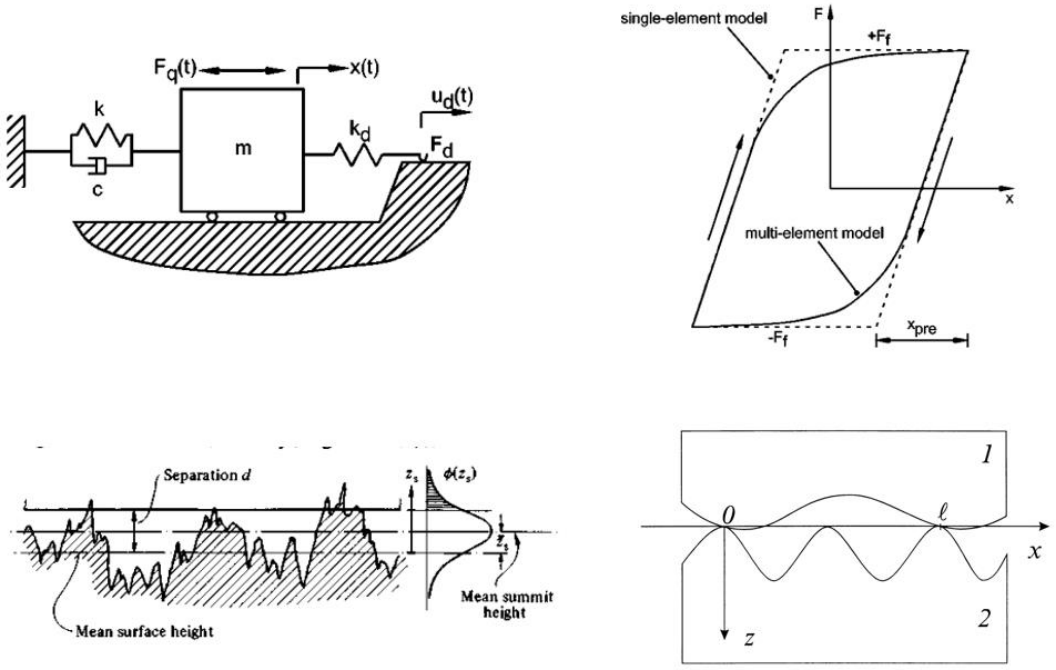

Figure 16 U. Left: Single-DoF structural model with hysteris [3], U. Right: Cycling loading with partial slip [3] L. Left: Contact of rough surface with smooth flat [24], L. Right: Shape of bodies in contact [7]

Static friction is usually modeled with numerical models, as dynamic systems introduce a lot of uncertainty and other more complex phenomena such as vibrations and impacts. Most of the methods model the stiffness of the two bodies when in contact in a generalized way, regardless of the exact geometry and roughness. This is again one of the ways to simplify a friction study. Hertz calculated the contact patch of two spheres when Young's modulus and Poisson's ratio were known along with the dimensions. Other models try to examine the friction force in relation to the relative velocity of the bodies, especially near the static limit. Coulomb's model states that step change is a constant value against the velocity direction. The improved Coulomb's model also adds stiction, which leads to increased friction values at null velocity [1]. The Stribeck effect, presented by R. Stribeck in 1901, was expressed for lubricated applications but can also be applied to dry conditions. Friction values peak at zero speed and follow a descending trajectory up to a constant value. In lubricated applications, Stribeck also adds an intermediate zone where friction

reaches a minimum before ascending to a stabilized value. Karnopp [9] proposed a zone near the zero point where friction accepts the static value rather than the dynamic value to overcome simulation difficulties. Other models, such as the Bengisu and Akay model [11], introduce a linear zone up to the maximum friction point to mitigate the uncertainty of Karnopp's model, while others describe a hysteresis zone near the zero point, where values can follow certain curves depending on the rate of change of the velocity of the bodies.

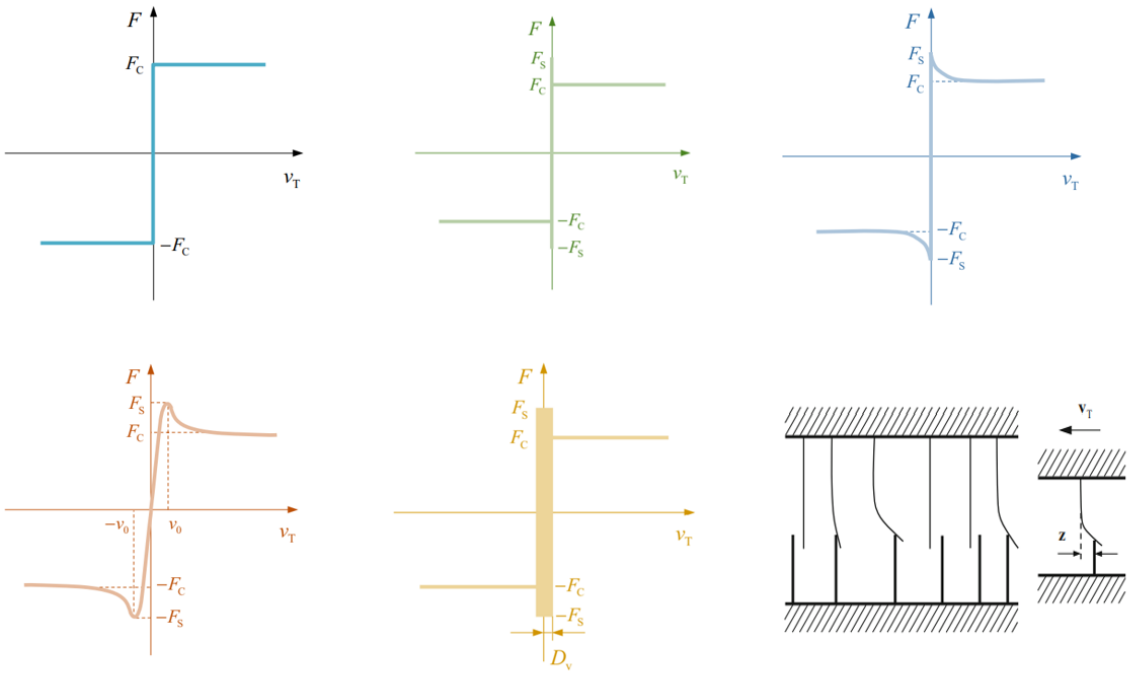

Figure 17 Different friction models according to literature [2]
Upper form left to right 1) Coulomb, 2) Coulomb with stiction, 3) Striberg
Lower from left to right 1) Bengisu Akai, 2) Karnopp, 3) LuGre Model (Bristle model)

Dynamic friction, on the other hand, is usually interpreted by simple models that dissect the total contact area into points that come into contact with their respective neighbors. The entire body, or each point, is marked with a specific stiffness, and differential equations lead to the extracted friction force. Dahl's model [12] added a stiffness coefficient for each body, or as a function of length, that is chosen based on the brittle or ductile nature of each material. The bristle model [13] and the LuGre model [14] are the early versions of many modern models based on asperities. In their considerations, the asperities of the contact bodies are modeled by single bodies that come into contact with each other. Each body has a specific length and stiffness, which can be further modeled by a series of springs and dampers [3,17]. Dividing each asperity into discrete bodies is a common practice used to calculate the mean deformation of the plane in contact as well as the average asperity height. The Leuven model [15] was the first description of the LuGre model that included asperities' deflection, and elasto-plastic models go a step further by adding the energy captured by the deformation of the asperities and explaining hysteresis based on the elastic and plastic properties of the sum of the asperities. As stated by F. Marques [2], the models tend to have similar attributes when force is plotted versus velocity, yet the sum of the models leads to a clear hysteresis region near static conditions. Current models try to introduce asperity damping, where asperities are formed from the pad and

disc material composition expressed by statistical functions for the volume percentage or the mechanical properties at each point.

At this point, it is worthwhile to discuss the nature of the asperities, the reasons they exist, and the impact they have on total friction. Asperities are considered the peaks of the roughness profile of each body. Given the nature of the composite materials used in the pads and the initially increased roughness of the disc's surface, those components have a lot of irregularities on their surfaces. Pads are composed of hard fibers such as steel and other metals, as well as ceramic elements and a polymer or organic matrix that bonds the pad shape, as seen in Chapter 1. The surface of the pad is not flat but presents irregularities due to the different compositions, which create a 3D surface topography consisting of peaks and cavities. Only a portion of the pad's overall surface area actually makes contact with the disc [18], as the pressure rise causes several plateaus to occur. Unless there has been significant wear on the pad material from excessive use, those plateaus make up less than 30% of the entire surface. The local characteristics of the composite material are related to the position and size of the contact areas. Increased hardness values are typically present in plateaus, as a result of a local rise in the volume percentage of metal fibers, which are surrounded by a softer lining.

The lining matrix helps with braking-related dampening. The material contacting the disc deforms both plastically and elastically as brake pressure increases as a result of Hertzian pressure. Peaks made primarily of metal deform less and bear a greater percentage of the load. As the metallic fibers deteriorate and come into contact with the adjacent lining, local stiffness reduces, followed by local deformation and an increase in overall contact area. Heavy run-in cycles, temperature, and repeated braking can all hasten this effect. The pressure varies locally along the pad's surface as a result of the metal-based peaks appearing sharper than the remainder of the pad. This variation can introduce bending moments into the disc, which enhance vibrations and squeals and leave visual concentric marks on the disc. Numerous studies [19,22] have demonstrated an increase in CoF with time until a steady value is reached, which is attributed to the local plastic deformation of the various peaks of the pad that ultimately leads to greater surface area and thus increased force.

Additionally, to asperities' deformation, other effects also occur at the microscopic level. Thermal induction affects the chemical and mechanical properties of the pad, leading to an even bigger contrast from soft to hard areas, and debris tends to stick to the contact surface, affecting the phenomenon. Contamination of the surfaces also occurs as volatile components are trapped in the contact volume, and oxidation of the fibers and the disc alters the nature of the contact. That can be minimized by optimizing the shape of the disc, as seen in Section 2.3.

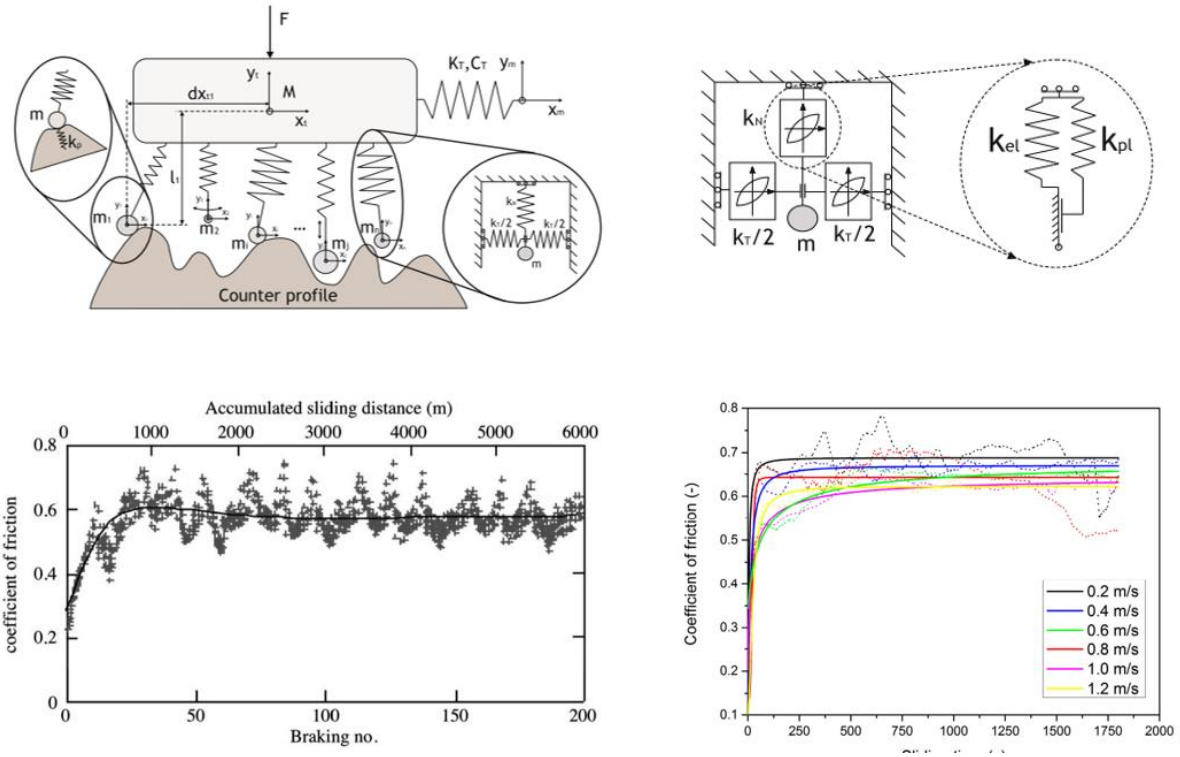

Figure 18 Models and results from literature. Upper: Asperity model with elastic-plastic modulation [16] L. Left: CoF values through time [17], L. Right: CoF values for different velocities [22]

The behavior of the asperities and the presence of foreign substances provide an explanation for hysteresis. The surfaces are forced to adapt to the new circumstances as the pressure builds. Cleaning the plateaus and the areas around them of volatile materials is necessary, and as each matrix element's elastic zone approaches its plastic limit, the overall stiffness of the pad is continually changing. Once all the reactions from each plateau are summed, the deformation stops, and friction is at its maximum. On the opposite side, elastic unloading takes place rapidly, but wear particles are trapped in the newly free spaces, and the total decompression phase is slowed down because the ideal total plateaus' surfaces are corrupted.

A statistical analysis focused on interpreting the asperities inherent in a strong model was published by Ogilvy [20]. In his model, he made the assumption that the two surfaces were represented by a height probability distribution throughout the material's length. By changing the sigma and lambda zero parameters, several profiles can be generated under the assumption that height p(h) follows a Gaussian distribution.

$$p(h) = \frac{1}{\sigma\sqrt{2\pi}} e^{-(\frac{h^2}{2\sigma^2})}$$

A flat, smooth surface is pressed against one Gaussian surface, and the vertical distance dh of the two bodies can be calculated at any point. If dh is smaller than the height of the point, the surface is readjusted by using elastic or plastic models. This deformation is equivalent to a reaction force, and summing all the individual

contact reactions produces the total load W applied to the smooth surface. The model can be used to acquire information about the reactions of the two surfaces to different statistical and qualitative parameters of the surface. K. Moerlooze et al. [18] expanded the research of previous authors on a concept similar to Ogilvy's but far more complex. He assumed the pad was a free-body M attached to a horizontal spring and a counter-profile. The asperities are modeled as free bodies of mass m_i attached to the pad by springs of different length l_i and stiffness k_i. The model also includes the elastic-plastic behavior of the bodies by adjusting the spring with a composite spring, one for each zone, according to the Maxwell-Slip model. The equations of motion for the pad (M) and the smaller asperity masses (m) are included in matrices forming a differential equation of the form:

$$\dot{q} = Aq + B$$

$$\dot{q} = \begin{bmatrix} 0 & I \\ M^{-1}K & M^{-1}C \end{bmatrix} q + M^{-1} \begin{bmatrix} 0 \\ F \end{bmatrix}$$

Due to the non-linear elements of the model, solving the equations requires an iterative process. This model is able to predict the Stribeck curve and replicate the qualitative behavior of hysteresis and CoF convergence over time. Both models attempt to build an effective model that is based on statistical values containing as many parameters as possible. Incorporating Gaussian distributions for the profile indicated in Moerlooze's study or using statistical distributions for the spring stiffness based on chemical analysis of pad materials might assist in future research.

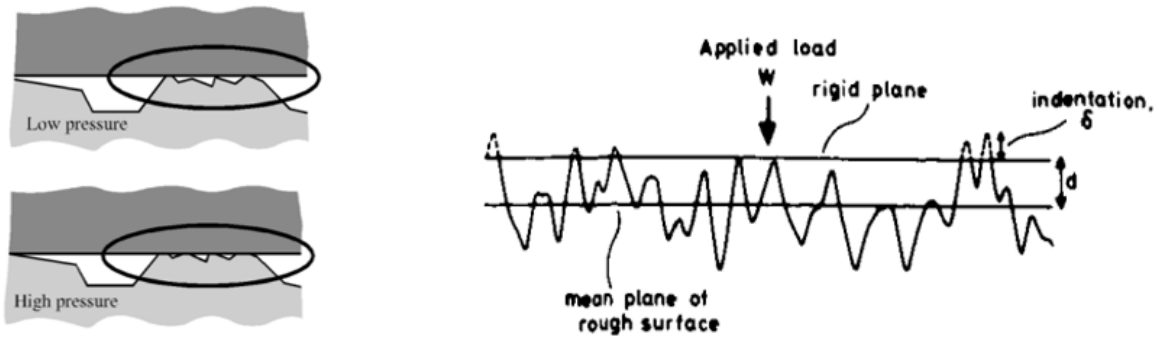

Figure 19 Asperities in contact: Left: Ogilvy's model [17], Right: Contact expressed by flat and randomly (Gaussian) distributed surface [18]

The final paragraph of this section is devoted to research related to other phenomena of braking contact. Goryacheva [20] analyzed Wear using mathematical models and also introduced damage fields for the asperities represented as random profiles. She also accumulated different wear models and their respective conditions, including Rhee's model. X. Liu [21] is among the many publishers in the field of friction dynamics for brake systems, as he described brake judder and squeal and conducted modal analysis on brake discs, correlating it to the sound emitted during braking. He also described the dynamic wobbling of discs due to different plateau pressures and a system of damping elements on various points of the disc. Brake squeal is covered extensively by many other scientists, as clearly stated by Liu. In a different paper, N. Kinkaid [22] summarizes squeal research, presents early and current approaches, and correlates squeal

with dynamic models. After an extensive presentation, he states that squealing is still an unsolvable problem but refers to analytical and FEA models that improve our comprehension of the problem.

The short overview of tribology-related variables in brake disc analysis is now complete. Predictions of friction values, vibrations, and local impacts can be produced more accurately by closely assessing the asperities. Although it has been established that no model can completely account for all potential scenarios, the complexity of the tribological contact between the pad and the disc is once again made abundantly obvious. Up to now, only qualitative descriptions have proven to be fairly precise.

2.3 FEA & CFD Simulations

FEA stands for Finite Element Analysis, where CFD stands for Computational Fluid Dynamics. Those powerful terms are the usual tools to analyze bodies that are subjected to some kind of stress or are included in a domain where fluid motion is present. In contrast to analytical models, FEA and CFD are usually provided in a software that aims in including as many scenarios as possible. For this reason, the computational time is increased in comparison to mathematical approaches, and the code is not always available for edit, therefore the simulation method may not suit entirely the application. Nevertheless, they are easy to use, can be modified by the user to describe the model in a good way, and do not demand interaction of the user and the solver environment. Both tools are based on bisecting the objects into smaller volumes consisted of nodes each one with its own properties. The values of the properties of each node are changed through iterations which ultimately converge to a smooth change of values in close regions and also counteract the inputs the user applies.

In brake studies, FEA are used to simulate the braking phenomenon and calculate the stress on the components. Studies include mechanical and thermal parameters, depending on the wanted outcome. Additionally, it is common practice to simplify the model, by neglecting parameters that have minor effects and assume constant values derived by other simple calculations. A. Lindgren conducted stress analysis on the Koenigsegg Regera braking system, where braking force and energy dissipation are calculated by a simple weight transfer analysis. This is a common technique used, as on most occasions the point of interest is the ultimate strength of the design in extreme conditions.. In most studies, the objects studied are the brake disc along with the brake pads, and all other bodies are neglected. On some occasions authors include the calipers and the wheel to represent the system in a more realistic way. Often the input is constant fluid pressure, constant deceleration, constant heat flux on the surfaces of the disc, or even constant force applied by the pad. All of the above are approximations that aim in reducing total computing time. As already seen in entity 2.2, it is extremely difficult and inefficient to accurately describe the braking system as thermal and mechanical elements are present along with fluid dynamics, wear, non-uniform materials, and varying road conditions. Simplifying the system can lead to faster results which are safe to use under the correct safety factor.

Heat transfer has a major influence on the final stresses on the disc's surface, since the highest temperatures are on the points of pad-disc contact. Heat is transferred by conduction, convection and radiation. Neys [23] studied the brake heat generation and dissipation in order to develop a brake temperature calculation model for an in-car warning system. In the paper of Talati & Jalalifar [24] it is stated that 93,4% of the generated heat is absorbed by the brake disc. A. Belhocine & M. Bouchetara [25] also claim that over 90% of the heat is consumed by the disc. They considered the pads as an entering heat flux receiving a constant value. Heat flux was calculated by the formula of Reimpel:

$$q_0 = \frac{1-\varphi}{2}\frac{mgv_0 z}{2A_d\varepsilon_p}$$

where z = a/g is the braking effectiveness, a is the deceleration of the vehicle [ms^{-2}], φ is the rate distribution of the braking forces between the front and rear axle, and Ad: disc surface swept by a brake pad [m^2], v0 is the initial speed of the vehicle [ms^{-1}], ε_p: is the factor load distribution on the surface of the disc, m: is the mass of the vehicle [kg], g: is the acceleration of gravity (9.81) [ms^{-2}]. Belhocine also state that radiation can be neglected, which is also common consideration across literature. W. Bena et Al. [26] conducted

thermal stress analysis on commercial Volvo truck, considering uniform pressure and uniform wear models. J. Jamari et Al. [27] conducted also a simple thermal analysis to derive the cooling improvements of ventilated vs solid discs. A. Belhocine et Al. [28] conducted FEA analysis on the frictional contact of vehicle braking including similar formulas and coupled the results with CFD simulations for accuracy improvement. T. Valvano et Al. [29] used an uncoupled thermal and static model to predict thermal distortion, describing adequately the thermal model. Y. Yildiz and M. Duzgun [30] compared different cooling geometries in a structural stress analysis using FEA introducing variable pad pressure to the disc. J.Yin et Al [31] present an equivalent moving model to better predict stress analysis of the disc, and propose improvements of the structure of the braking disc, achievable by sintering or 2-phase casting. A.Afzal [32] also include the Belhoncine equation proposing a simple FEA model that includes heat transfer and can be solved by computing software. Additionally, Afzal refers to previous studies regarding wear, thermal analyses, and stress calculation on brake discs, and showcases possible disc designs to improve cooling. From all of the above, it is evident that the research on braking simulations is extensive and ongoing, and different models are proposed frequently to cover different areas of interest. Most of the models are based on simplifications and cannot describe the entire braking event with complete accuracy, due to the high number of unknown parameters.

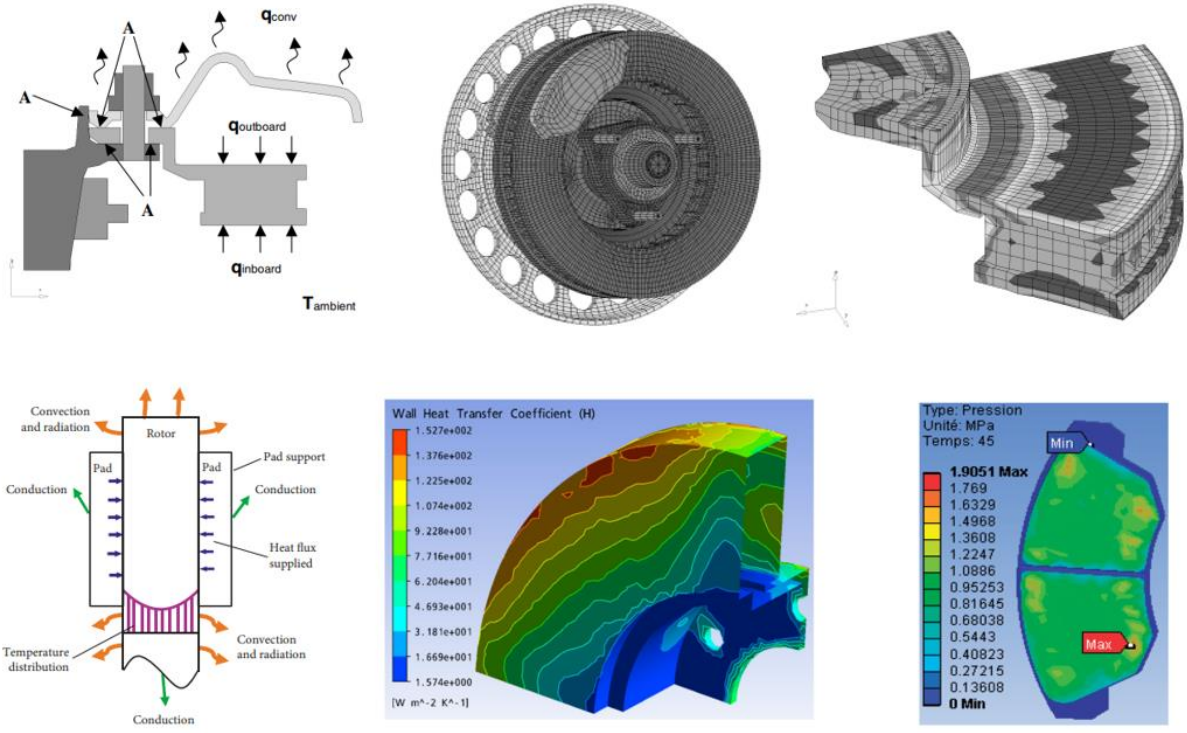

Figure 20 Braking system FEA models from literature. U. Left: Thermomechanical analysis, U. Middle: Mesh for complete brake disc, U. Left: Mesh and stress plot for brake rotor. L. Left: Thermal flow in Disc/Pad pair, L. Middle: Heat transfer coefficient in brake disc rotor, L. Left: Brake pad stress field

Apart from FEA providing static or dynamic tools, CFD can also be used to study cooling effects of different designs [33]. CFD simulations are demanding a lot of resources especially in complex studies of rotating bodies including components with small and critical dimensions. To improve heat transfer studies, CFD simulations are obligatory in parallel. Authors use CFD either coupled or de-coupled with thermal

simulations to acquire the best possible knowledge of each braking system, in cases where this is critical. This includes motorsport and hi-end production cars' design, where the braking events produce excessive heat which interrupts the aerodynamics of the car. Ducts are used to increase cooling and manage the airflow of the hot air stream. Few studies have been published on this matter, since most manufacturers disclose their innovations. Systems are simulated by moving wall boundaries which majorly affect the cooling performance, or by either multiple reference frame or rigid body motion. The former adds the forces by the rotation to the volumetric region of the disc, while the latter physically rotates the parts in the space. This is more accurate, yet computationally expensive, and requires exceptional description of the boundary conditions of the bodies.

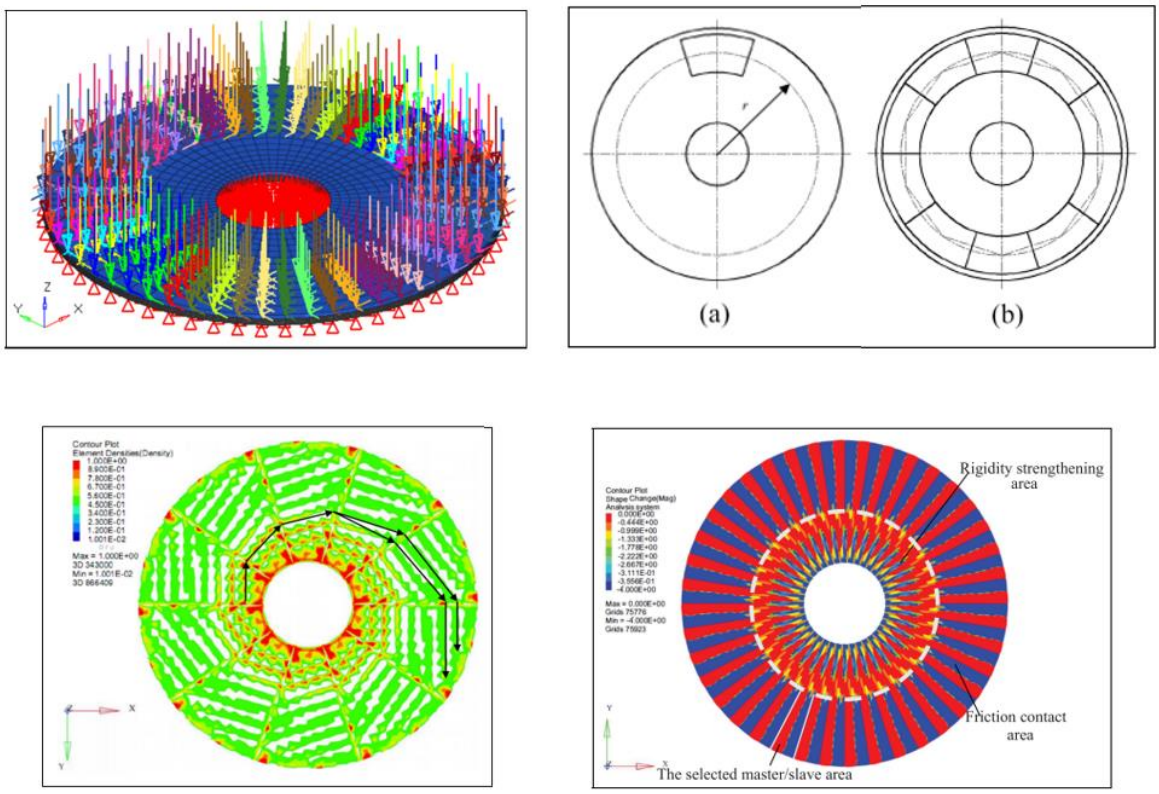

Figure 21 Jian Yin et Al [31], equivalent moving load method application for heavy duty brake disc optimization.
U. Left: FEM of internal structure, U. Right: Equivalent moving load method characterization
L. Left: Density of optimized internal structure, L. Right: Optimized result

Based on the complicated nature of this system, CFD is used for specific operations when examining specific sections of the disc. C Preda et Al [34] studied the contribution of the vane shape in cooling effect. I. GÜLERYÜZ [35] studied the vane shape in relation to the cooling behavior for heavy-duty vehicles. A. Lindgren [36] wrote his thesis on improving the brake cooling brake duct for a hyper-car braking application using CFD. A. Vdvoin et Al [37] depict the challenges of accurately simulating both airflow and thermal effects of the braking system. The interactions of the wheel flow were examined by C. Cravero [38] et Al, which also studied the flow of racing car's braking system along with thermal analysis [39]. In their paper, they use a model consisted of 45 million cells of high quality ratio to capture the streamlines inside the wheel and produce the temperature map of the composite brake disc. J. Campbell-Brenna [40] also studied

the heat dissipation of different vane designs, with a simpler model focused on the brake disc. Many coupled approaches are used for combining heat transfer mechanisms with the results of CFD iterations and vice versa [37,41-43]. The coupling of the two systems allows for a more accurate characterization of the disc's state. A. Vdovin provided the model shown in figure 22 which generates the heat transfer coefficients based on CFD velocities which are fed to their thermal code that calculates the temperature field. This field is then returning to the CFD solver to recalculate the flow and the coefficients needed. In their study, they validated the model by experiment with relatively small deviations, considering the complexity of the system.

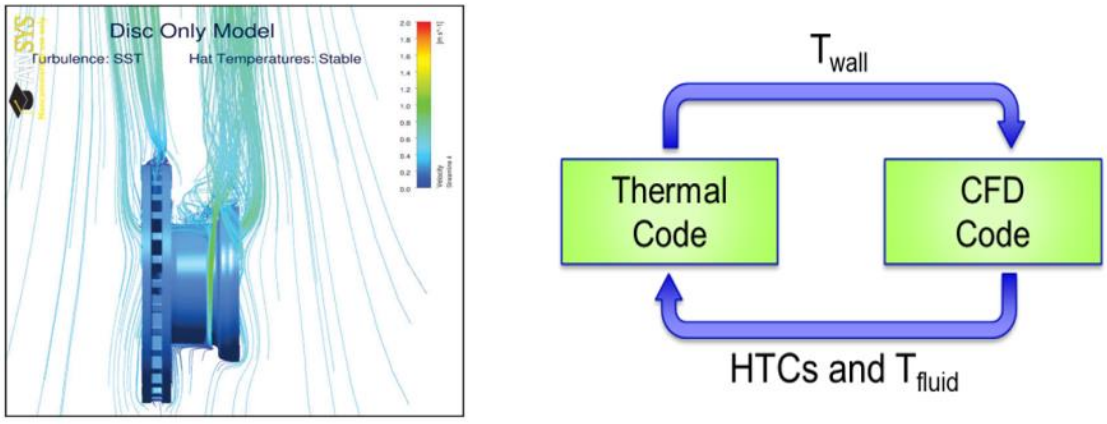

Figure 22 CFD Concepts and examples.
Left: CFD thermal model for brake disc and bel [33], Right: Simplified example of a coupling process [29]

2.4 Wear Models

Simulations are also used to analyze and predict wear of the pad and disc using FEA simulations on the contact area. Wear is a significant factor in the system's stability as non-uniform wear can lead to instabilities and judder, while some amount is desirable. As per A. AbuBakar and H. Ouyang, [44], the rough surfaces later become smoother as wear progresses. According to section 2.2 this can be explained based on the nature of asperities that rapidly become smoother after the initial braking, and then slowly degrade. In their model, AbuBakar and Ouyang used Rhee's formula of wear:

$$\Delta h = kP^a(\Omega)^b t^c$$

where h is the wear displacement, P the normal contact pressure, Ω the rotational disc speed (rad/s), r the pad mean radius (m) and a, b and c are all constants which remain to be determined. Other studies also use this formula [45-47]. For each step, the wear displacements are calculated for each node. The nodes' coordinates are adjusted in the axial direction and the process continues until the desired time. Increased wear is noted on the outside part of the pad, and even more so in the leading part of the pad as it touches the disc. As time passes, their model showed that the area of contact greatly increases, which as per 2.2 improves friction. A. Söderberg et Al. [48] used Archard's law assuming a proportional wear rate to the normal pressure and velocity at each point. Similarly, the outer part of the pad was worn more, due to the increased force applied as area increases towards the outer diameter of the disc.

G. Ostermeyer [49] created an even more localized model based on Cellular Automation. The model estimates the size and properties of asperities and particles trapped in the contact surface and alters their respective size through iterations. The model is studying the meso-scale of the feature at the size of the particles involved. The contact area is represented by a grid of rectangular shaped elements, which are given discrete height values, which change through each iteration. Ostermeyer's model can be used to predict the evolution of the patches formed in the surface of the brake disc through time, and generate a basic idea of the material interaction used in each application.

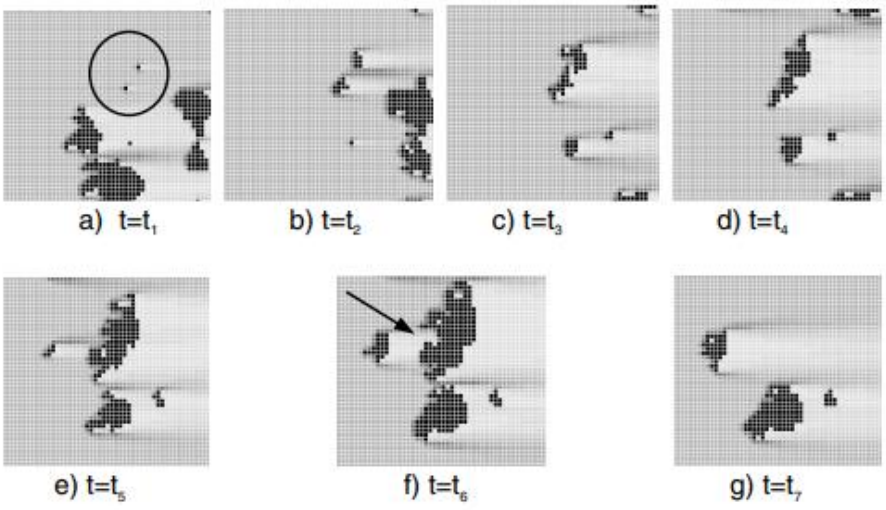

Figure 23 Cellular Automata model calculations through time [6]

2.5 Scope of this Thesis According to Literature Review

So far, the nature of braking systems, and materials used has been presented. Various models have been described from the engineering world regarding different aspects of the braking event, with the focus of these model varying, depending on the aim of each study. Some researchers try to improve the contact recognition and deliver accurate predictions of CoFs and friction forces, and others focus on a bigger scale, such as total wear, vibrations and thermal effects. Liu et Al. [50] experimented with the opposite problem to decrease lubrication resistance. After simulations and experiments they state that dimples can be used to lower the total friction in lubrication films but the optimal geometry and density of the pattern relies on the working conditions and the rotational speed of the parts. Similar proposals have been published by Greiner et A.l [51] who used bio-inspired patterns to alter sliding friction. Chen et Al. [52] utilized different shapes and patterns in wet clutches and noted a pressure field change as they applied different geometries, sizes and densities of features.

The current thesis is based on those observations, and transfers the initial idea to the braking world, in the attempt to increase braking efficiency by adding textured surfaces onto the braking discs. By introducing textured patterns to the area of contact, bending of the components is produced in addition to traditional shear. The normal stresses due to bending are transformed into an additional resisting force to the disc, increasing the total drag force. The first step of this thesis is proving the aforementioned assumption by testing deferent surface patterns on an FEA tool. Different surface features will be examined, aiming to the proof of the idea, which can be the basis for future observations and practical applications. The concept applies to racing and motorsport applications where increased braking momentum can improve the overall performance. On the other hand, this is not desirable in conventional vehicles as components will suffer from wear if friction increases further. By proving a theoretical concept this thesis is then focusing on additional experimental proof to support the findings of FEA analysis. The final part of this thesis is the design of a custom testing rig to further prolong investigation into the future by testing the concept using disc on disc experiments in an altogether economic manner.

Chapter 3 Development of the FEA model

In this chapter, the development of the FEA model using ANSYS Mechanical will be described in detail, from the initial setup up to the creation of an effective tool for comparing different geometries. The employed geometries were initially generated in ANSYS Designer and afterwards in SolidWorks 3D, allowing for finer parametrization of the features being studied. The procedures described in this chapter contain the initial stages of the primitive model, which allowed the revision of the approach used in order to develop a reliable model.

After introducing the bending stresses, the aforementioned attempts to provide an improved understanding of the tribological properties. Resolving the initial convergence challenges caused by the relative movement of the bodies in the model enables the use of a symmetry-based consideration that lowers the degrees of freedom and hence the error. The mesh of the bodies in contact and the stiffness of the two bodies are thoroughly examined since they have a major impact on the accuracy of the results.

The model is then used to assess a range of elements from both the quantitative and qualitative perspectives of the design in its final form. In an optimization procedure, the number and shape of various bumps are altered to extract the maximum amount of information possible while taking computation time into consideration.

Finally, utilizing a consistent mesh and identical input parameters for each design, the results of the finalized models for each geometry are displayed and contrasted.

3.1 Simulation Model Setup

In order to provide sufficient data to back up the hypothesis given by this thesis concept, FEA was chosen as the method to model the subjects. Using static simulations, the bodies in contact can accurately be represented and the contact conditions can be parametrized for different inputs. Once the idea of the model is finalized, the setup determines the accuracy of the final results. Models of poor quality can be affected by the discretization of the bodies involved, or the tested conditions, something that should be avoided. A good model on the other hand, recreates the same results for the same inputs, and presents similar behavior when testing different conditions. For this reason, the setup phase of the model is the most crucial.

The steps of the simulation's setup are as follows:

- Initial approach
- Improvements on the approach
- Final model and conversion to Symmetry model
- Definition of contact stiffness correction
- Mesh Characteristics.

The key to evaluating the various models is to follow this procedure, resulting in results deemed satisfactory with consistent model behavior and proper body contact. Given an acceptable model, the mesh determines the model's computational efficiency and accuracy, which, given hardware limitations, must also take geometric characteristics into account. Each setup phase will be described separately from the others. For instance, meshing or contact parameters are not explained during the "initial approach" phase, but on a later entity.

3.1.1 Initial Approach

When it comes to modeling brake discs, the first decision is in regard of the phenomenon under examination. Either it is stress, fatigue, vibrations, thermal stresses, friction, or wear, the model must be specific to the property under our scope. The aim of the study is to extract the tangential force Fx generated in each scenario based on the conditions and inputs of the system. Our approach is a parametric one regarding the improvement of the friction coefficient and its general response to geometry variations. The pad-to-disc contact is the point of interest, while thermal, vibration, and squeal metrics are neglected.

Having this in mind, the model is based on the assumption of a linear disc section in direct contact with the pad and having an adequate contact area. The brake pad body has equal length and supported by the backplate body. The bodies' materials have the actual properties of the materials as well as the same thicknesses used in the actual assembly of the car. Although the pad in reality is smaller and thus would pivot around its symmetry plane after touching a wavy surface, the proposed model eliminates this effect so that the results are consistent over time. This is achieved by considering the pad of adequate length, touching almost the entire disc body. Furthermore, in real life, given the relative stiffness of the touching materials as well as the external support of the pad by the backplate, the pivot rate would be small and balanced by the local deformation of the pad surface.

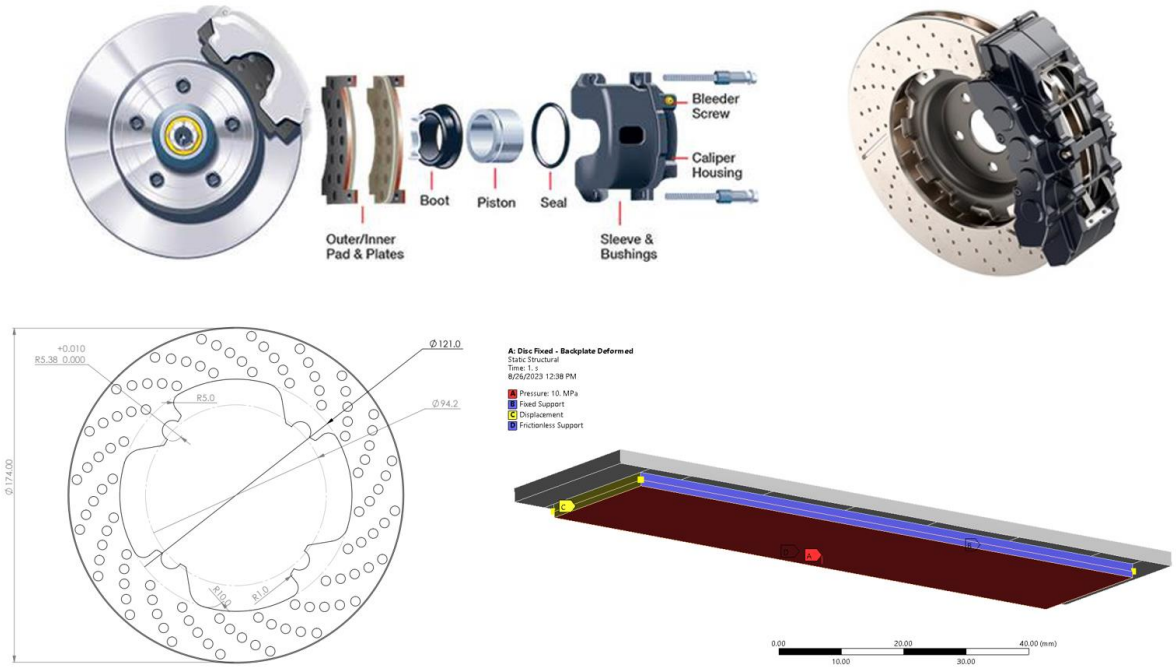

Figure 24 Brake disc's designs and simulation model design.
U. Left: Exploded view of Disc assembly, U. Right: Brake disc and caliper with 4 pistons
L. Left: Prom Racing FS brake disc 2021, L. Right: Thesis ANSYS FEM model of brake disc

In every automotive braking system, brake pads act in sets of 2, one on either side of the disc. In this way rotating moments applied on the disc around the x-axis are zero. The first modeling approach considers the free face of the disc fixed, representing the symmetry of its half plane, for simplification. To restrict the lateral movement of the pad and backplate, they are bonded with each other and a frictionless type of fixture is applied to their side faces, as to allow vertical but not lateral movement. The inputs in the system are the velocity of the free face of the backplate and the pressure applied to it. This is equivalent to the pressure of the brake fluid transferred by the piston(s) to the backplate. The force reaction in the Y direction (perpendicular to the contact) can be calculated as the product of pressure applied and the area of the face of the backplate.

The materials for the disc and pad are chosen so that their mechanical properties lay as close as possible to the real attributes of a Formula Student brake system. Grey Cast Iron steel is chosen for both the disc and backplate. The major factors influencing our study are the Young's modulus and the Poisson's ratio, as they define the Shear Modulus, and the overall behavior of the bodies. The specific roughness for each surface in the real case is also neglected, in an attempt to create a reliable first model before further improvements. For the frictional contact, friction coefficient is given a value corresponding to the upper limit achievable, and is then utilized to produce the tangential force based on the nominal load. For isotropic and homogenous materials:

$$E = 2G(1 + \nu)$$

For the brake pad, material is unknown as the manufacturer discloses the datasheet, thus the research refers to the literature, where Young's Modulus and Poisson's Ratio are usually derived from experiments. The

brake pad used is an alloy of ceramics, metals, plastics, and resin, coated with protective films, with presence of organic components. The actual value of E is not clearly defined as the brake pad is not a homogenous alloy with a clear structure; rather, dissimilar regions can be observed within its structure. In this paper, the Pad material properties are attributed with a fixed value after cross-referencing values used or found in other papers, and they can be seen in table 1.

In a well-defined static analysis, the inputs (force, moment, and displacement) can be chosen by the author, as long as the fixtures' placements allow for constant reactions in equivalent scenarios. In this sense, for practical reasons the brake disc is fixed to represent the symmetry. Although in reality the disc is rotating, in FEA analysis the perspective can be chosen based on any coordinate system. Considering the disc as fixed, enables the allocation of pressure and velocity on the back plate, equivalent to the real scenario. As seen from the disc, the brake pad/backplate is in relative motion, hence the displacement input on the backplate surface.

The initial model considers the simultaneous application of both the pressure and the displacement Y. After careful evaluation of different geometries, the model was weak in convergence, and the results were inconsistent with each other. Braking can be considered as two independent actions: pressing and rotary displacement. The pressing part is produced by a hydraulic system operating in a range of 30–90 Bars for small racing vehicles and 50–120 Bars for Formula 1 cars, and the pads move approximately 1mm before complete contact. The enormous pressure applied enables the travel of this distance almost immediately, and no considerate rotary displacement has been completed during that time. After noticing this, the first upgrade to the initial model is the separation of the two actions into two time steps.

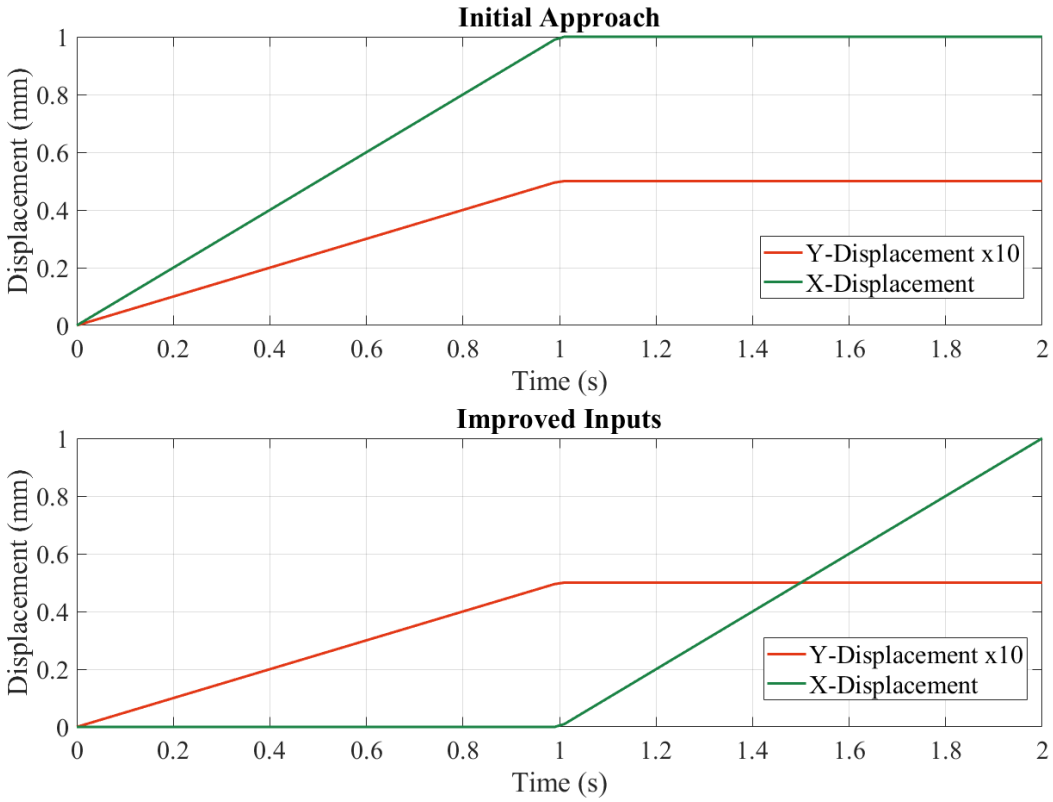

Figure 25 Input parameters for structural analysis. Upper: Initial approach, Lower, Improved model

The analysis chosen to implement this change uses the "substeps" method, with the two steps being independent of each other. The first step aims at the initial touching of the friction surfaces, while the second one aims at expressing their relative motion with constant pressure applied. Ramp functions are used for both pressure and X displacement, and the number of substeps in each step is found after fine-tuning the model to an adequate convergence. The accuracy of the model is confirmed by acquiring the same results using different mesh sizes and methods for the same scenarios, something that was not achievable using the simultaneous approach.

This approach generated the first tentative proof of the assumption of friction coefficient variation based on the geometrical shape of the brake disc. Unfortunately, the FEA model is not in accordance with the actual phenomenon occurring during a braking event, due to the considerations taken and the size of the objects. One additional issue at this point is the inaccuracy of the deformed state of the bodies involved, by the assumption of the pressure input. Using this method, the DoF of the backplate allow for excessive deformations across the points of the body, and pad and backplate are deforming in an attempt to recreate the negative geometrical pattern of the disc. Although a reaction force must counteract the pressure applied, this force is not constant across the span of the surface of each body. This is due to the ability of the pressure to be expressed by the integral of dFy over dA.

$$P = \int_A dFy$$

In this sense, areas with greater freedom of movement (top of the bump) are allocated with less force, while the areas near the bottom of the bump are highly compressed, increasing the reaction force in the total area. It is evident that the backplate cannot behave in this manner, especially at high speeds, and its bonding area to the pad evidently creates strong reactions to these deformations. The model has been positively upgraded by the displacement application, allowing it to examine boundary conditions in detail. The application point of the displacement was examined in depth. The concept is to create a realistic FEA model without inconsistencies near any body's edges. For this reason, the Brake disc is designed to be slightly bigger in both the z and x directions. The following scenarios for the displacement input application were examined:

- Pad free surface – Face selection
- Pad free surface – Longitudinal sides (x-axis parallel)
- Pad free surface – 4 Nodes
- Pad rear surface – Face selection

After FEA analysis, the free surface/face selection is the best to apply the displacement where results lack stress concentration near the edges. Severe internal bending moments caused by the fixtures are also avoided in contrast to other concepts. The elements in this concept seem to work in the best way along the thickness. Although changing the input application location improves the model, the model is far from perfect. One unsolved issue is generated by the expansion of the material in the lateral directions due to the compression of the brake pad in the vertical direction. The frictionless boundary condition does not allow this, yet it cannot be disabled as the model will not be properly constrained. To overcome the problem, the bodies are cut in half using the XY parallel plane, and a symmetric boundary condition is applied to all bodies perpendicular to the z-axis. In this sense, the z movement of the bodies is restricted to their elastic ability, and the frictionless condition is not part of the model any more.

The symmetrical concept is shown to be closer to reality, and results also indicated this in many occasions not presented in the current paper. The lateral expansion is still present, but the consistency of the reactions is improved. FEA models tend to exploit any non-defined or partially defined boundaries, as deformation of the bodies is reduced. With the symmetrical approach, the XY plane is in contact with one side of the bodies, and the issue is mitigated.

3.1.2 Final Model and Conversion to Symmetry Model

To fix the issue reported in the last section, the inputs of the model must be reconsidered. During the brake actuation process, the piston is traveling inside its housing coaxially with its centerline axis, pressing the backplate vertically. The backplate then drives the pad in the same direction, which comes into contact with the disc. The motion occurs regardless of the geometry of the disc due to the geometrical constraints of the piston housing and the piston's external diameter, and in some occasions, the backplate is also restricted to excessive lateral movement and rotation. Given the observations in 3.1.1:

a) The free face of the backplate in the model must be moving in the Y direction with constant displacement across each point of the surface.
b) The pressure on the piston flat surface is not constant

In reality, for flat discs, a 3-point bending effect is created when the piston acts on the backplate. The piston applies a force that is reacted by the sum of the local pressures on the disc. Directly above the piston, pressure is higher, while on the sides of the backplate that lie outside of the contact with the piston, pressure decreases. Furthermore, due to inertia, part deforms more. Of course, the stiffness and the relative position of the backplate to the pistons are designed to mitigate that effect, and it can be considered insignificant in our model. The first improvement to the model is based on the application of vertical displacement on the free side of the backplate instead of pressure. This means that the reaction force will vary in the fixture of the disc. If the amplitude of the feature used is greater than the displacement δY applied, areas exist were no contact takes place, something that should in general be avoided. This observation plays a significant role in the parametric behavior of each design, as seen in Chapter 3.3. Finally, the stress and pressure are also expected to vary in different areas due to changes in material compression.

Using this method, the relative stiffness of the three bodies has a significant influence on the relative compression of their elements. The softer the material, the greater the deformation and energy storage. In order to reduce the complexity of the model, the deformation of the backplate was examined closely to determine if its use in the model is necessary. The three bodies are modeled as springs, and a compression load F is applied. The equivalent spring constant K_{eq} can be acquired by:

$$K_{eq} = \frac{K_1K_2 + K_1K_3 + K_2K_3}{K_1K_2K_3}$$

In the case of composite bodies, the K constant is not equal to the Young's modulus, as thinner bodies are stiffer in compression perpendicular to their width, while thicker ones allow for greater proportional deformation, as in the case of springs with equal dimensions except for the length. Given that K links elongation and applied force, the stiffness can be calculated:

$$\sigma = E\varepsilon$$

$$\frac{F}{A} = E\frac{\Delta l}{l_0} \rightarrow F = \frac{EA}{l_0}\Delta l \rightarrow F = K_i\, x$$

Where K_i is the equivalent constant of the material given its original thickness l_0, along with the Young's Modulus and the Area of the force application, and x is the relative compression that the body is subjected to. Substituting the average data for the FS car, the attributes of each material are shown in table 1.

Application	Material	Young's Modulus (GPa)	Poisson's Ratio	Design Thickness (mm)	Stiffness (N/mm)
Brake Disc	Cast Iron Steel	110.0	0.30	2.3	47826
Composite Pad	NAO Pad	1.6	0.27	3.5	457
Backplate	Cast Iron Steel	110.0	0.30	2.3	44000

Table 1 Material properties for structural analysis in ANSYS Mechanical

The Pad is softer by two factors compared to the other two bodies. Considering that two springs in series are closer to the value of the softer spring, the bonded pair can be simplified by ignoring the much stiffer backplate. The percentage stiffness difference for a simpler model ignoring the 3rd body is found:

$$K_{eq} = \frac{K_1 + K_2}{K_1 K_2}$$

The compression of the three bodies (assuming flat geometries) is calculated based on the free body diagrams and the stiffness calculated. To maintain equilibrium, the external force must be transferred through the nodes. Considering each node based on Newton's 3rd law:

$$F_i = F_i'$$

$$K_1 x_1 = F$$

$$K_2(x_2 - x_1) = F$$

$$K_3(x_3 - x_2) = F$$

$$K_{eq} x_{eq} = F$$

The equations are solved in matrix form using the values from table 1:

$$\begin{bmatrix} K_1 & 0 & 0 \\ -K_2 & K_2 & 0 \\ 0 & -K_3 & K_3 \end{bmatrix} \begin{bmatrix} x_1 \\ x_2 \\ x_3 \end{bmatrix} = \begin{bmatrix} F \\ F \\ F \end{bmatrix}$$

Or for the simplified system:

$$\begin{bmatrix} K_1 & 0 \\ -K_2 & K_2 \end{bmatrix} \begin{bmatrix} x_1 \\ x_2 \end{bmatrix} = \begin{bmatrix} 0 \\ 0 \end{bmatrix}$$

And the compression of each element can be written in matrix form.

$$\begin{bmatrix} \delta l_{disk} \\ \delta l_{pad} \\ \delta l_{backplate} \\ \delta l_{eq} \end{bmatrix} = \begin{bmatrix} x_1 \\ x_2 - x_1 \\ x_3 - x_2 \\ x_3 \end{bmatrix}$$

$$\begin{bmatrix} \delta l_{disk} \\ \delta l_{pad} \\ \delta l_{eq} \end{bmatrix} = \begin{bmatrix} x_1 \\ x_2 - x_1 \\ x_2 \end{bmatrix}$$

The solution of the systems is found in the table 2, showing the relative difference between the two concepts.

	3 Bodies	2 Bodies	% Difference
Spring Equivalent	448.2	452.8	0.01
δl_1 (mm/1kN)	0.021	0.021	0.000
δl_2 (mm/1kN)	2.188	2.188	0.000
δl_3 (mm/1kN)	0.023	-	-
δl_eq (mm/1k0N)	2.231	2.209	-0.010

Table 2 Comparison of stiffness change for the models using 3 and 2 bodies respectively

Each spring added in series is only contributing negatively to the total stiffness of the system. Considering only the spring with the fixed end, its deformation is calculated by its own stiffness and the force applied (equal through each node). In this sense, the x_2 deformation derives from the x_1 and the stiffness of the second spring, and so on. In this model displacement is the input and both systems must be compressed by the same value. This means that the 1.03% difference must be compensated by the other two springs proportionally. After simulating the two models, the difference in force lies within 1.5%. The simpler model is adequate for the purpose of this paper and shall therefore be used if it is also verified by the FEA model.

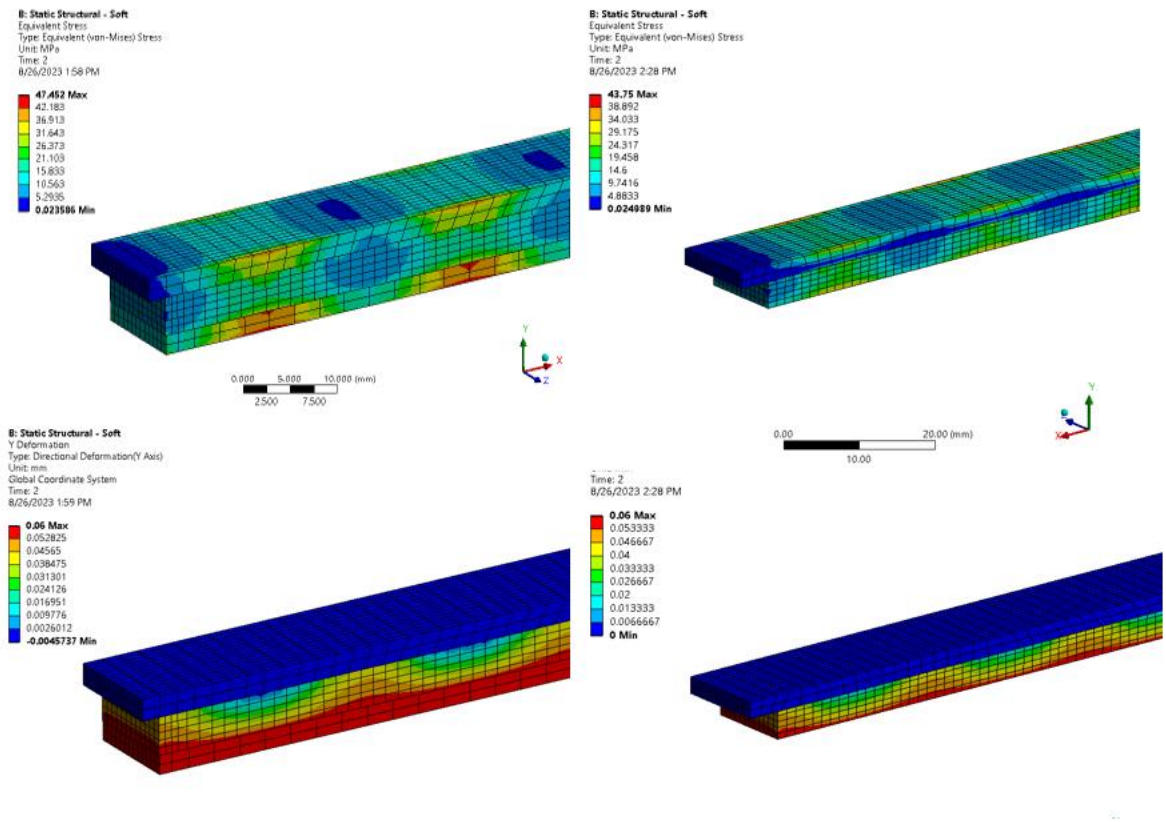

Figure 26 Results of structural analysis for model with 3 and 2 bodies.
U. Left: Model 3 bodies – Equivalent Stress, U. Right Model 2 bodies – Equivalent Stress.
L. Left: Model 3 bodies – Y Deformation, U. Right Model 2 bodies – Y Deformation

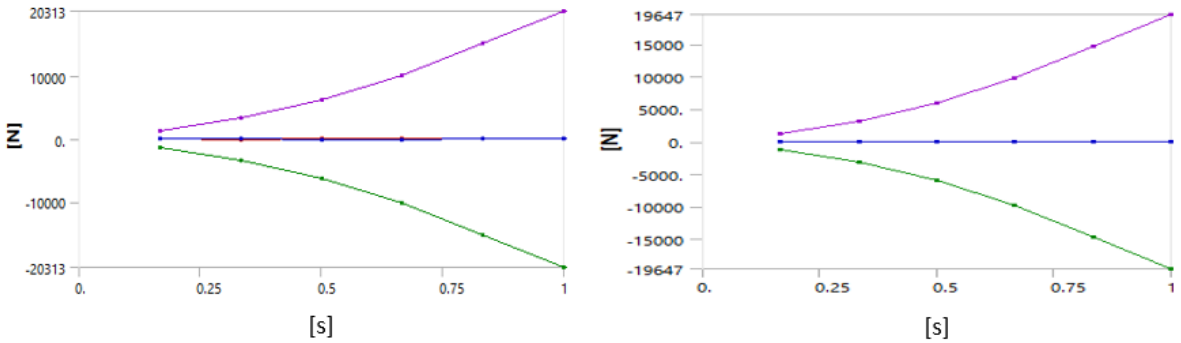

Figure 27 Force reaction for model with 3 and 2 bodies. Purple line represents backplate, blue the pad, and green the fixture on the disc side

3.1.3 Contact Details and Analysis Settings

After simplifying the model to its most efficient and realistic form, the contact between the bodies is examined in depth in this section. Contact analysis results differ based on the way the simulation environment handles the calculations. The master/slave definition is common across many platforms and plays a key role in the efficiency of the system. In this section terminology derives from the ANSYS Mechanical environment. The contact in this case is modeled as asymmetric and the pad is the contact body acquiring finer mesh, being the softest. The contact points are detected as the points of the pad that come into contact with the surface of the disc. This allows for better results, both arithmetical and visual. The formulation is kept as Augmented Lagrange, which, after iterations, was found to converge systematically with reasonable computational time. Apart from that, it was found that adding a force convergence control and a displacement convergence control improved the accuracy of the results for different meshing parameters.

The major parameter influencing of fine-tuning the model was the choice of the Normal Stiffness Factor (NSF) parameter. This parameter enables a better description of the problem to the software specific to each application, the aim of the model, and the geometries and materials involved. For pure bending problems with similar materials involved, the value is kept low (0.05–0.3). For problems with different stiffness of materials involved or where penetration is restrictive, the factor is increased. This factor can only be found through an iterative procedure, as every application is different from each other. In the model, penetration must be kept extremely low to avoid implications for the width of the feature, hence the NSF is optimized for this reason. Penetration values below 5% of the amplitude value of the feature were the aim of the optimization to avoid a severe influence on the results. Penetration is not something that should be inexistent and may even be desirable in some cases in the analysis. For example, sharp edges in the features introduce great stress concentration, which can be avoided with logical values of penetration. This is evident in rectangular patterns, where the Normal Stiffness Factor limits the excessive interaction of the two volumes yet allows for realistic expression of the penetration. In real-world applications, sharp corners are always manufactured with small radii values and are then worn down from the interaction between bodies involved. In this sense, any penetration present must be within logical limits so as to represent the expected wear of the disc without overpassing it. In the figure, penetration values and shapes for different values of the NSF.

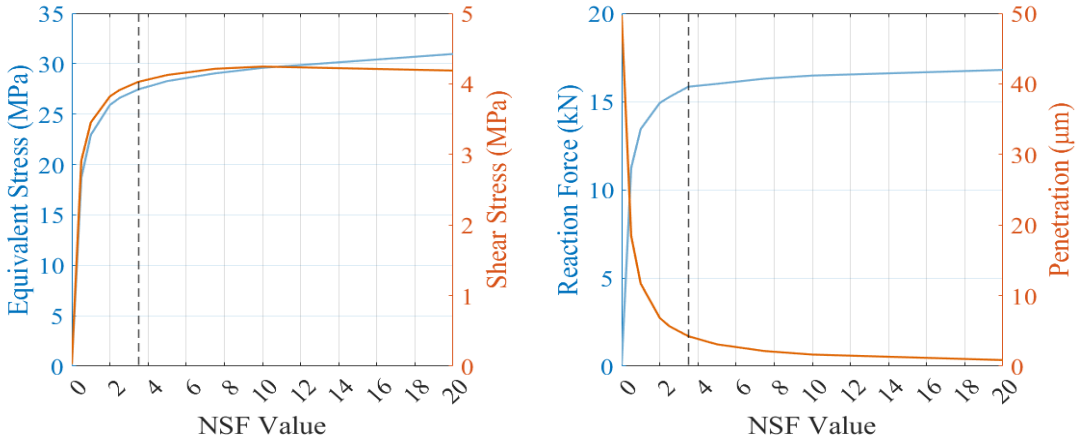

Figure 28 Model behavior for different NSF Values.

Left: Equivalent & Shear Stress vs NSF, Right: Reaction Force and Penetration vs NSF

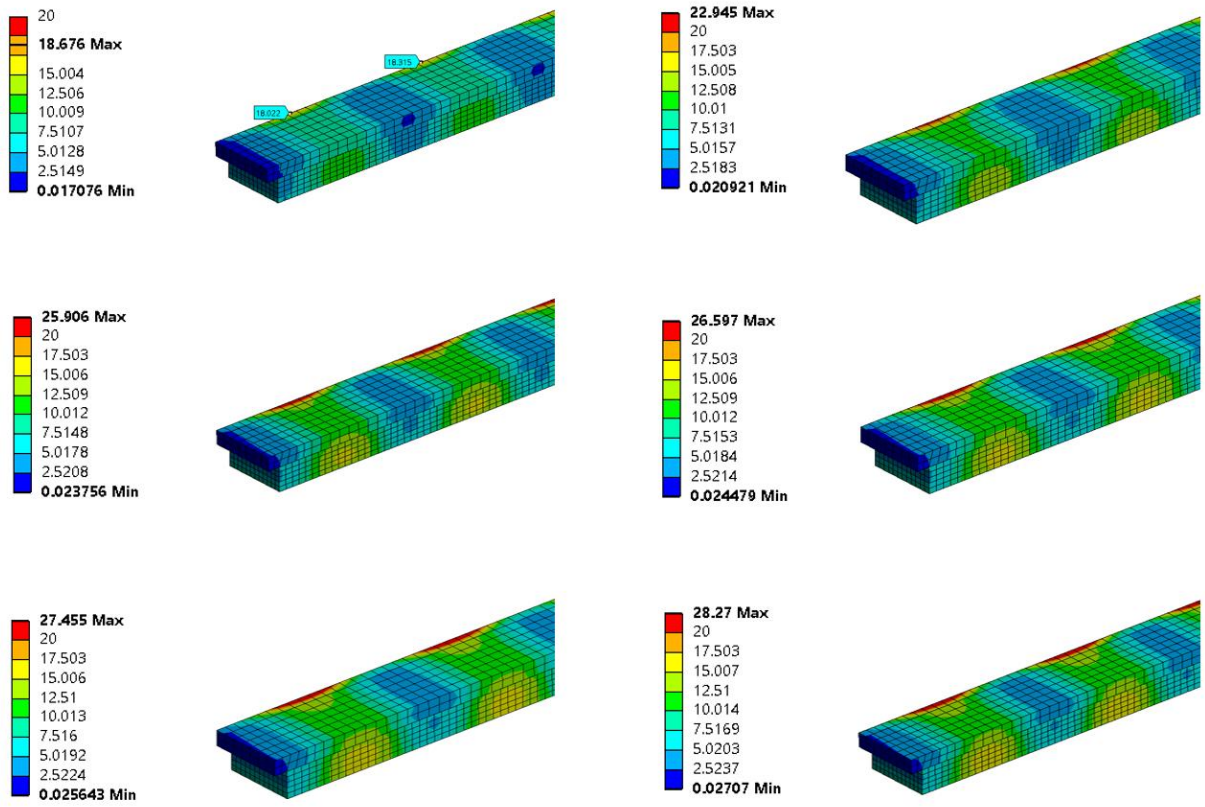

Figure 29 Stress plots for different NSF Values
NSF value from left to right and top to bottom: 0.5 – 1.0 – 2.0 – 2.5 – 3.5- 5.0

The final value of 3.5 was used in the analysis, as results were within the target penetration values, and the brake pads deformed naturally as seen in figure 30 this value is approximating very good the actual phenomenon, allowing for the desirable penetration value of maximum 10% of the feature amplitude. The features used in the plots had an amplitude of 0.035mm and the pad was displaced by 0.050mm, allowing for full contact. Stress is transferred also in a natural way through the elements, and convergence is good for different scenarios.

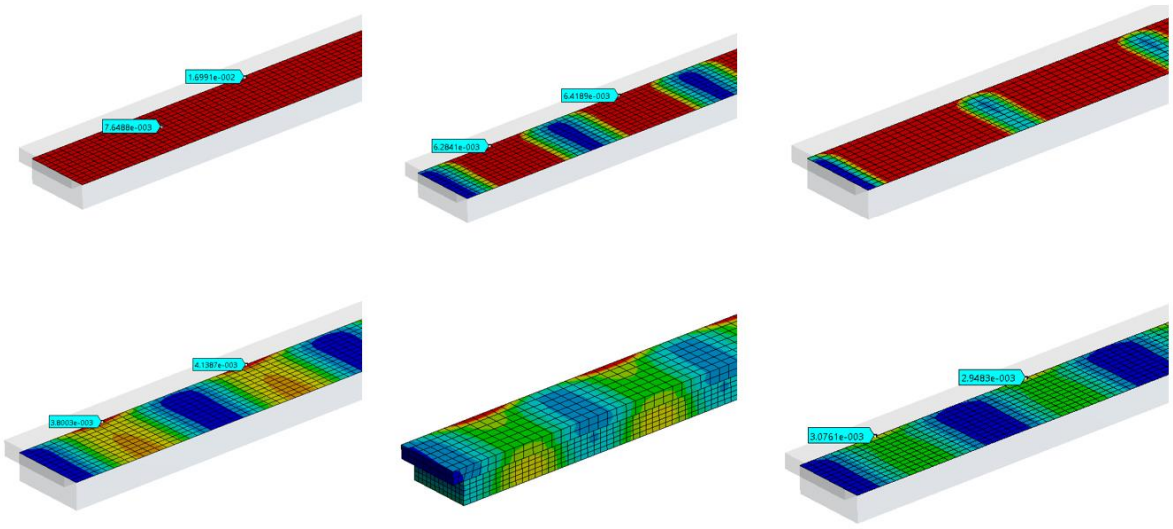

Figure 30 NSF Penetration plots for different NSF values
NSF value from left to right and top to bottom: 0.5 – 1.0 – 2.0 – 2.5 – 3.5- 5.0

3.1.4 Meshing

The final process of the setup definition is in regard to the mesh of the bodies involved. Mesh is the discretization of the bodies through space, and may vary in quality and size. Smaller elements increase accuracy and computational time, and good quality is represented by consistent results, minimal to none stress concentration areas and good boundary conditions' adaptation. Bodies with one dimension significantly longer than the others are classified as thin plates. In thin plate FEA, enough elements must be provided through the body thickness to enable the accurate description of the body deformation. In this application, the pad mesh must be chosen carefully, as it the pad is subjected to greater deformations, and layer thickness of the mesh is critical. In this iterative part of the model's definition, the following properties are examined:

- Vertical elements of Pad & Disc
- Width (z parallel) elements of Pad & Disc
- Size (x parallel) of Pad & Disc
- Mesh control of the features to improve their description.

The aspect ratio of the elements has a big impact on the attributes of the model. The target was set to a 50% ratio whenever possible, as this improves the deformation ability in every direction. Always considering the x direction as the scope of the research (the geometrical features are changing along the x-axis), long elements are unable to interpret the geometry of the disc, while short, narrow elements highly increase computational time and may be subjected to internal shear forces. The multizone method was used, with a skewness target of maximum 0.3. Target quality is set at 0.95, Smoothing to Medium, and Transition to Slow.

Finer meshing results in better solutions with longer computational times. In order to find the best element size for the disc, examine the quality of the mesh over the variations in its length. Given the long aspect ratio of the features, only 2 elements are used in the vertical direction and a size of 1.0–1.2 along the x direction. Seven elements across the width were used to aim for a better aspect ratio of the elements. In specific cases, mesh control was applied near the feature to improve disc-pad contact. The elements of the pad were proven to have greater influence over the result of the simulation, it being the softer. To determine the best size, the convergence time was examined for elements in the range [0.2, 2] mm. The computational time follows an exponential decrease by the size of the elements, while the convergence is logarithmic.

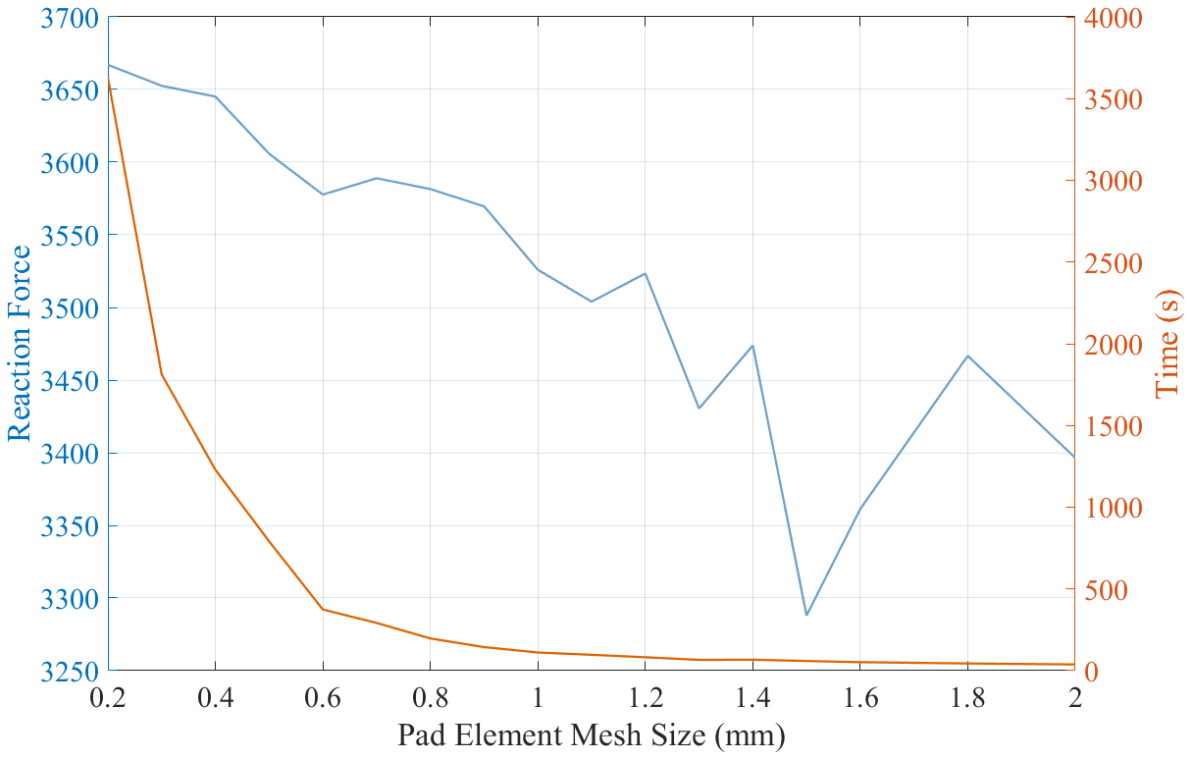

Figure 31 Reaction Force and Time convergence of the model vs Pad Element Size.

At this stage, the model setup is finished and all the critical parameters are considered to set a satisfactory basis of evaluating the different geometrical patterns designed. The final model has good computational time, very good convergence, and can be applied to any geometry with little to no user changes, and low geometrical sensitivity. Stiffness and boundary conditions are taken into account extracting smooth results without excessive stress concentration or penetration. The model is simplified to the maximum amount to reduce complexity without compromising equivalency to the full model, which would consider also the backplate and the pistons. Yet as already mentioned, the scope of this thesis lies in the relative evaluation of different geometries in a parametric way to confirm the proof of concept. The exact values for brake simulations are not the key feature of this study, as that would be very limiting to a specific application rather than concluding to a general idea. Considering all of the above, the model is satisfactory to use, and the comparison of the models will be presented in the next sections.

3.2 Parametric Investigation

Once the FEA model is set, the different geometrical features are designed to create the so-called "bumps" and “peaks” across the surface of the disc. The total number of different bumps forms the texture of the surface and each kind of bump is characterized by its own features. Features are divided into shape, size, aspect ratio, orientation, periodicity, and hierarchy of arrangement in the case of multiple kinds of features used in the same disc. Based on the observations of Chapter 2.1, bumps are designed to have a consistent shape along the radius of the disc and are positioned at a relative angle $\Delta\theta$ from each other. Their size must be chosen to introduce only bending stresses to the pad, avoiding any critical phenomena such as side crushing of the material from sharp edges. For elements along the radius, the periodicity is limited by the angular span of each feature and the space between the next ones. Combined with the size and aspect ratio, the minimum length of each feature can be found. This study is qualitative and, according to 3.1, examines flat specimens, so the periodicity of features relies on the dimensions of the specific project, and is not directly equivalent any final design.

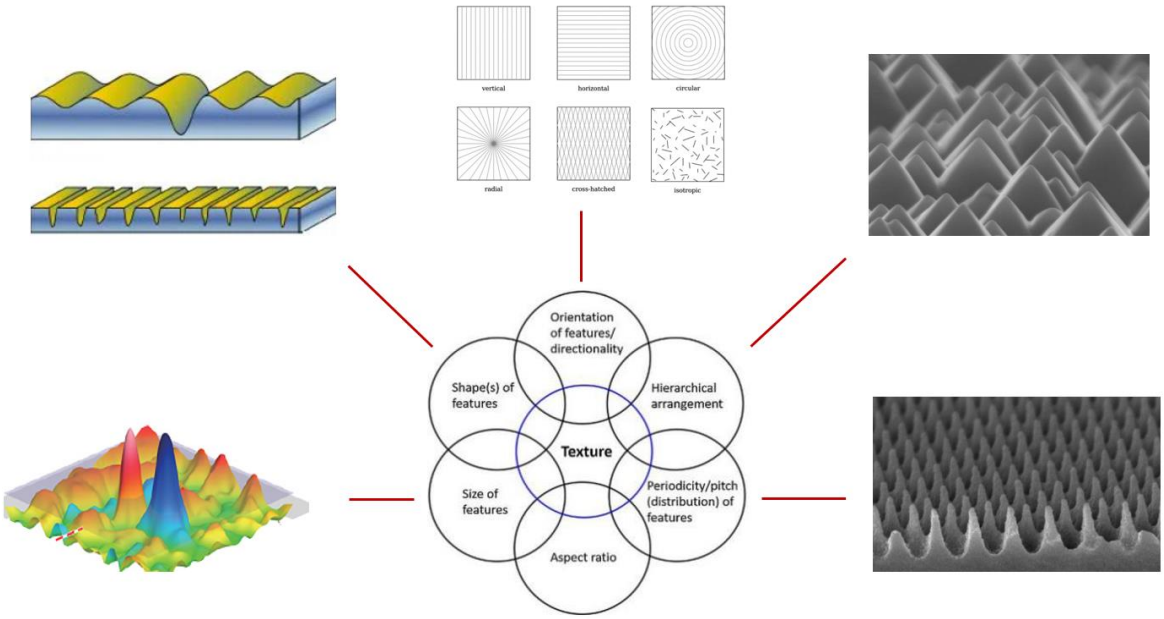

Figure 32 Different texture parameters to examine for Features used in simulations

Although an optimizing process would exploit every available geometrical pattern to extract the maximum profit, current research is also focusing on creating realistic models, not only a theoretical basis. Shape of features is restricted by manufacturing capabilities, both for the prototype test pieces and the real discs, and no examination of extremely complicated features was tested, as their manufacturability is poor. Traditional machining (milling and turning) cannot produce sharp edges and negative, and grinding techniques used to treat metallic components also suffer from the same incapability. Rectangular features are the most achievable, as only X-Y motion of the milling tool is required. Further improvements can make use of 3D machining to create smoother transitions and more intricate surface patterns. Specimens may be manufactured utilizing EDM machining, which is cost-effective for large production scales, or even DMLS Printing. Surface quality for the aforementioned techniques is usually poor, so surface treatment must be

undergone. Finishing steps within the machine can also improve surface quality, except for DMLS, where the layer height of the printing determines the quality.

Sharp corners and steep changes in bump height have by definition a bad impact on the behavior of the system, introducing vibrations and excessive stress and wear. The concept of the paper introduces normal stresses along with shear, something can be achieved exceptionally by establishing total contact between pad and disc throughout the feature. This contact is limited by the bending stiffness of the pad, which was examined in the previous chapter and must also be a considerable factor. I.e., frequent changes of the feature height and its second derivative are set to fail. The part of the bump that extrudes towards the pad is called the entry of the feature, while the part that restores the initial height (bottom of the bump) is the release of the feature. In this chapter, the effects of the following features will be investigated, corresponding to the entry and release of the used bumps:

1. Flat Disc
2. Sinusoidal Feature
3. Rectangular Feature
4. Wavy Feature
5. Ramp Feature
6. Ramp & Wavy Hybrid Feature
7. Double Amplitude Hybrid Feature

The characteristics of each feature can be observed in figure 33.

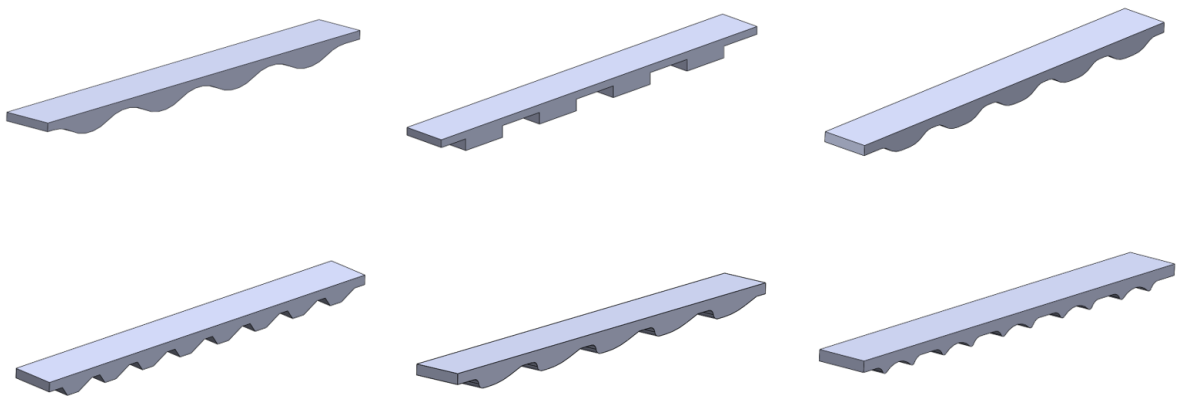

Figure 33 Different features to be examined in simulations, exaggerated amplitude of features for reference.

The discs' parametric investigation includes the design of the feature and the application of sets of different scenarios to each disc. All discs are subjected to two separate and independent y-direction displacements of 30 m, 40 m, and 50 m. It was decided to simulate the braking pressure applied by the pistons at a pressure of 50 bar, a typical value for FS applications. For this reason, specific values of displacement were tested that simulate close results to the expected value and include a wider range for better conclusions. To further understand the behavior of the features, each displacement is tested on 12 different amplitudes varying from

10 m to 100 m. Amplitudes greater than the maximum y-displacement are also evaluated in order to extract the qualitative response of the top of the bump. Cases with an amplitude smaller than the displacement represent total, or near total, contact between the two bodies and are indicative of the behavior of both the top and the bottom of the bump. The following subsections introduce some of the properties for each feature.

3.2.1 Flat Disc

The flat disc represents the common brake disc of all automotive braking systems. The disc surface is completely flat, as this non-featured disc is used to acquire a relative basis for later comparisons. Since no amplitude of the feature is present, data points are extracted for different y-displacements, which will be later interpolated based on the required normal force target. The products of this interpolation will be used for comparison with the other geometries to extract theoretical results.

3.2.2 Sinusoidal Feature

All the geometrical features are considered the projection cut of the area between a curve tangent to or coincident with the bottom surface of the Flat disc and that bottom surface. The sinusoidal feature is constructed by a series of sinus waves along the x-axis. This feature lacks flat surfaces as it is a constant curve. Reduced pad bending stresses are expected along the curvature of this feature, as there aren’t any steep grade changes. The lack of flat faces at the bottom of the feature is equivalent to smaller pressures, as most elements are not in maximum possible compression. Thus, greater displacements must be used to derive the same reactions as the other discs.

From a manufacturing perspective, the feature can be produced either by EDM, 5-axis Grinding, or 3D Milling. DMLS is not a good option since layer thickness values cannot capture the desired geometry of big curvatures near the end of the feature.

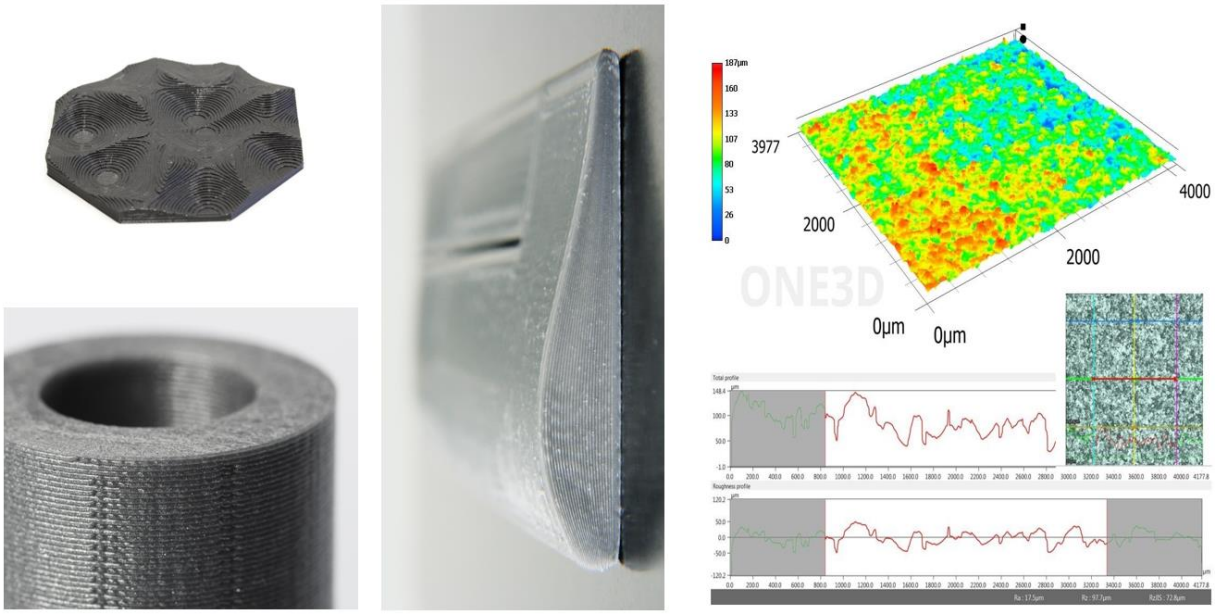

Figure 34 Surface imperfections of 3D printing manufacturing method

3.2.3 Rectangular Feature

The rectangular feature consists of a series of identical rectangular cuts. This feature is ideal for milling manufacturing as the tool can follow a simple XY plane motion to accurately capture the geometry. The biggest disadvantages of this feature are the stress concentration near the entry and the release of the bottom faces, which would increase the wear of the pad and produce vibrations in the system due to their non-linear nature.

For a given bending stiffness of the pad, the length near the vertical side face where the two bodies are not in contact can be calculated.

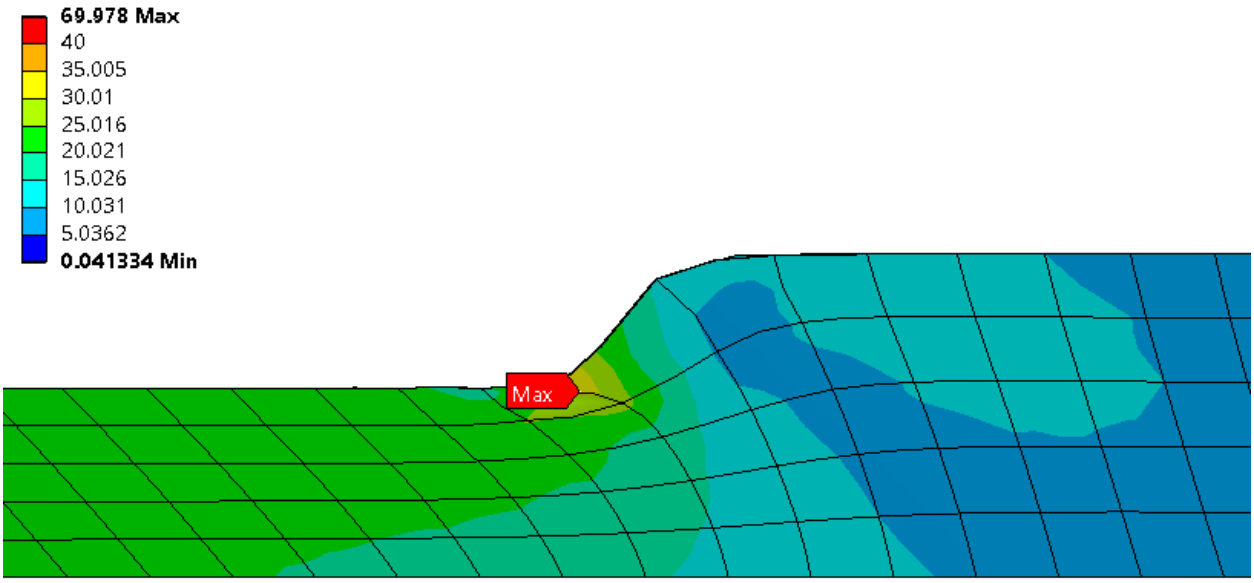

Figure 35 Stress concentration near the free edges of the rectangular feature. Magnification x45

3.2.4 Big Fillet Feature

Although the rectangular feature introduces many disadvantages compared to the sinusoidal one, the abrupt change in disc height also introduces great bending moments. This phenomenon can be exploited by introducing a double fillet to smooth the step between the two levels. Apart from the reduction of corner stresses, this adjustment allows smoother contact through the entire length of the disc, thus generating greater forces. In order to determine the correct fillet size, the grade of the pad material from the rectangular cases is examined and the geometry adjusted appropriately. The number of features and their length can also be evaluated using the Big Fillet feature. Apart from the amplitude check, designs with 4, 5, and 6 bumps were tested, which resulted in different force reactions. In theory, as the number of bumps increases, the instances of the brake pad being subjected to bending also increase, thus resulting in a higher CoF. This assumption is validated, as per Chapter 3.3.

3.2.5 Ramp Feature

Although the wavy geometry is a first improvement on the rectangle concept, areas near the start of the release of the bump are not exploited to their maximum capability. The inertia of the body does not allow for perfect contact at the point where the derivative of the grade of the curve changes. This is the steeper change in the geometry. To solve this issue, the bumps are redesigned using ramp features in the form of straight inclined lines, whose grade allows for smoother contact between the two bodies. Although the ramp feature introduces non-linear elements at the corners of each end, they do not greatly affect the model as some penetration is allowed, and the relative grade difference stops excessive stress concentration in the edges. This idea improves the release of the bump, yet it cannot match the wavy entry effect with changing grade along the curvature of the feature, leading in greater bending stresses.

3.2.6 Ramp & Wavy Hybrid Feature

Using the experience of the previous chapters, the feature is redesigned with wavy entry and ramp release to exploit the benefits of each feature. A slight improvement over the Wavy design is expected; after all the two ideas are similar. The efficiency of the contact at all points allows for a shorter bottom flat face and the replication of the feature from 5 to 8 times. Emphasis is given to the entry bending with proper release to avoid gaps. This procedure is iterative and not covered to the most optimal design in this paper.

3.2.7 Double Amplitude Hybrid Feature

This feature is the first to introduce double amplitude. The motive is to exploit the flat part of the bottom face to create an internal bump, which will double the bending frequency due to entry events. Unfortunately, creating additional bumps destabilizes the effect of the flat face. Pressure is reduced, as seen in the Sinusoidal attempt, and there is not enough length for a proper release. Additionally, this feature increases the manufacturing time and complexity of EDM negatives and creates fragile mini bumps that are subject to wear due to their summit form.

3.3 Parametric Analysis Results

A sort of review of the different features used has already been presented. The features were chosen based on the quality characteristics they introduce, starting with simple features such as the Sinusoidal and the rectangular and leading to composite features that treat entry and exit in different ways. Once the mesh, the inputs to the system, and the boundary conditions were chosen, every design was tested in the total range of feature amplitudes as well as different parameters for some features. The Ramp and Wavy Hybrid was tested for 5 and 8 extrudes, and further parametrization has been carried out on the Ramp feature for the grade of the ramps. All scenarios were tested both for 30 and 50 m of pad displacement. Finally, extensive analysis has been carried out on the ramp feature for an amplitude of 35 m, and conclusions have been drawn on the contribution of the entry and exit geometries.

A special tool was developed in Matlab that allows the manipulation of the data from the FEA models. Values from ANSYS Mechanical are quantized, meaning only specific values exist for reference data sets. Amplitudes of 10 to 100 m were simulated, and using the tool, values in that range can be extrapolated which can also predict values outside of this range. It must be clear that the data are based on the vertical displacement input, and in some cases they may be similar if the Amplitude of the feature is greater than the displacement value. For example, given y = 50 m, any rectangular feature with an amplitude larger than that will behave the same way, as the peaks come into contact with the pad while the rest of the feature and the bottom faces maintain a positive gap to the pad without further contribution to friction generation. For this reason, if the target value for the extrapolation corresponds to a point with an amplitude greater than 100 m, the last FEA value is used.

3.3.1 Fx Reaction versus Feature Amplitude

Plotting the friction reaction in correlation to the feature amplitude allows for a better understanding of the qualitative behavior of each feature. Figure 1 clearly indicates the behavior of each concept, especially the non-contributing phase of rectangle-based features, for amplitudes greater than the displacement. The diagram is divided practically into two zones, one in which forces decrease linearly and the second in a constant phase already explained. The point where zones are separated is the critical point.

Amplitude of Feature = Displacement of Pad

The near-linear behavior in the first zone can be explained by focusing on the areas where displacement is larger than total amplitude and therefore total contact takes place, apart from simulation gaps near the edges due to stiffness of the materials. From the point where the total point is achieved, every step lowering the amplitude is equivalent to pure compression of the pad material. This is because the pad volume already attached to the disc surface does not contribute any more, and since the disc is practically incompressible, any further compression is connected with the rest of the pad volume. This volume has a rectangle cross-section; therefore, by Hooke’s law, compression is linearly connected with force increase. In other terms, the features only contribute to changing the way the pad approaches the disc and the percentage of area between full and least compression. Those are respectively met at the tops and bottoms of the features. Features also have an impact on the transition between those two zones as they introduce different bending into the pad material. Sinusoidal and Hybrid features preserve their curvature in both zones, as different amplitudes correspond to disc peaks with different curvature, and the contact area decreases constantly but

at a slower rate. For this reason, their diagrams can be simplified into two lines, one corresponding to full contact based on Hooke's law and the other to the geometrical alterations of curvature, which are less steep and start after the critical point.

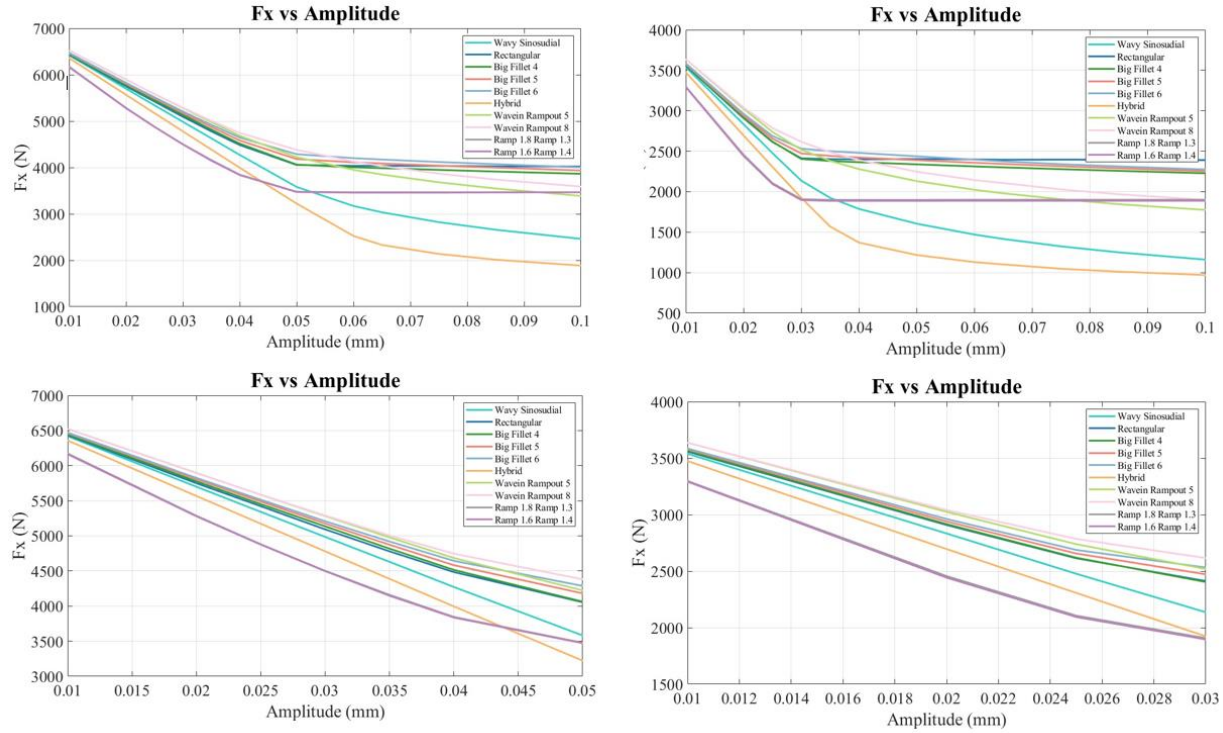

Figure 36 Extrapolation of Fx based on the FEA results
U. Left: Compression 50μm, Amplitude range [0.01,0.1], U. Right: Compression 30μm, Amplitude range [0.01,0.1], L. Left: Compression 50μm, Amplitude range [0.01,0.05], L. Right: Compression 30μm, Amplitude range [0.01,0.03]

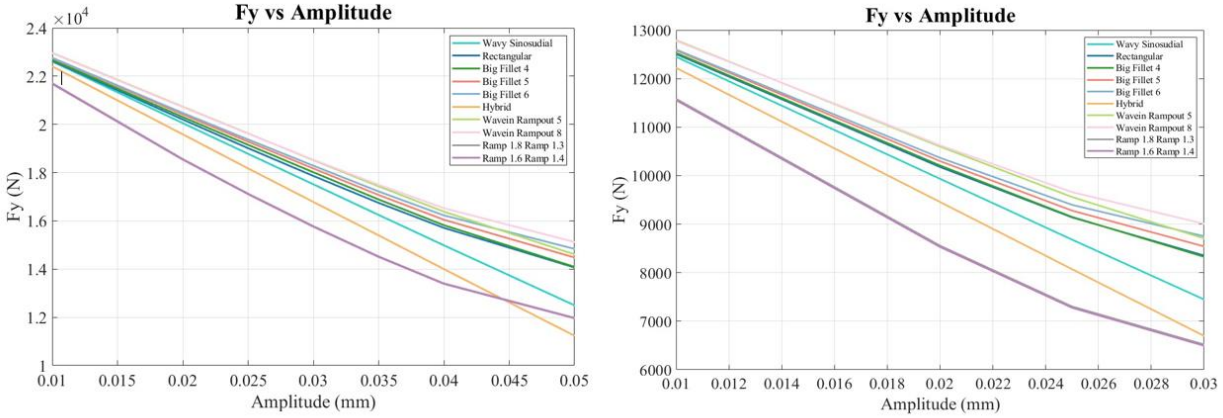

Figure 37 Extrapolation of Fy based on FEA results
Left: Compression 50μm, Amplitude range [0.01,0.05], Right Compression 30μm, Amplitude range [0.01,0.03]

From the diagrams, one may assume that specific features are inferior to others based solely on the position of each curve on the diagram. This is incorrect, as a change in feature also means a change in the way the height of the contact area is distributed. Therefore, vertical force reaction is not constant across all models for a specific amplitude. In figure 36 the vertical force reaction for different features in the first zone can be seen.

A similar trend is observed for each feature's corresponding line in the Fx and Fy diagrams. In the following sections, data will be analyzed in a feature-based and CoF-based way to extract the maximum information from the data points. The decimal numbers on the legend are related to the degrees of the ramp, while the integers refer to the number of features across the length of the disc. Total disc length: 100 mm.

3.3.2 Stress and CoF Diagrams Across Features

One exceptional way of characterizing each feature is by visualizing the stress and COF throughout the study. Bar graphs can contain adequate information about each feature, such as the mean value, the range of FEA data points, and any other user-introduced quantity. Stress is a valuable aspect of the model, as the optimal design must avoid concentrations in sharp corners or due to excessive bending. Displacement is minimal and the latter is unavoidable; Visualizing stresses across different models can be very helpful.

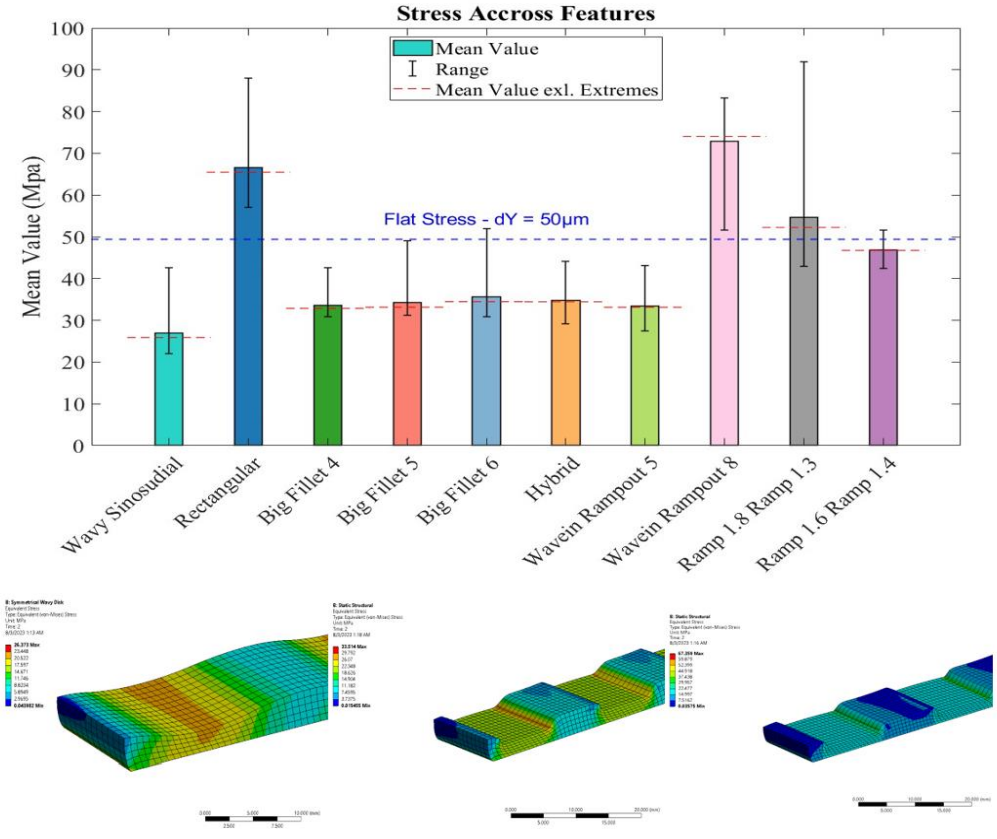

Figure 38 Equivalent Stress across features. Upper: Comparison for all models tested
L. Left: Wavy Sinusoidal feature, L.Middle: Big Fillet 5 feature, L. Right: Rectangular feature

Figure 38 shows stresses across all features tested. The data are based on the 50-m displacement model, and all measurements are accounted for. A large variation across measured stresses is shown, and some features treat the pad smoothly while others present even double values of equivalent stress. On some occasions, FEA and CAD models cannot accurately represent the feature for small amplitudes, and for this reason, the red dotted line represents the mean stress value excluding extreme values. In this case, maximum and minimum values are excluded. The correlation between the red lines and the bars shows that good convergence exists across the model, except for specific values. Sharp-edged features have a tendency to increase stress, which is lowered by introducing smoother ramps. On the other hand, smooth bend edges like the Fillet or the Wavy present stresses even smaller than the flat scenario. This diagram must be further analyzed since no force value is present. This means that stresses on the Wavy disc are not directly comparable with those on the flat disc since the area height distribution is different. Yet, the variation in each feature is indicative of the range expected even for an increased nominal load. This observation is further justified by the images in figure 38, as sharp-edged features are clearly loaded in an unsuitable way.

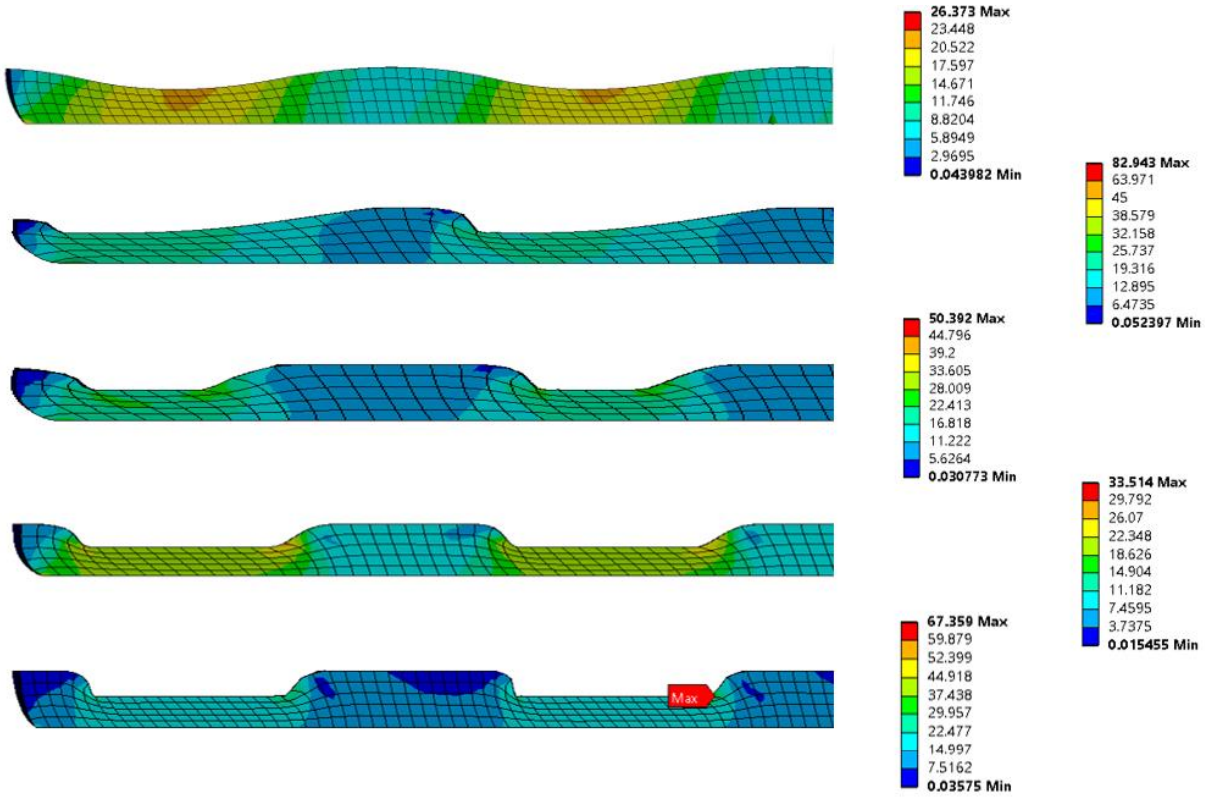

Figure 39 Equivalent Stress plot comparison for different features. From top to bottom: 1) Wavy Sinusoidal, 2) RampIn-RampOut, 3) WaveIn-RampOut5, 4) BigFillet5, 5) Rectanglular

CoF trends are presented for each feature in ascending order in figure 40. All the features present a preliminary proof of concept by being constantly above the flat disc scenario, even in the most unfavorable FEA runs. The total increase in CoF is not something revolutionary lying within a range of 3%. Considering the stiffness limitations predicted in Chapter 3.1, this increase is desirable and can hardly be increased. This is also the first diagram from which rational conclusions result. The increase in CoF is proportional to the increase in features, as can be observed from the various "Big Fillet" designs. The same can be deducted

from the wave-in-wave-out feature. Furthermore, the grade of ramp features has a small impact on the improvement of friction between relevant models. One way of verifying the features's impact is by measuring the contact area of the flat peaks among the features. "Big Fillet 6" has a total peak area of 432.9 mm2. While WaveIn RampOut8 has 189.4 mm2, meaning that CoF is not directly relevant to the percentage of area nearest to the pad but is based on the entrance and release of the bending through the feature. Additionally, the proportional relationship described above also indicates that an increased number of features is equivalent to increased bending, therefore improving COF.

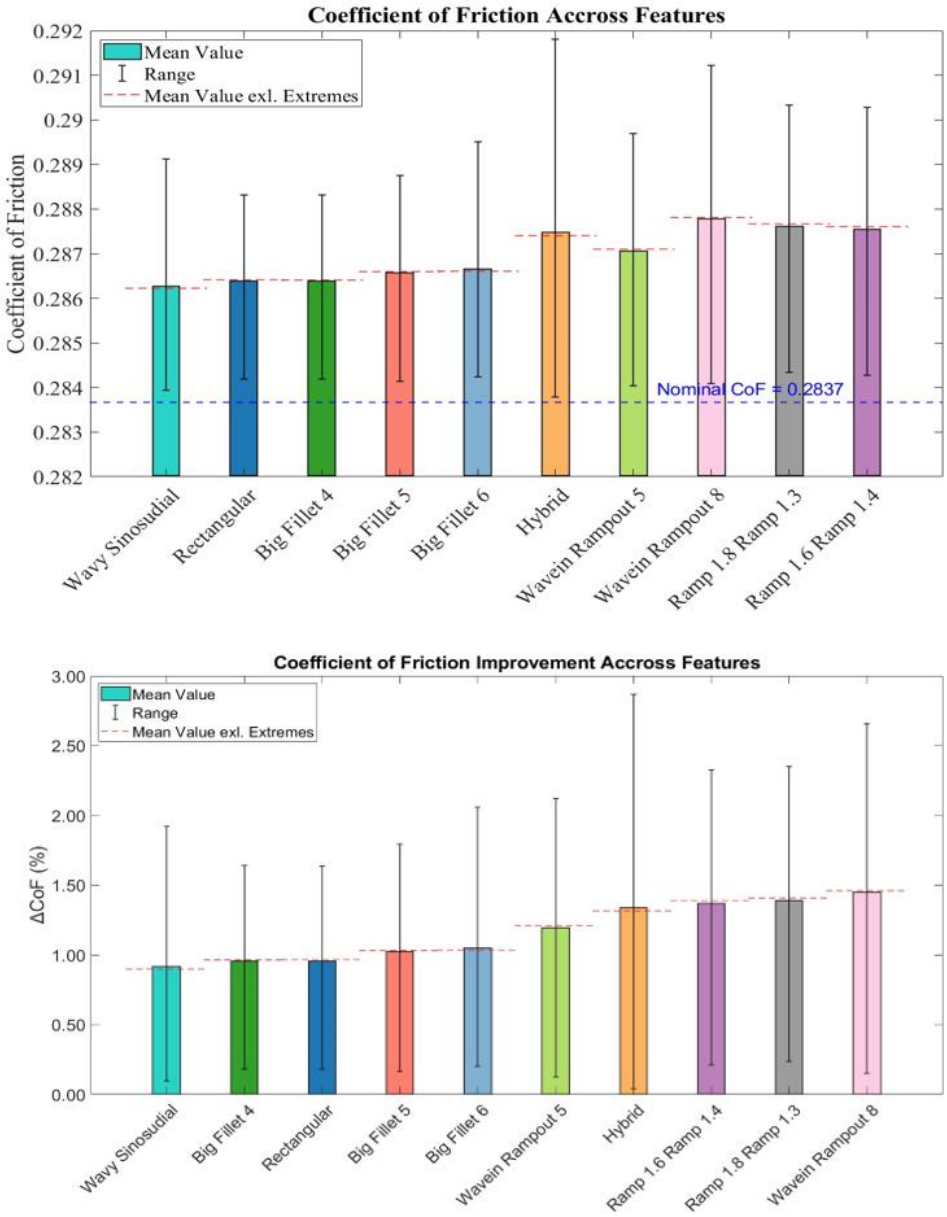

Figure 40 Comparison of CoF values across features. Upper: CoF mean and extreme values for all scenarios, Lower: CoF improvement from baseline mean and extreme values for all scenarios

The bar diagram in figure 40 indicates that the qualitative characteristics of the feature are responsible for the response rather than solely the number of features. "Big Fillet 6" presents lower CoFs than WaveIn-RampOut 5, even though it contains one more peak per disc length. This difference is only equivalent to 0.143%, as the improvements are really small. Interestingly enough, the "Wavy" feature is the least effective, as it treats the disc in a smooth way, while the best attributes are found on features optimized for optimal material entrance with appropriate release mechanisms. One proposal for future research is adding an increasing ramp in place of the flat peak to further increase the 3-phase phenomenon and add progressive bending even on the currently flat surface. This was not tested in the present paper, research was targeted for features that can be manufactured, and even the Ramp Feature with high grade is near the limits of the capabilities of most machinery.

3.3.3 Interpolation and Quantitative Analysis

Using the custom MATLAB tool to interpolate the results, plots are derived for both 30 and 50 m of deformation for various reaction forces. This entity is opting for the comparison of features within their working range to avoid using non-achievable values. The interpolation is based on the sets of consecutive data and is expanded until zero feature amplitude, or the maximum achievable force by the feature, and the lower value found from FEA, considering amplitude is already double the deformation. One keen observation is that all features should converge to the same value at A = 0 m, but the linear scheme was preserved as this area is outside of the manufacturing range. For this analysis, Equivalent Stress and CoF values are also presented, giving maximum acknowledgement of the datasets acquired from FEA runs.

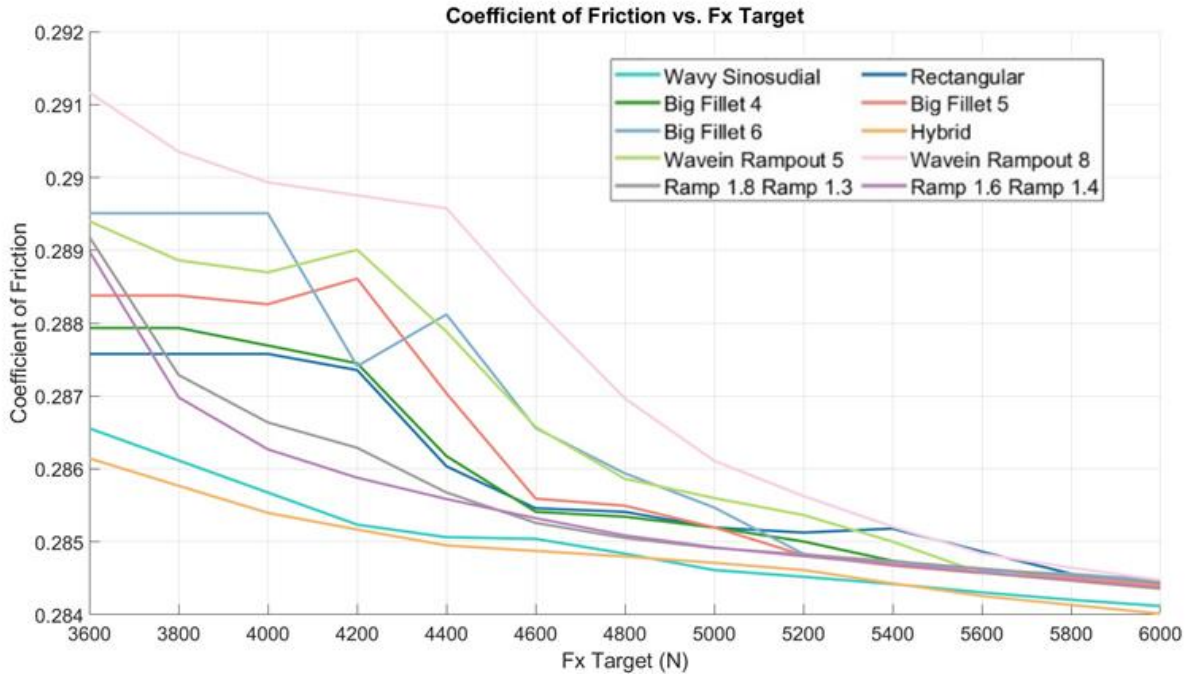

Figure 41 Extrapolation of CoF values across working range for all features

Figure 41 provides valuable feedback from the measurements. Increased Fx values are equivalent to small amplitudes, and the pre-described convergence is indeed shown from the data, proving a rather reliable

model. The only two features beyond this scope are wave-based features that behave differently, as seen from the low CoF values throughout the range of targets. Flat lines at low Fx values indicate the inability of the feature to produce forces in this range. The jog point of each curve is the critical point, and an exponential decrease of CoF is shown for all features after the critical point. Additionally, families of features present the same tendencies, such as the purple and gray lines for RampIn-RampOut, and the BigFillet family also shows common behavior, also shown in the following figures.

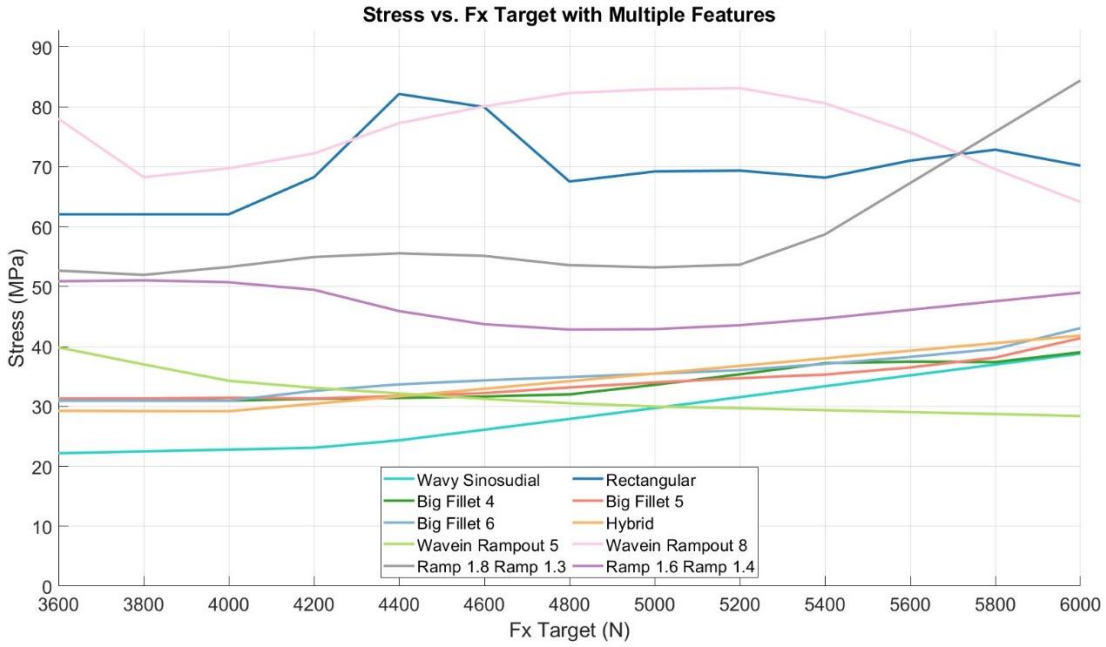

Figure 42 Extrapolation of Equivalent Stress values across working range for all features

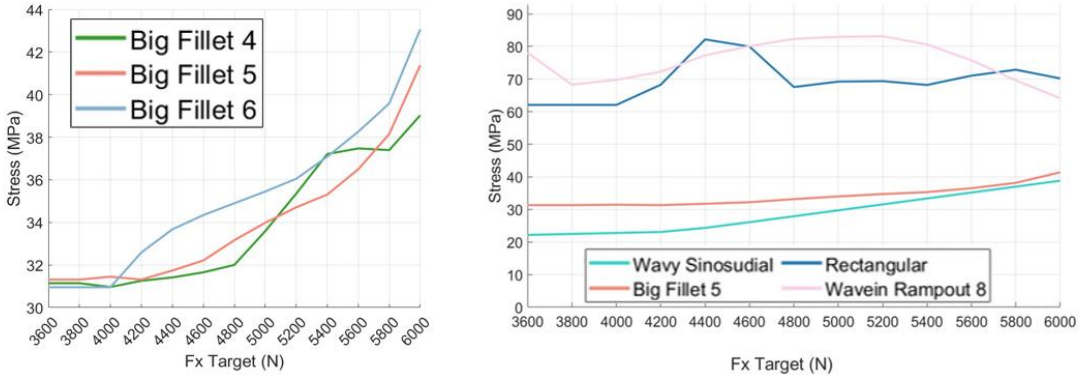

Figure 43 Equivalent Stress values for families of features. Left: Big Fillet variations, Right: Qualitative comparison of Eq. Stress values for smooth vs sharp edged features

Figure 42 captures the Stress behavior of each feature for the working area. Rectangle-based features present anomalies, probably due to inaccuracies from the sharp corners. Penetration allowance has a significant impact on the reaction force, as the graph only shows maximum values of stress taken from quantized time steps. Extreme points may indicate a statistically bad point. This is minimized by smooth features using fillets, where a uniform shape is presented. Figure 41 also shows that features introduce bending, as the curves equivalent to more peaks show greater stress due to the increased amount of times the two surfaces contact each other in the feature area.

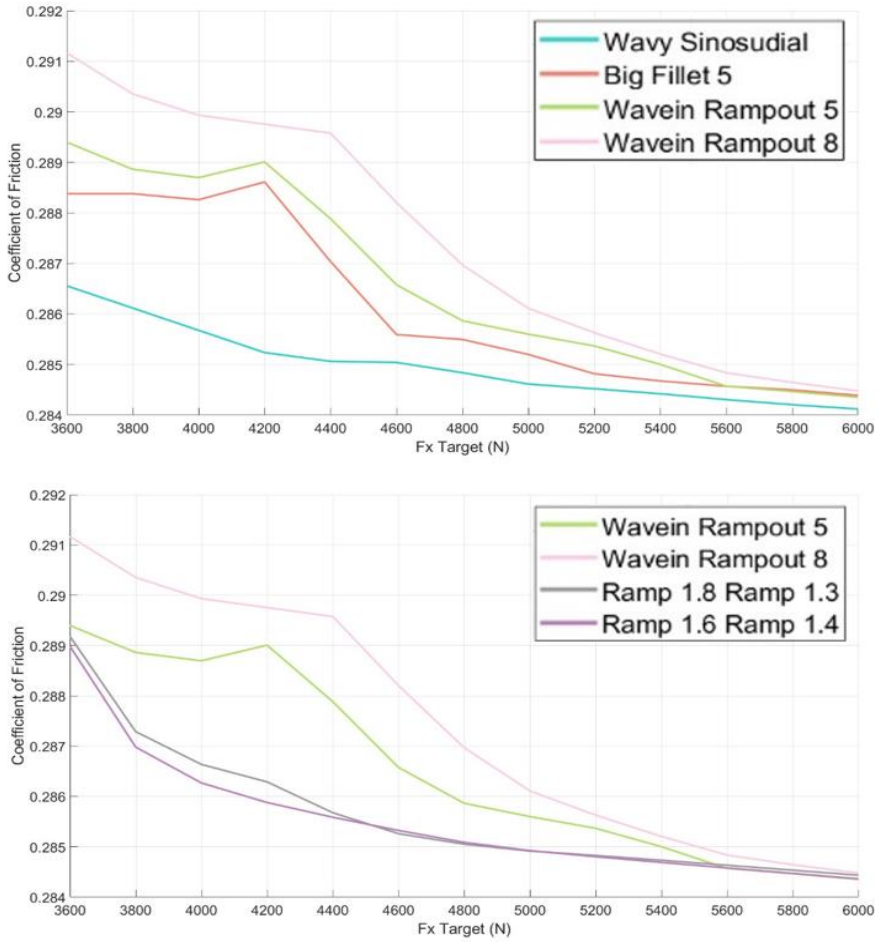

Figure 44 Coefficient of friction for families of features. Upper: WaveIn RampOut features compared to Wavy Sinusoidal and Big Fillet feature, Lower: WaveIn RampOut features compared to RampIn RampOut features

3.3.4 Further Investigation of Features

In this section, the RampIn-RampOut feature is further investigated to extract the maximum possible information. Specifically, the grade of the ramps is tested in different designs, and the coefficient of friction is measured for each model. Geometrically, the models are equivalent to other designs with eight bumps, apart from the Entry and Release of each peak. Different sets of grades are tested, always considering low penetration values and high accuracy. For this reason, grades in the range of [1.0–2.2] degrees were tested

in various pairs. Assuming that the greater impact on the CoF is attributed to the entry geometry, the investigation continues in order to prove this theory and also test the impact of the release curve as well.

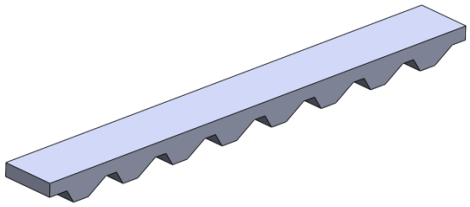

Parametric Study with A = 0.035 for the Ramps					
Ramp In, Ramp Out - Half Model - 8 Extrudes					
	Ramp In (deg)	Ramp Out (deg)	CoF	CoF diff (%)	In - Out (deg)
Flat Disc	0.0	0	0.2837000	0.00000	
Case 1	1.4	1.8	0.2856625	0.00687	-0.4
Case 2	1.6	1.8	0.2857377	0.00713	-0.2
Case 3	1.4	1.5	0.2857448	0.00716	-0.1
Case 4	1.6	1.5	0.2858213	0.00742	0.1
Case 5	1.4	1.2	0.2858214	0.00742	0.2
Case 6	1.8	1.6	0.2858454	0.00751	0.2
Case 7	2.0	1.8	0.2863691	0.00932	0.2
Case 8	2.2	2	0.2859640	0.00792	0.2
Case 9	1.6	1.3	0.2858769	0.00761	0.3
Case 10	1.8	1.4	0.2859020	0.00770	0.4
Case 11	2.0	1.5	0.2864415	0.00957	0.5
Case 12	1.8	1.2	0.2859531	0.00788	0.6
Case 13	2.2	1.6	0.2865461	0.00993	0.6
Case 14	2.0	1.2	0.2865023	0.00978	0.8
Case 15	2.2	1	0.2866423	0.01026	1.2

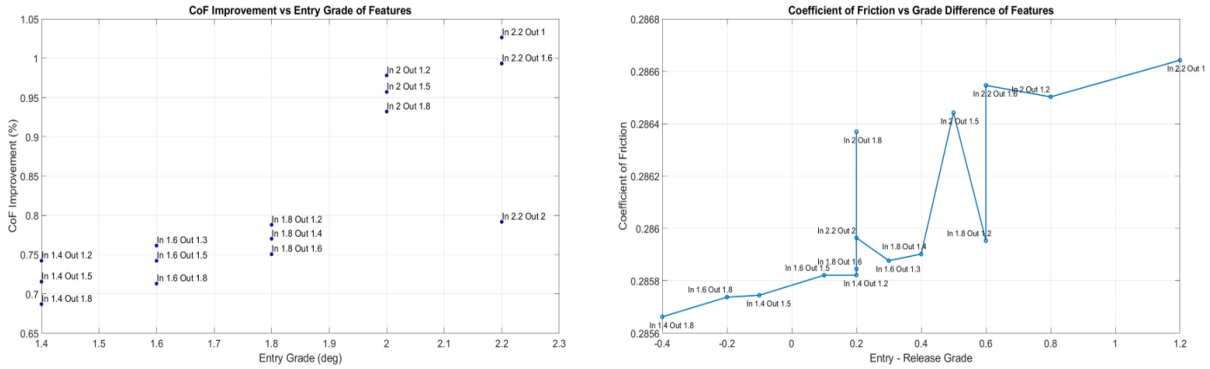

Figure 45 Opimization results for RampIn-RampOut feature.
U. Left: Design of the feature in exaggeration, U. Right: Comparison of results with increasing grade difference, L. Left: Results for % of CoF improvement from flat design, L. Right: Results for CoF value

The designs were sorted based on the difference between the two grades, favoring the entry inclination. Negative differences (entry smoother than release) were also tested, and in the case of the same gradient difference, they are sorted in ascending order based on the entry characteristics. As seen from the figure, friction is improved for steeper grades, and even more so for bigger grade differences. Negative differences are not a good option, while the data indicate pushing the disc to stress limits on the entry side to achieve maximum results. An Improvement range of 0.35% is shown between the worst and the best feature, and overall, 1.03% from the baseline. According to figure 40, this is not beyond the maximum improvement record, although figure 40 shows that those values are met in features larger than the pad displacement; therefore, comparing them with these investigation values is not ideal. The difference in bending can be compensated by the selective choice of different gradients for the entry and the release. Higher grades are required for the entry, while smoother ones are required for the release. A series of grade sets was simulated to extrapolate the accuracy of this statement. The grades were selected so that they satisfy design consistency for feature amplitudes up to 100 m. As observed from the table in Figure 45, the choice of the gradient slightly impacts the final CoF and should be considered a final fine-tuning process after the feature has been selected. Every theoretical observation is not accurately transferred to the real world due to roughness and manufacturing incapabilities. The positive sign given by the investigation is in regard to the

overall improvement of the friction phenomenon by tweaking the geometry, which is therefore the needed proof of concept.

3.3.5 General Observations

As observed from the figures throughout this chapter, the proof of concept exists in the FEA modeling world. Introducing geometrical features to enhance disc bending actually increases the friction coefficient and overall braking force. Features have an impact on the total area of contact as pressure is further varying on the surfaces of both components due to height distribution. The needed displacement of the pad to achieve the same force values is larger. The concept is verified by locating the behavior of the CoF for each feature near the highest amplitude. In those areas, the pad is in total contact with the peak of the feature, which is usually equipped with the biggest curvature. The entry and release "corners" are mainly in contact with the pad; bending is enhanced, and the tangential force percentage to the perpendicular increases; in other words, the CoF is improved. Although this proves that geometrical bending is beneficial, one cannot design the braking disc based on huge amplitudes, as the entire disc is no longer used and redundant weight is carried over. Yet, the correct feature choice can improve friction values even at smaller amplitudes—at least theoretically. Fortunately, the current FEA model presents a stable behavior across features, and penetration values between the two bodies are of the same order, as shown in figures 46 & 47, as already indicated, this is an acceptable magnitude, as contact stiffness would otherwise heavily increase, influencing the results negatively, and real body roughness is larger than this value. One can assume that penetration in this model is equivalent to the deformation of the asperities during the start of the real contact. Finally, for greater loads, penetration converges for all models, indicating a good stiffness correction factor choice.

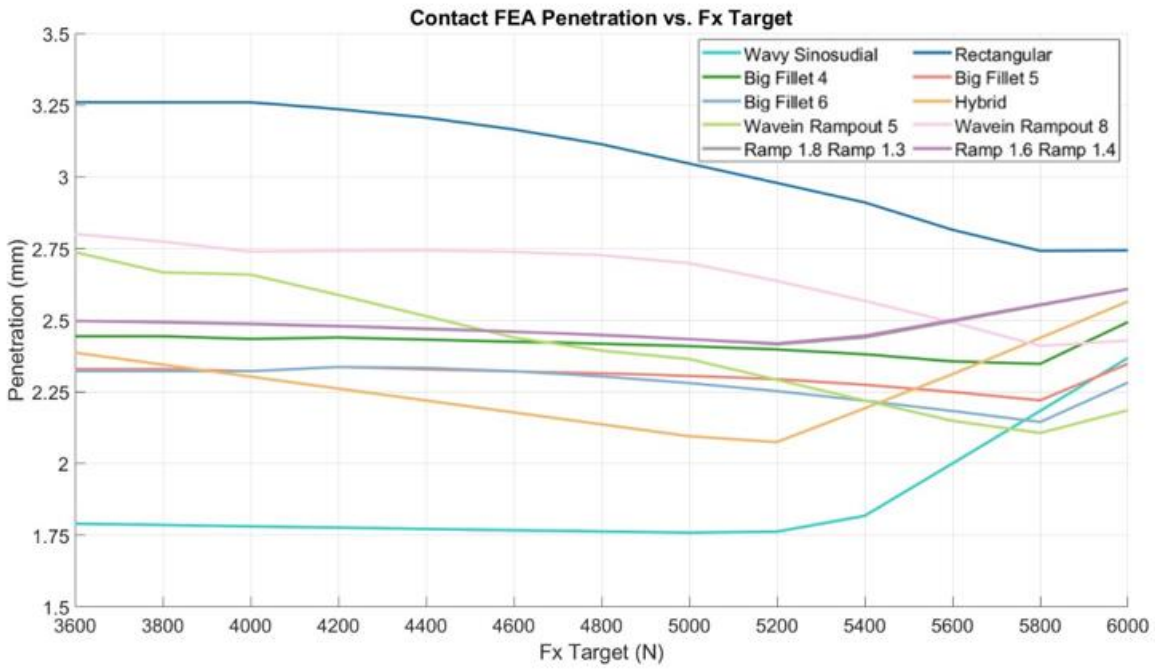

Figure 46 Interpolated disc-pad Penetration values of the FEA model across all features

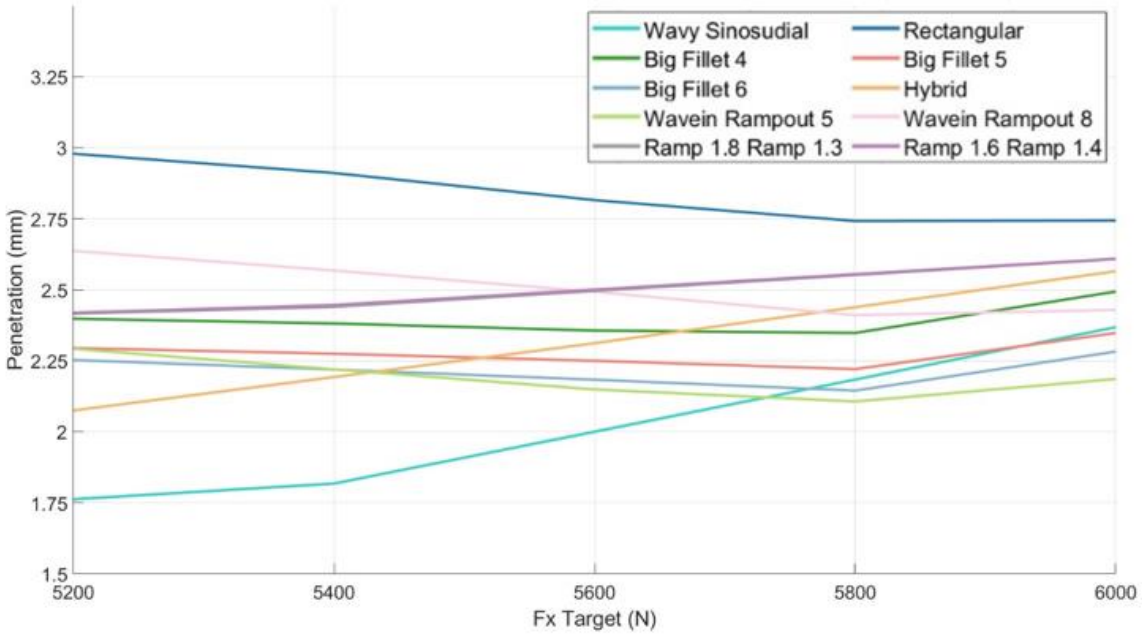

Figure 47 Interpolated disc-pad Penetration values of the FEA model across all features focused in convergence area

Chapter 4 Experimental Investigation

The delivery of a FEA proof-of-concept that utilizes actual data obtained through experimental tests is the focus of this chapter. The creation of test prototypes is the first step of action, which will be evaluated using a tribometer rig based on the findings obtained in Chapter 3. The prototypes were created utilizing a smaller-scale geometric pattern and will afterwards go through the pin-on-disc test. The feature selection is important because it influences the results and is affected by the manufacturing process, which, depending on the process, can fail to transform CAD files into precise 3D models. The fabrication technique was chosen based on the application, the time available, and the resources available. Specimens were examined and measured prior to testing to establish a correlation between the theoretical design and the actual objects. The pin-on-disc rigs do not completely capture the phenomenon, but the goal of the tribometer testing is to translate the proof of concept into the real world. As a result, a unique tribometer rig with novel features is designed for disc-on-disc tribological investigations. The assembly aims to be a fully functional, affordable method for assessing the characteristics of contact cylindrical rotating systems. In this way, the area of contact rather than the pin tip determines the results. Furthermore, the bespoke tribometer is easily adaptable to a variety of studies in the future, including liquid applications for wet clutches.

4.1 Specimen Fabrication

Based on the observations of the proof of concept in Chapter 3, cylindrical specimens for the pin-on-disc experiments are designed. The available pin-on-disc tribometer for the measurements is the TRB-3 by Anton Paar, a renowned tribometer found in many professional labs and known for its accuracy. This experimental rig uses a rotating chuck to secure the prototype in planar movement, and the pin is positioned at the desired radius to measure friction. The user chooses a preset normal force representing the vertical load of the pin. The chuck has a maximum holding diameter of 60mm, so the discs are designed with an outer diameter equal to that to maximize the available range. The inner diameter of the specimens is set at 20mm and the nominal thickness at 3.5mm for discs with features and 2.5mm for the flat disc. The thickness is minimal to reduce the manufacturing costs of DMLS printing. In our approach, eight bumps are used for each disc to ensure a smooth transition between peaks and bottoms during the test. The features chosen were: (a) a ramp-in-ramp-out feature with antisymmetric grades for the ramp; and (b) a wavy feature, as they introduced either high CoFs or smooth stress fields accordingly. The Wavy feature is formed by fillets of variable radius in the radial direction, and the curvature radius increases towards the outer diameter to enhance the angular character of the design rather than straight lines eccentric to the center of the disc.

Manufacturing options that can accurately capture the small amplitude scale are:

a. SLS printing,
b. DMLS printing, and
c. EDM pressing with a negative geometry.

SLS is suitable for the fast production of low-cost plastic prototypes. These were used for the initial measurements before advancing to the more accurate and expensive DMLS printing. EDM was not chosen as the negative geometry of manufacturing greatly increases the cost and lead time for small quantities and is preferred for mass production. Once the SLS printings verified the varying CoF in comparison to the flat geometry, the production of DMLS-printed steel prototypes was opted for. This method allows a minimum layer thickness of 30 m, which is restricting, but after consideration of the 120 m amplitude of features, it was decided to utilize at least 5 layers for our geometry, reducing the inaccuracies of the quantization of the curvature in steps. The manufactured pieces were then sandblasted to improve their surface quality and further abraded using sandpaper.

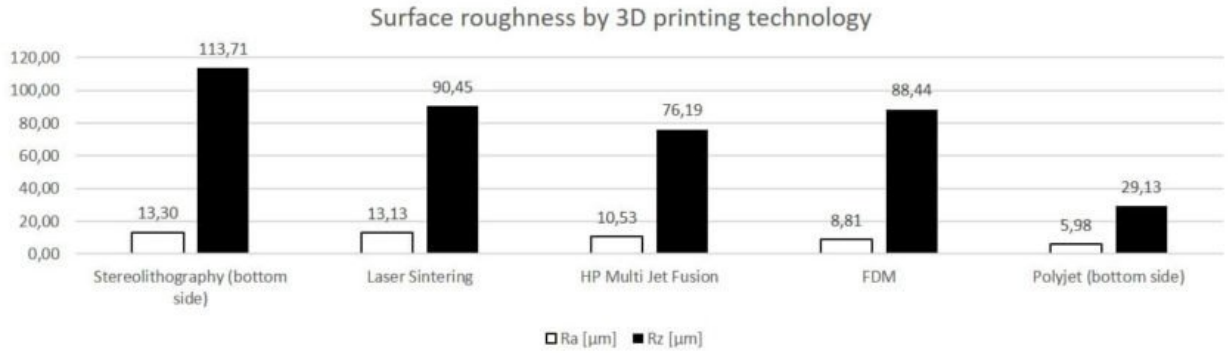

Figure 48 Typical roughness values of various 3D printing methods

4.2 Surface Topography

Printed prototypes are measured before any tribological testing, which has a destructive nature for the surface quality. To extract maximum information about the features, the BRUKER Contour GT-KO Optical Profilometer was used, with a measuring range of 1mm x 1mm areas and an accuracy of Although the area of measurement is very small in comparison with the entire area of the disc, the measurements are used to get a better visualization of the printed surface. Maximum data were acquired for the features by targeting the areas where grade changes significantly, as those points are responsible for altering the CoF. Finally, three sets of measurements were conducted, one for each disc.

- Flat disc – 4 points measurement
- Wavy disc – Double Fillet measurement
- Ramp disc – Measurement of the steeper grade

The software used automatically calculates crucial variables for our analysis. Using the mean plane of area, A, the variable Z is determined to measure the vertical position of each point from this plane. The Z-height distribution is indicative of the quality of the disc's surface. This surface can be further evaluated by the following metrics:

a) Sa - arithmetical mean height: Expresses the mean absolute value of the difference of the height of each point to the mean height of the surface.

$$Sa = \frac{1}{A}\int\int_{A} |Z(x,y)|dxdy$$

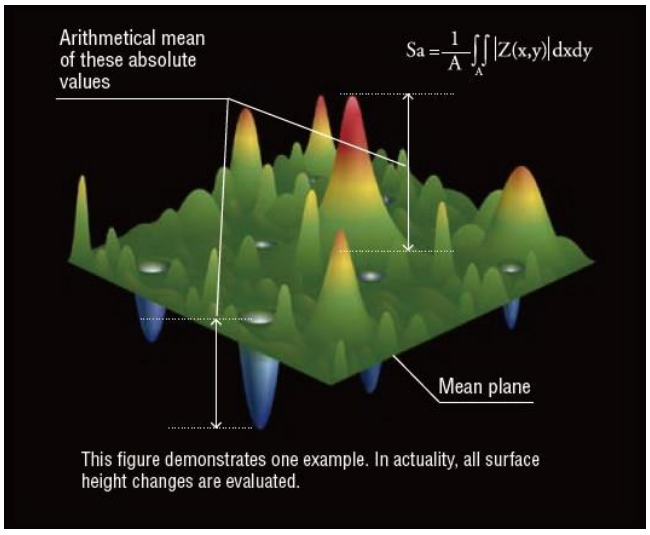

Figure 49 Qualitative demonstration of Sa variable

Sku – Kurtosis: Expresses the sharpness of the roughness profile

$$Sku = \frac{1}{Sq^4}\left[\frac{1}{A}\int\int_A Z^4(x,y)dxdy\right]$$

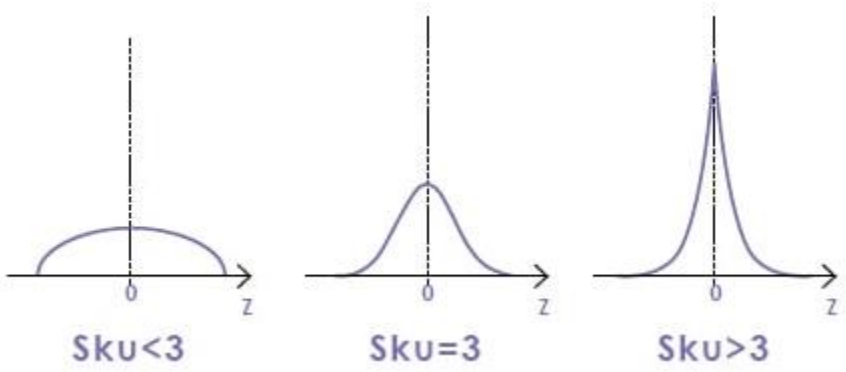

Figure 50 Sharpness of the asperities expressed by Sku variable

b) Ssk – Skewness: Degree of bias of the asperities. Negative values indicate height distribution skewed above the mean plane.

$$Ssk = \frac{1}{Sq^3}\left[\frac{1}{A}\int\int_A Z^3(x,y)dxdy\right]$$

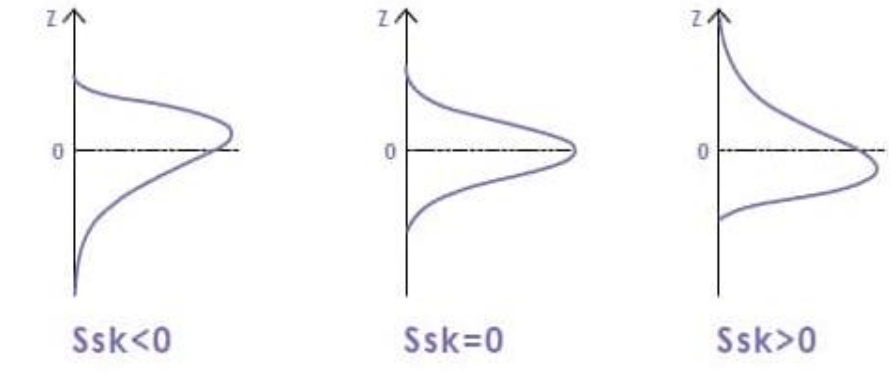

Figure 51 Shape of the asperities expreessed by the Ssk variable

c) Sp, Sv – Maximum and minimum heights from mean plane.

$$Sp = \max(z(x,y)\,, \qquad Sv = min(z(x,y)$$

d) Sz – Maximum Height: The sum of the absolute values of Sp and Sv.

$$Sz = |Sp| + |Sv|$$

e) Sq – Root mean square height: Value of ordinate values, equivalent to standard deviation of heights

$$Sq = \sqrt{\frac{1}{A}\int\int_{A} Z^2(x,y)dxdy}$$

Measuring the flat disc before the experiments is proven valuable in understanding the roughness quality of the manufacturing technique used. The measurements of the flat disc are valuable to understand the roughness of the entire manufacturing process, including the sandblasting. Roughness values are similar on all 3 discs but harder to measure on inclined surfaces, as the inability of DMLS layering also contributes to asperities of unequal characteristics at the edge of each layer. The software used by the profilometer does not allow extraction of the data points; hence, custom diagrams cannot be produced, and valuable information cannot be visualized.

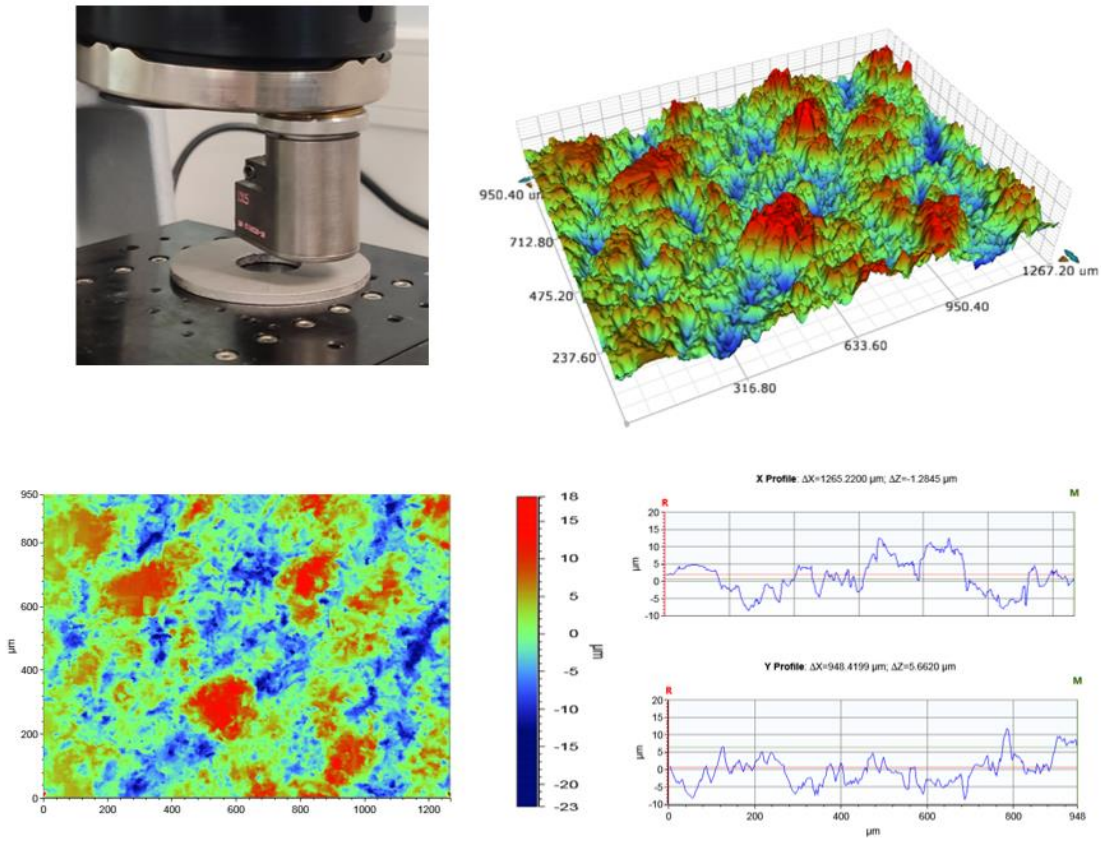

Figure 52 Surface topography measurements. U. Left: BRUKER profilometer and disc specimen, U. Right: 3D representation after scanning, L. Left: 2D representation after scanning, L. Left: X and Y surface profiles compared to the reference thickness

After evaluation of the profilometer data, the flat disc has increased roughness in comparison to the ideal flat model. In a real-life scenario, this would result in increased wear of the pads and gradual smoothing of the disc's surface. Additionally, vibrations are expected during our experiments as the lateral moment introduced on each side by the asperities would differ heavily between local points, as seen in Chapter 2. In an attempt to provide uniform conclusions about the disc's surface, data from the four positions is combined to extract the average values for our surface quality. The results are shown in table 3.

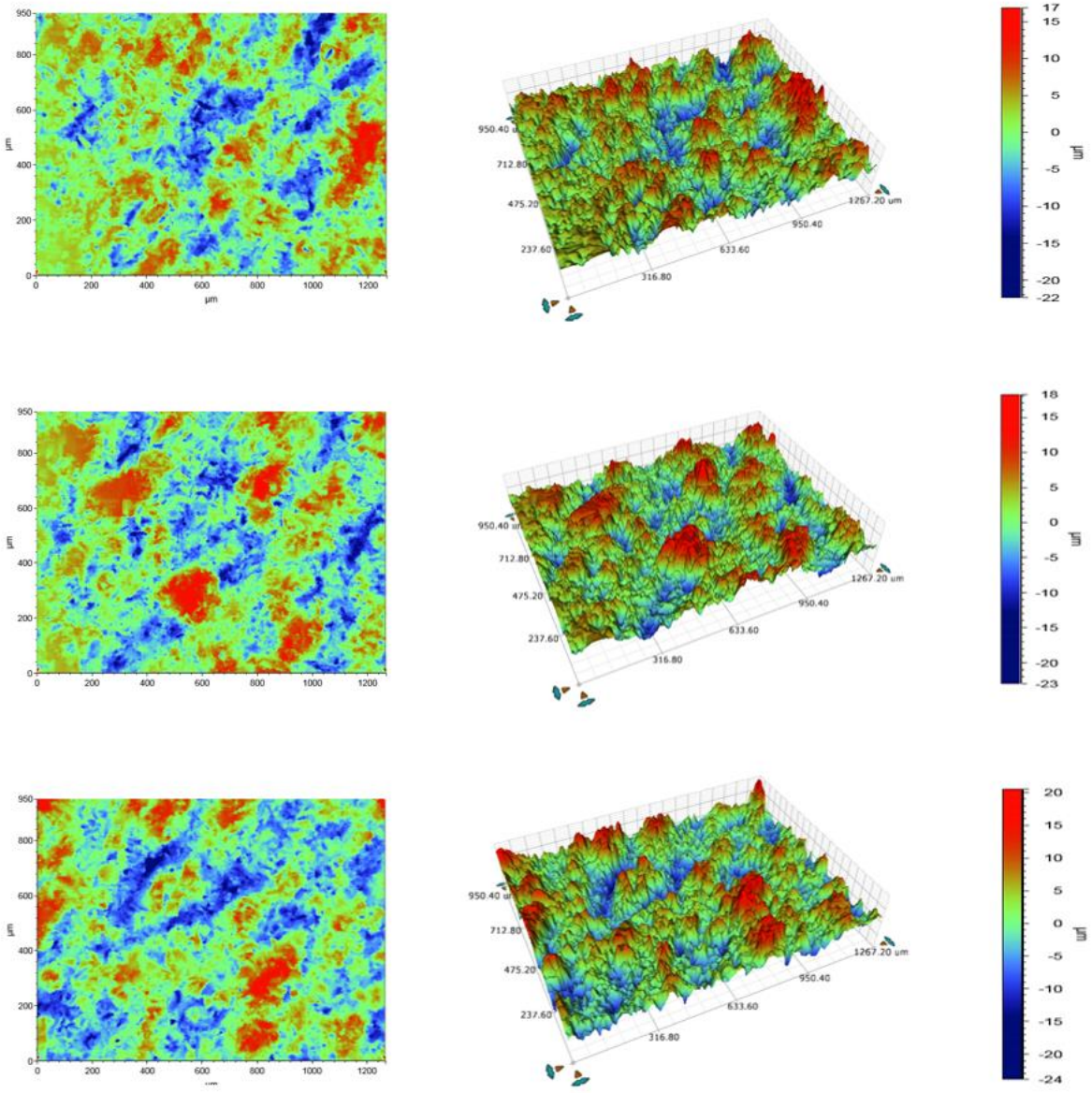

Figure 53 Profilometer measurements for the flat disc, sets of 2D, 3D and scale. Upper: Measurement point 1 Middle: Measurement point 2, Lower: Measurement point 3

The measurements of the two discs with features are used to extract the relationship between CAD geometry and the 3D model. The quality and dimensional accuracy of the features in the real models are evaluated, targeting the inclined plane of the ramp feature and the entry/release point of the wavy feature. Extreme peaks (Z positive) and bottoms (Z negative) are expected to disrupt the uniformity of the feature and increase surface roughness. After measuring the aforementioned areas, analytical results are exported, and the software performs a flattening process on the total area. Sp and Sv values are comparable to the flat disc ones and do not represent the highest and lowest points but rather the bigger relative peaks and pits. This is equivalent to creating a new coordinate datum system with the XY plane coincident with the inclination of the Ramped disc, or tangent to the curvature of the fillet, at the median Z coordinate of the feature.

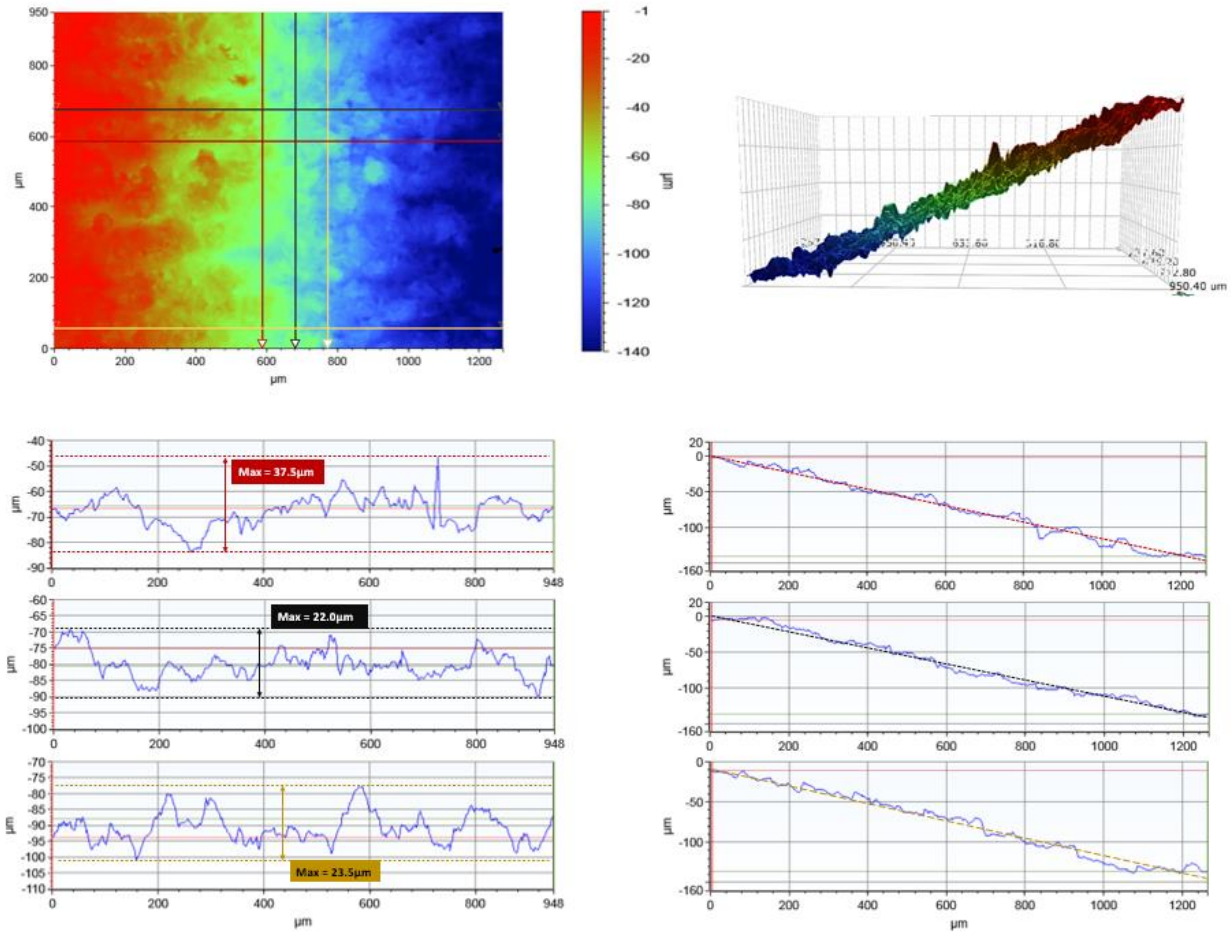

Figure 54 Profilometer measurements on the Ramp Featured disc.
U. Left: 2D representation and scale (1), U. Right: 3D representation in side view,
L. Left: Y profile for the points in (1), L. Right: X profile for the points in (1)

The measurements on the Ramp feature are of good quality, resembling the desired feature. In top view, five zones are observed, whose Z median is descending gradually from the left to the right. The dark red area highlights the highest points of the feature; green is at the median Z coordinate of the inclined plane; and dark blue represents the bottom of the feature. Two transient areas on either side of the green area are observed, in which asperities vary largely in shape and size due to manufacturing inaccuracies. The absence of extreme peaks in the blue area or pits in the red one is a positive aspect, indicating the gradual decline

of the Z values. As seen from a side view, the surface can be further improved with finer surface treatment methods, such as 5-axis grinding or dying the part into special solutions. The Z values measured at different points in the area are present in the figure clearly showing the linear behavior of the disc profile in the feature area.

On the other hand, the image captured during the measuring of the Wavy feature exhibits lower degrees of accuracy in comparison to the intended design. The demarcation between different regions lacks clarity, and their interactions are indistinct. Furthermore, the positioning of the green area undergoes vertical displacement and width fluctuations. Utilizing the metrics obtained from the X profile, the presence of three arbitrary zones can be established: two horizontal and one inclined. Regrettably, the fillet's radius is not distinctly discernible in the image and appears to be disrupted. Although a wavy curve can be applied to the dataset, the fitting process yields substandard results, and the roughness functions as a statistical noise filter for the data. In this report, the unprocessed data are presented; areas of high contrast in darker shades indicate sharp variations akin to peaks or valleys. The concentration of contrast points exceeds the desired values. The anticipated length of the fillet ranges from 1.55mm to 3.1mm. Consequently, the profilometer fails to encompass the entirety of this feature. The data demonstrates a height variation of approximately 100 m, which is lower than that specified in the CAD file.

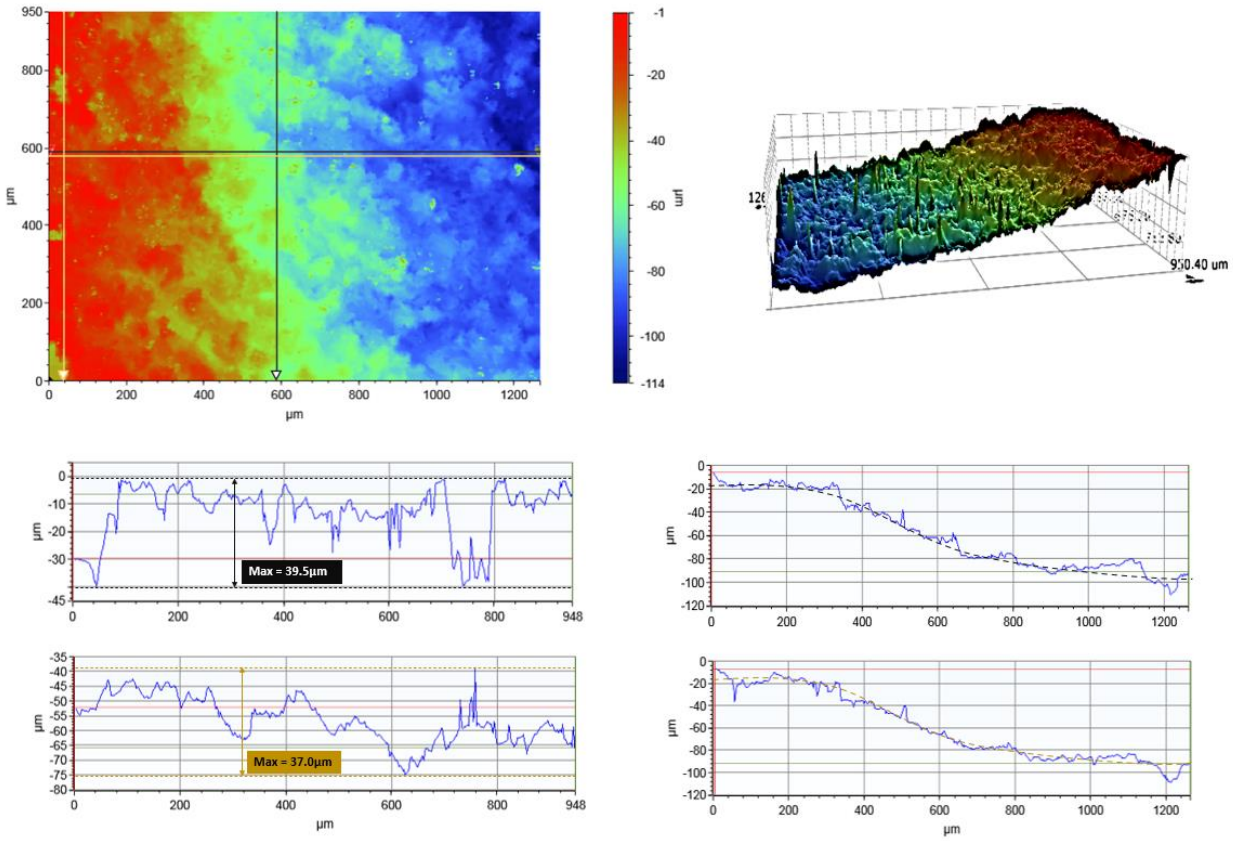

Figure 55 Profilometer measurements on the Wavy Featured disc.
U. Left: 2D representation and scale (2), U. Right: 3D representation in side view,
L. Left: Y profile for the points in (2), L. Right: X profile for the points in (2)

The surface topography of the discs indicates some primitive issues of concern regarding the experiments that will follow. Firstly, a lot of noise is expected in the data due to the roughness value. The manufacturing method is not optimal, as it introduces a lot of uncertainty about the accuracy of the measured values. On the bright side, a better understanding of the conditions of the experiment is available and can confirm the inability of the DMLS to produce curvy geometries. The data for all cases are presented in table 3.

Variable	Flat Disc	Ramp Disc	Wavy Disc
Sa (mm)	4.093	4.425	6.089
Sku	3.118	3.360	4.12
Ssk	0.01	0.07	-0.05
Sp (mm)	20.55	29.89	71.02
Sv (mm)	-23.95	-21.67	-39.10
Sz (mm)	44.50	51.55	110.12
Sq (mm)	5.163	5.627	7.771

Table 3 Surface quality variables measured with profilometer. Flat disc values are the average of the total points measured.

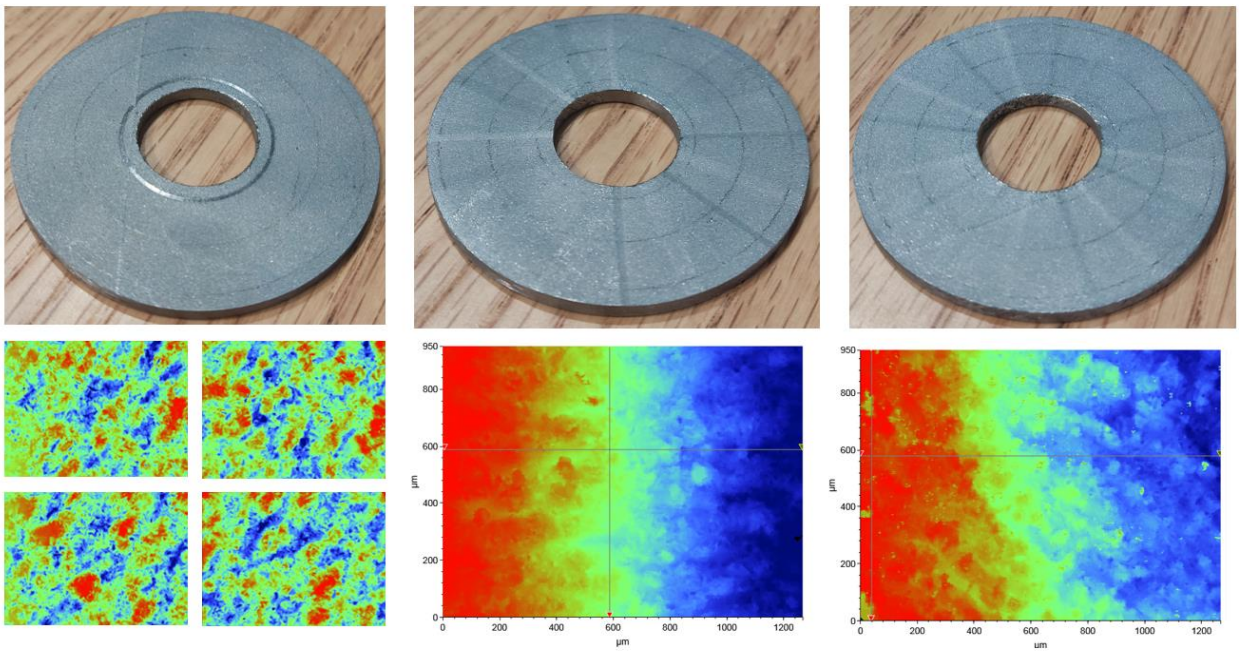

Figure 56 Surface comparison of all discs with Amplitude of feature =120µm, real model and 2D representation. Left: Flat disc, Middle: Ramp featured disc, Right: Wavy featured disc

4.3 Pin-On-Disc Experiments and Results

To evaluate the proof of concept, physical experiments are conducted on the Anton-Paar TRB3 tribometer. The specimens are cleaned from debris and dust, and every measurement set uses a new part of the sphere in contact. To minimize the impact of surface roughness, each disc is evaluated at 3 different radial coordinates (12.5–20–27.5 mm) and at 3 different rotational speeds (25–50–100 rpm). Each test has a duration of at least one minute, and the normal load is constant and equal to 1 N.The force was chosen after experimenting with different loads based on the non-disruptive performance of each load. Specimens must be tested in a non-destructive way to preserve the 3D nature of each geometrical feature.

Before conducting any experiment, the rig is prepared to reduce the error factor by leveling out the chuck and calibrating the sensors. The tribometer setup allows for accurate knowledge of the vertical load as the rig is balanced before its application by counterweights. Additionally, radius and speed setups are conducted, and the radius is controlled by a linear sensor, also tested during the setup phase. For the experimental procedure, the force reaction on the load cells of the tribometer must be stabilized during the one-minute total duration of each measurement. In most cases, the CoF reached a stable value within the first few seconds, but the experiments were carried out normally for the full duration. The data collected from each test are then compared using custom MATLAB tool to obtain further information. The tool has the ability to filter the data-points, using a moving average filter, which is proven useful, as experiments - especially the ones on higher speeds - induce a great amount of noise. The filtering process aims in reducing redundant disturbances and to provide understandable graphs with smooth curves. This does not necessarily relate to excluding disturbances of the experiment completely, as the qualitative characteristics of during the contact phase should also be exhibited. Smoothing out the data completely would deliver a linear curve, equivalent to the mean CoF value, something that blocks valuable information from the results.

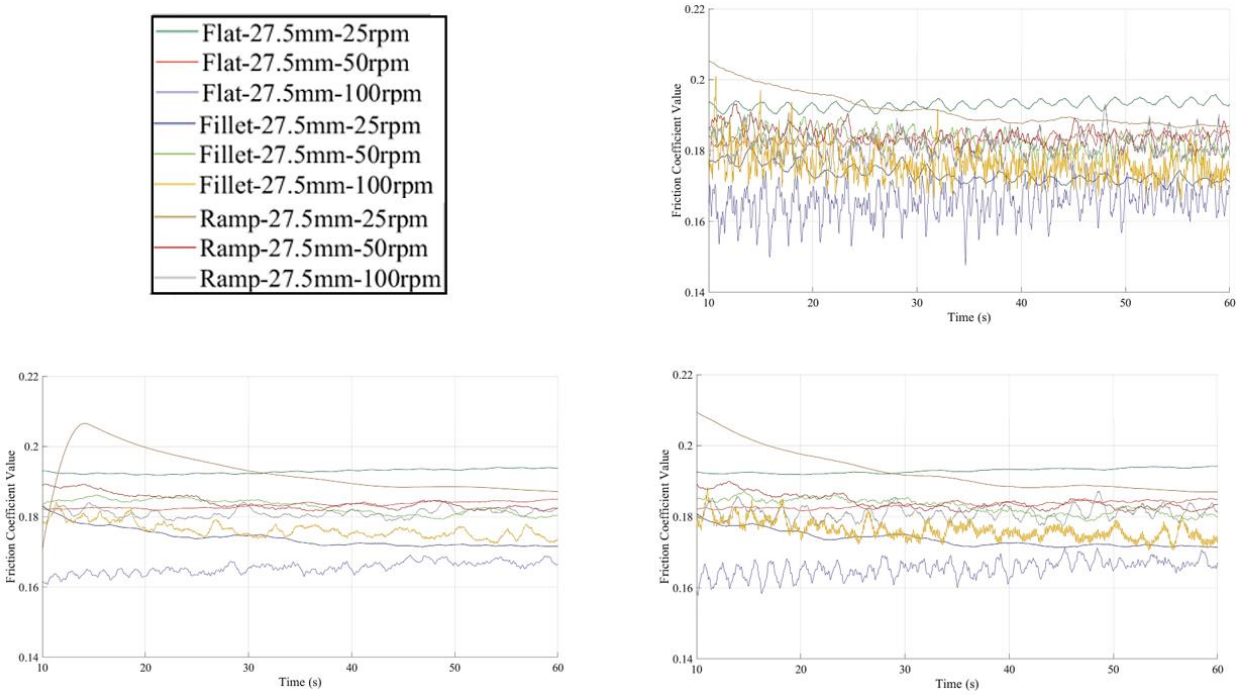

Figure 57 Filter application on all discs measurements at R=27.5mm.
U. Left: Cases shown, U. Right: filter 18, L. Left: filter 58, L. Right: filter 38

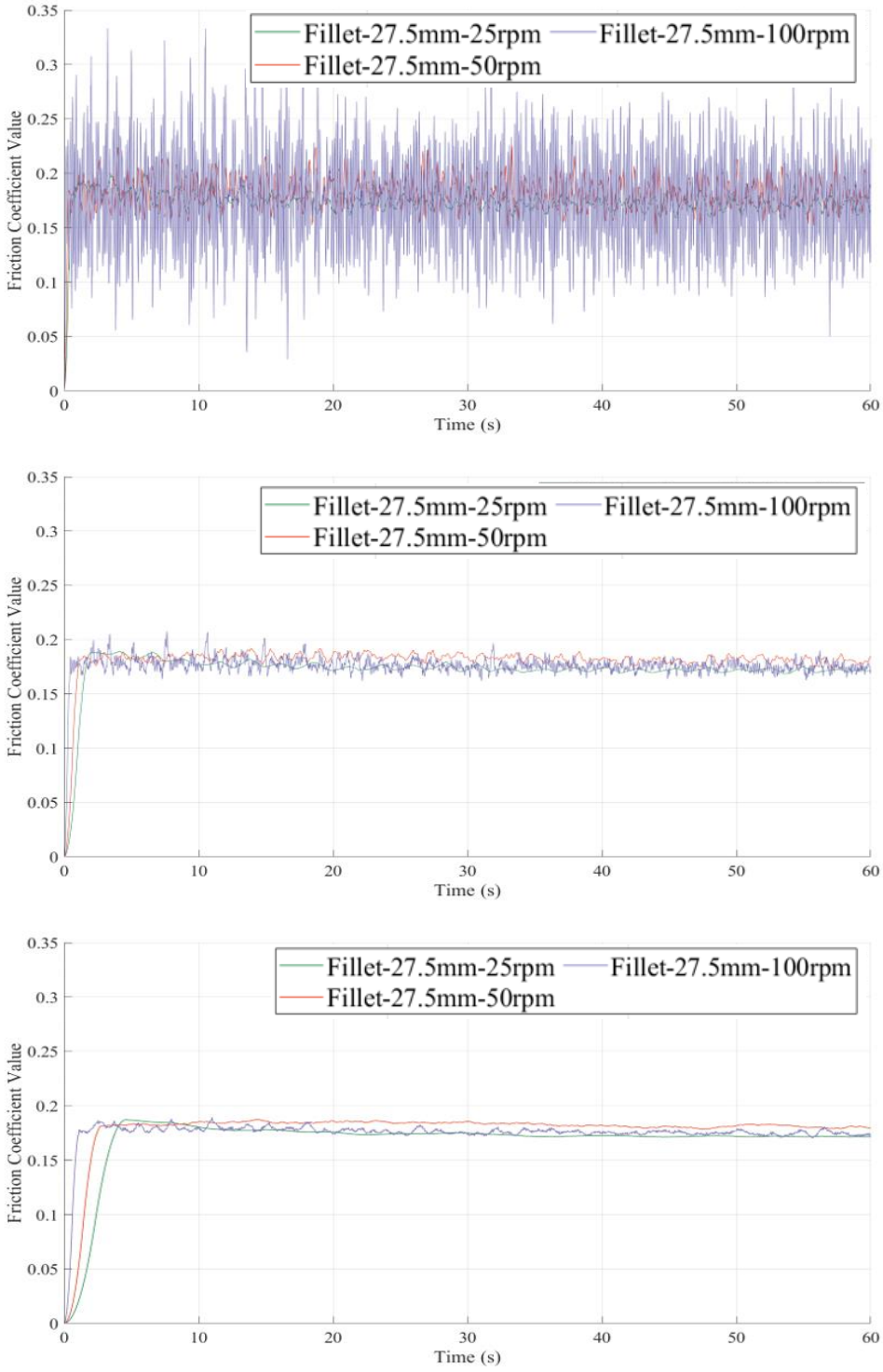

Figure 58 Filtering process on the Fillet featured disc, at R = 27.5mm.
Upper: filter 5, Middle: filter 25, Lower: filter 55

It is evident that the filtering process must take place to extract conclusions, as data are plummeted with noise. One other aspect of the filtering process can also be observed from the plots 57 & 58. The noise is not proportional exclusively to the rotational speed, but also varies for different radiuses. As the radius increases, linear speed at the point of the contact is the product of the two variables, thus little to no noise is expected for slow experiments in low speeds, and rather disturbed ones for points near the outer diameter of the disc that move in high speeds. This observation is further captured in figure 57, where 3 distinct moving average values have applied to the data. Each plot corresponds to one of the values 18, 38, 58 chosen for the filter. Although the curves appear smooth using the 58 filter, and relatively good for the 38 filter across all experiments, they cannot be considered suitable for every application. For slow experiments, the filters flatten the oscillations during the experiment and may even move the curves across the timeline as in the case of the 58 filter on the 25 RPM sets. Filter 18 on the other hand, fails to deliver an understandable image for higher speeds, yet it captivates the essence of slower ones. For this reason, different filter values should be chosen for different speeds, and plots describing data from different rotational speeds may have a different quality across the curves. Figure (next next) presents the values from the experiments on the flat disc for the nominal load of 1N, and the filtering effect on different speeds can be also observed, as the data were treated in the same way, to indicate the vibrations in higher velocities.

From a qualitative perspective, results for all experiments indicate two phases for each test run. In the first stage, the CoF is rising, which is a result of the speed control process of the motor until the nominal angular velocity is chosen. Measurements in this zone should be neglected, as the pin is also in a transient contact state, and the larger asperities are smoothed during the initial passes of the pin to a more uniform size distribution. The second zone is the zone of stabilization, where the load cell reaction remains constant with low fluctuations. The lateral force is quickly stabilized and remains near constant for the majority of the experimental time. The latter is important as it indicates both the presence of features in the form of fluctuations and steady experimental conditions. The experimental data suggest a great amount of inconsistency throughout the experiment. Those inaccuracies can be attributed to a variety of factors, yet a rather stable behavior should have been expected instead. First of all, the surface roughness of the specimens can be attributed for most of the inaccuracies. It bears double impact, as it affects both the surface in contact and the overall positioning of the disc in the rig. The backside of each disc is designed flat, but for many tests, the placement onto the chuck holders often exhibits a slight joggle, contributing to the deviations.

Tests are considered failed when the specimen becomes loose, leading to a force reaction incensement, which can be attributed to lateral pin contact in the direction of motion, thus increasing load cell reactions. To mitigate this, the discs can be subjected before future tests to grinding process to ensure a secure fixture on the rig and provide substantial thickness derived from the chuck teeth. The circumference of each can be further processed for finishing passes using lathe machining to ensure cylindrical tolerances.

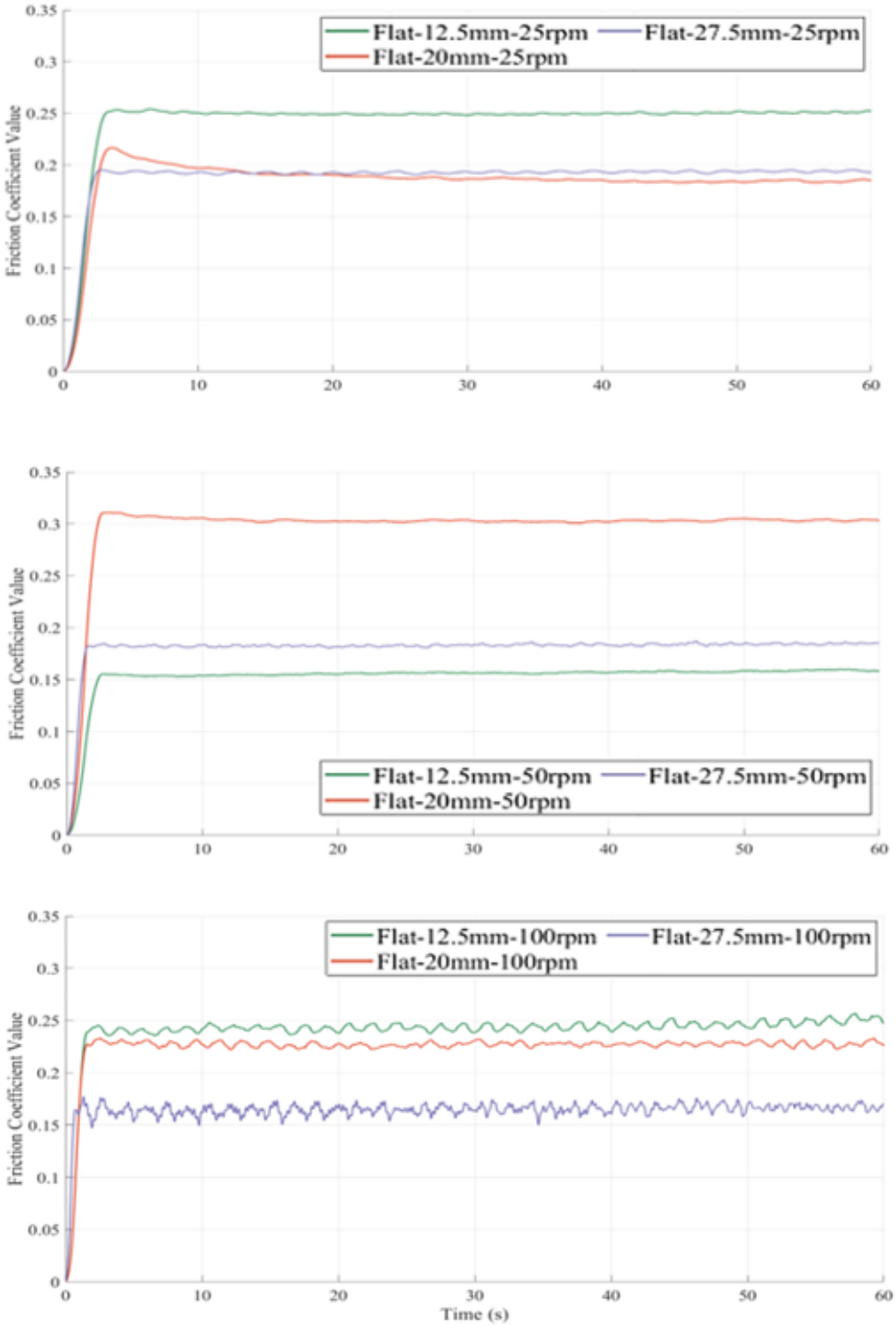

Figure 59 Data for flat disc - all cases.
Upper: Speed = 25RPM, Middle: Speed = 100RPM, Lower: Speed = 50 RPM

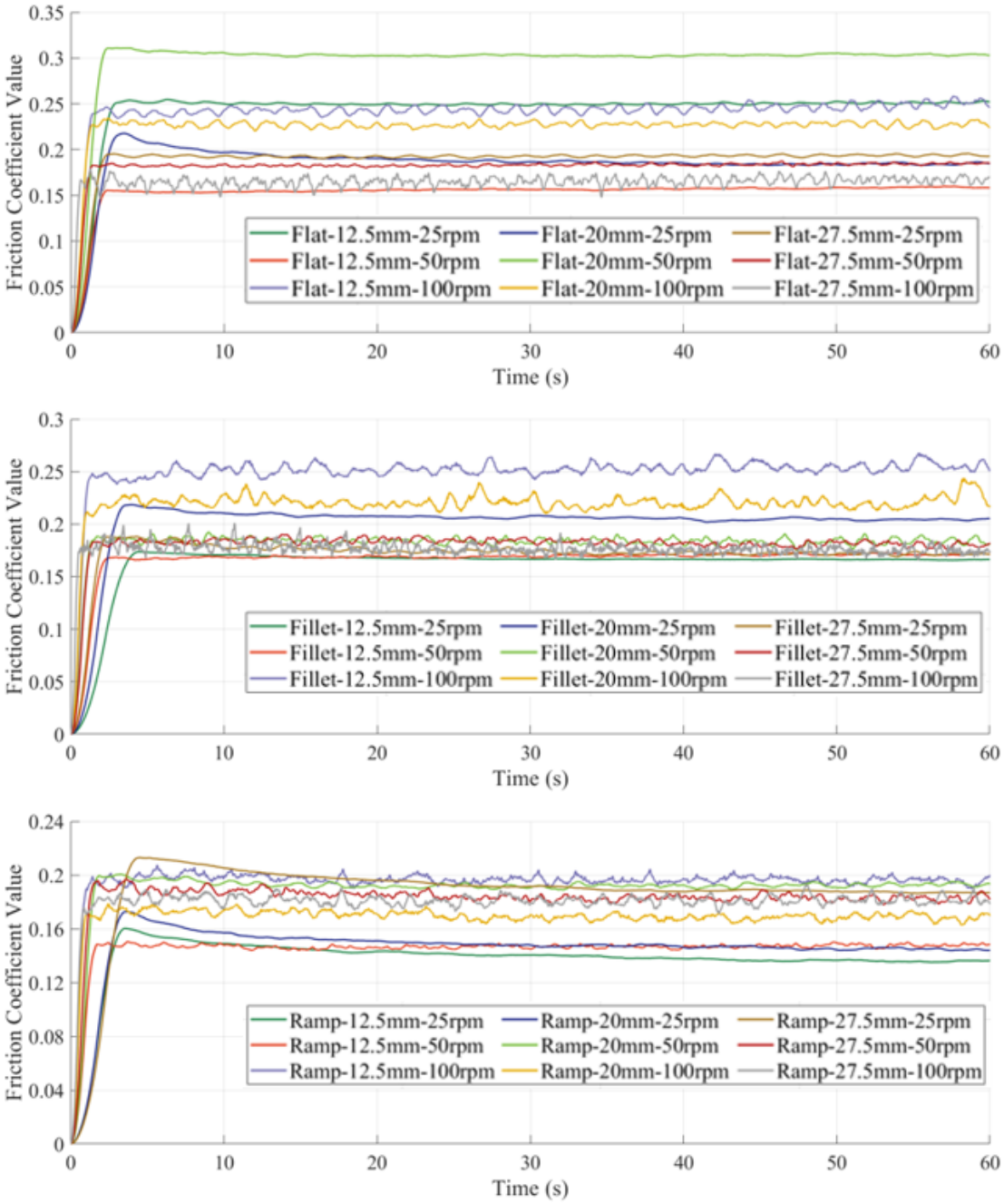

Figure 60 Data for all Cases, same feature per plot.
Upper: Flat disc, Middle: Fillet featured disc, Lower: Ramp featured disc

As already seen, data acquired during the testing phase are not completely accurate. In this section they are further compared into different sets of plots, each one introducing some common properties, ex. constant radius and/or rotational speed. In this way different features are compared on the same graph, and may reveal some insights on the overall performance of each disc, regardless of the faulty data points. The Flat feature had the greatest fluctuation in CoF values between different experiments, while the Ramp feature presented a rather stable state, yet not entirely desirable, as still some sets should be carried over again. Due

to cost limitations, only one disc was manufactured for each feature, and no grinding was feasible. The plots in figures 61 & 62 are created using the same filter value per plot, which once again indicates noise incensement along with linear speed of the contact point. No pattern can be noted from the constant feature & radius plots, yet for speeds of 50 and 100 RPM, values tend to exceed 0.2, while for 25 RPM values are mostly near that limit.

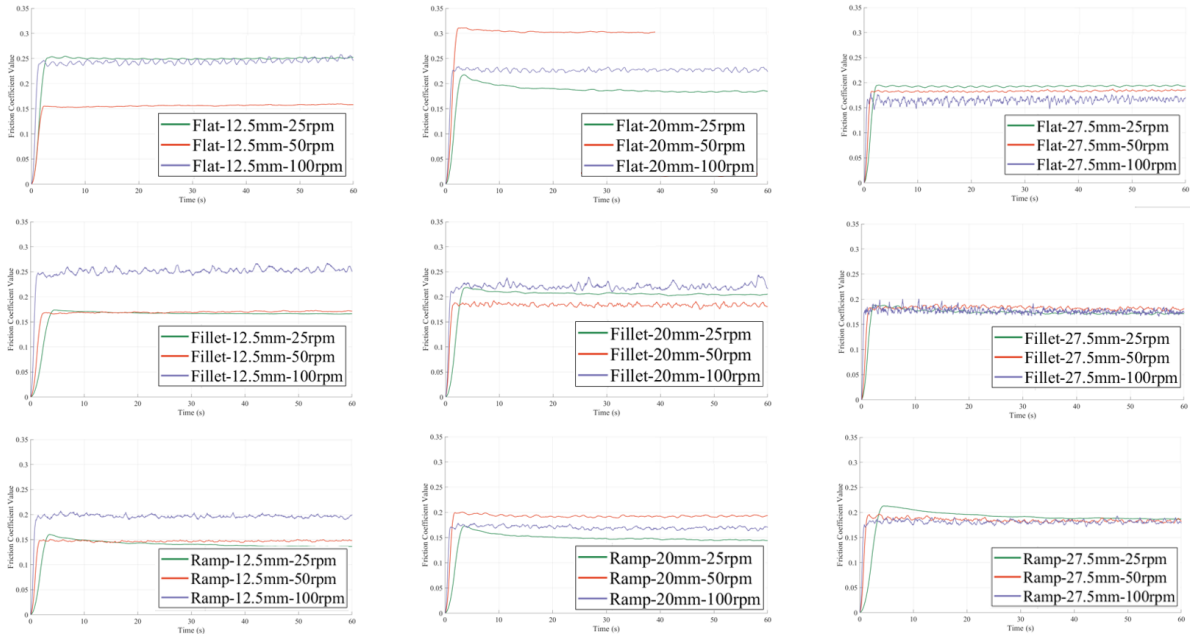

Figure 61 CoF data for all cases, grouped per feature and radius

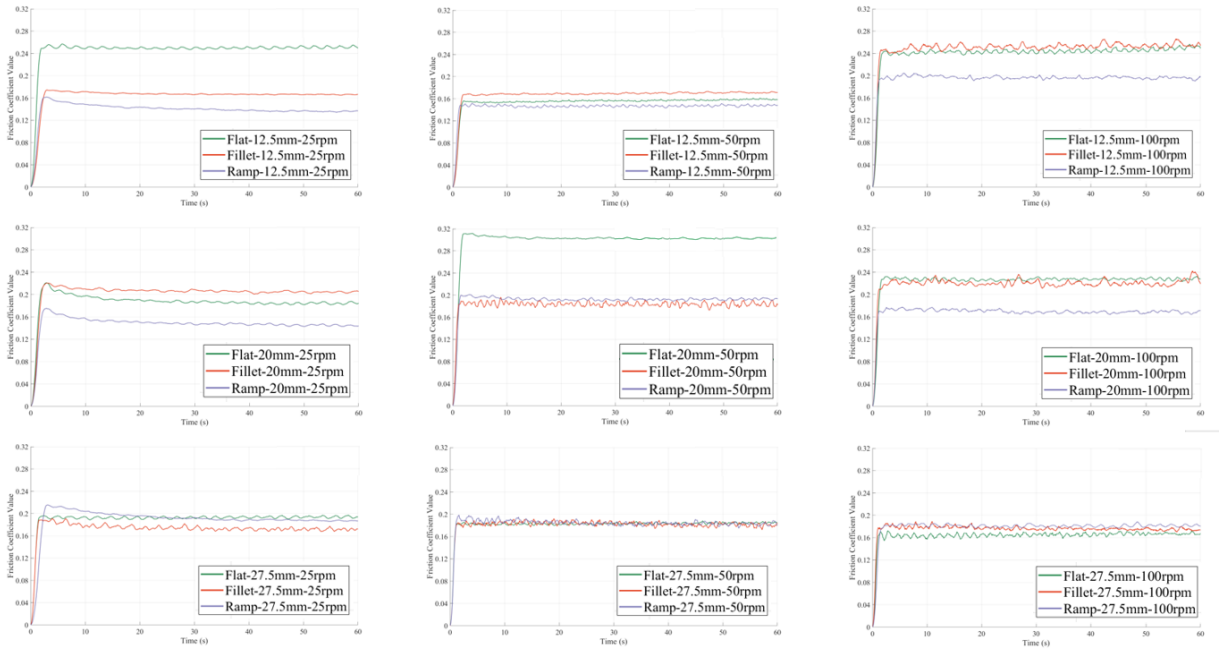

Figure 62 CoF data for all cases, grouped per speed and radius

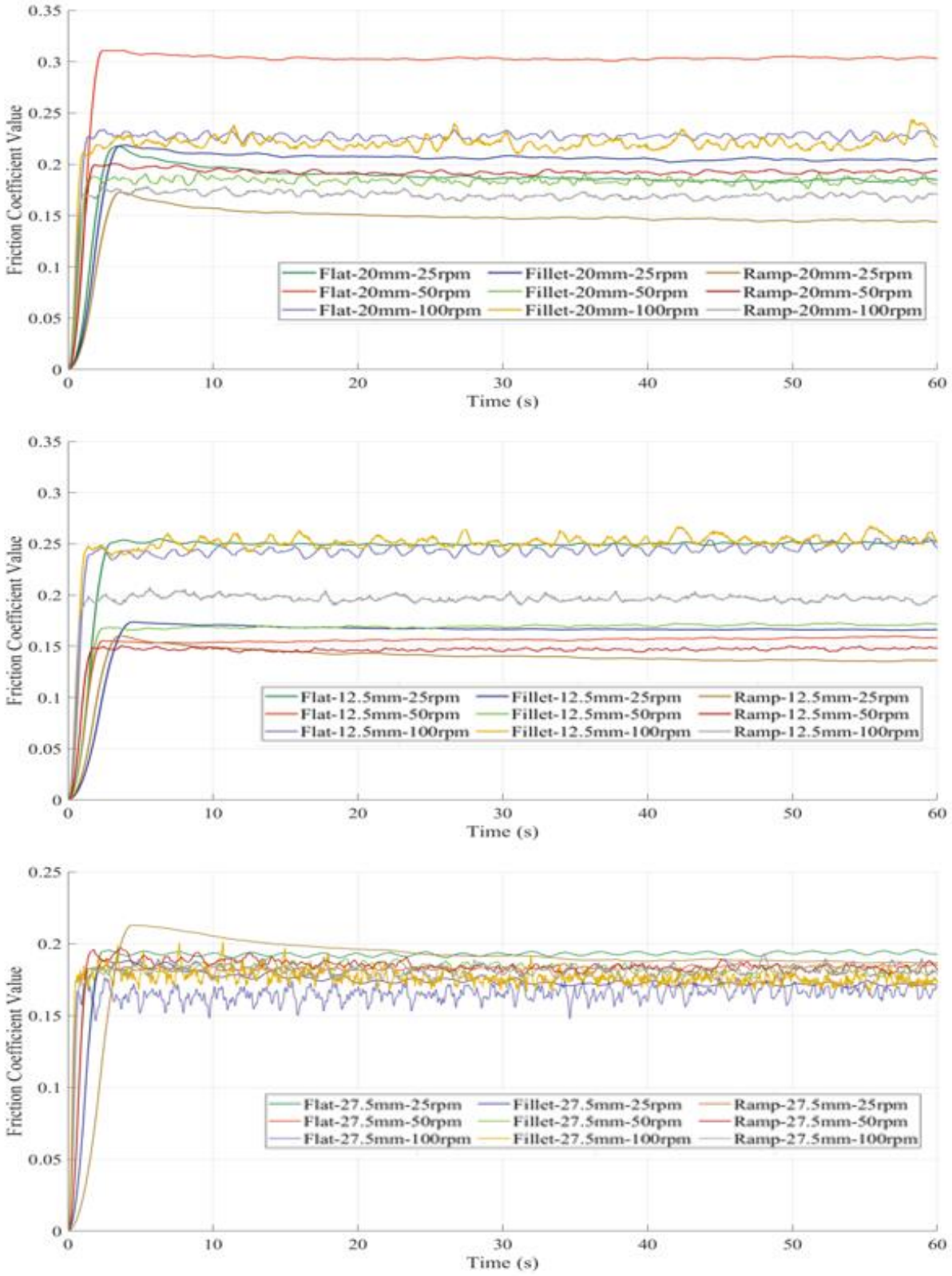

Figure 63 CoF data for all cases, grouped per radius. Upper: R = 12.5mm, Middle: R = 20mm, Lower: R = 27.5mm

When comparing the features using constant radius & speed, features have different behavior on each experiment. Combining figures 61 – 63 the proper coefficient is around 0.18, as many experiments indicate values similar to that. Using this information, the plots of figure 62 can be assessed, targeting the 0.18 value, and excluding plots or features within plots, that may deviate a lot from that either positively or negatively. In general, ramp feature appears to be improved to the fillet one. For the flat feature, conclusions are hard to be made, but the few times values are probably in the correct margin, they are a tad lower than the corresponding ones for the other two features. This is only a preliminary conclusion, as the data for the flat configuration are corrupted from misplacement on the chuck, along with other parameters. Besides, the flat disc was thinner in comparison to the other two, something that clearly has an impact using that specific rig. In figure 64, the CoF zone [0.10-0.20] is presented for the stable part of the experiment, where blue lines corresponding to the Ramp feature, do tend to be above the green ones (Fillet feature). The Flat feature appears somewhere in between, definitely lower than the ramp feature, but this is not a certain conclusion, for the reasons already explained.

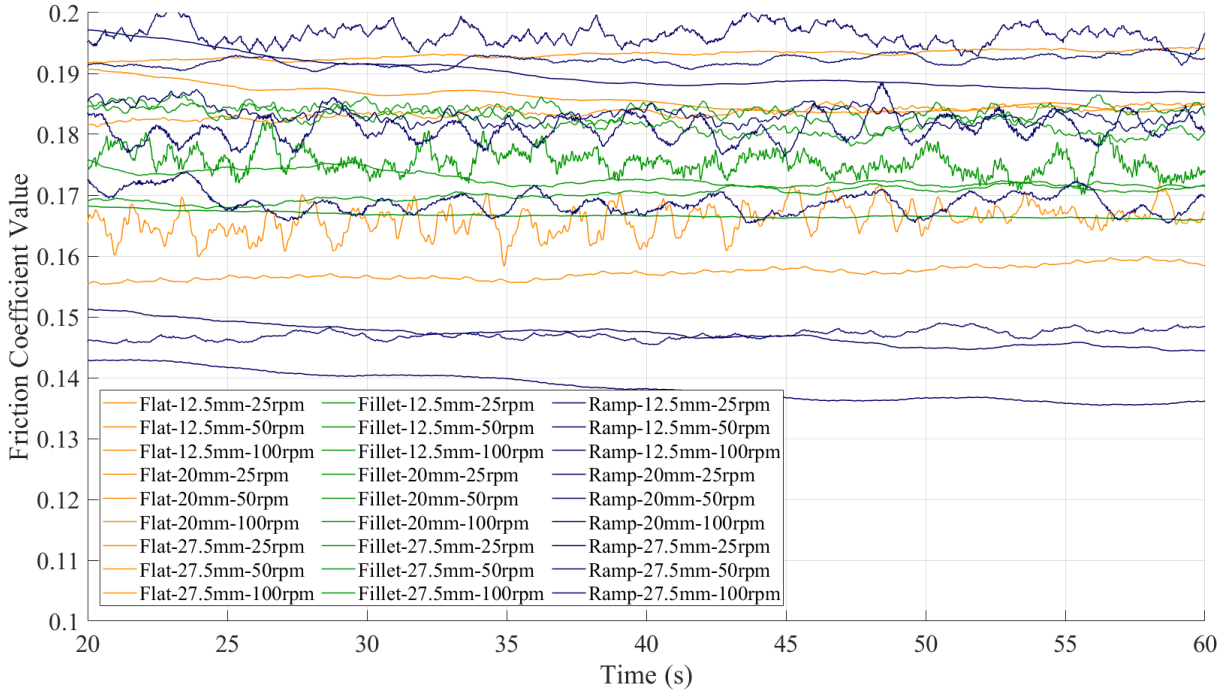

Figure 64 CoF for all cases, quantitative comparison near expected physical vaues

The experimental investigation has come to the end. Although results were not always of the best quality due to reasons already described, an attempt for the proof of concept has been made. Featured discs should undergo a surface treatment for future experiments, and increased thickness of the specimens may also aid in better convergence of the CoF across all conditions. Figure 64 indicates a slight improvement for the Ramp feature over the other concepts, but a hard conclusion cannot be made due to the disturbed nature of the datasets, yet focusing on the [0.16-0.20] area, Ramp features seem to present an improved average value of the desired properties. Based on chapter 3.3, the improvement should be in the range of 0-3%, proving that the experimental conditions are to blame. Furthermore, the experiment is pin-on-disc, which by its nature cannot represent braking phenomenon, as the pin is free to oscillate along with the feature, thus bending effects are minimal. Disc-on-disc experiments with greater nominal load might be able to improve

the accuracy of the results, and deliver higher quality for the contact, taking into account the entire span of the feature. Future research involves finer tuning of the experimental conditions for consistent results, and the possibility of extracting the proof of concept and the improvement of the CoF.

4.4 Design of A Novel Low-Cost Disc-On-Disc Test Rig

The final part of this thesis describes the steps and decisions during the design of the custom disc-on-disc test rig, which incorporates low-cost manufacturing methods along with other valuable features, such as low maintenance and easily assembled parts. The goal of the design is to create a rig that offers the ability to control angular velocity during the experiment, to provide an increased range of vertical height choices for the disc, and to allow movement of the rotating axis for setup. To ensure maximum adjustability during experimental sessions the discs used must be quickly replaceable, and the same applies to the vertical load chosen.

Most of the parts are custom designed and opted for CNC manufacturing in the prototype phase. To minimize cost, each self-designed part is created to be suitable for easy manufacturing, low cost of raw materials, and easy assembly. The rig must be capable of measuring lateral force reactions in a plane perpendicular to the rotation axis, and finally, the total stiffness must be adequate to minimize sensitivity errors during measurements. For the reasons described above, the complete assembly will be presented, considering both the static and the moving parts, as well as the sensors and control unit required for the operation. Standard bolts are used and the majority of the parts is made from aluminum, as loads are relatively small and it easily available in the market.

4.4.1 Goals and Constraints

The aim of the design is the delivery of a fully working prototype tribometer concept for disc-on-disc friction measurements. The manufactured rig should be able to produce satisfactory results for a range of different conditions and materials. The desired measured quantities are the lateral force reaction of the fixed probe (Load Cell) and the input moment of the used motor. The device should not be complicated, must be easily transferable by one person, i.e., have a low weight, and must incorporate three distinct positions for the main lever, equivalent to the Anton-Paar design, to allow for distinct setup and measuring states. Additionally, it must incorporate a pivoting mechanism to prevent overstressing of the specimen and adjustable counterweights for setup. The final goal of the design is to utilize innovative elements and select materials to reduce manufacturing costs and lead times. Based on the given goals, the rig must comply with geometrical and functional constraints. The device must have small dimensions to enable its use in almost every environment. A mechanism to adjust the plane of support should be used to ensure the flatness of the two discs, and the range of motion of each component must be limited either by fixed conditions or positive stops of some kind. Friction materials should only come into contact on their designed contact faces and avoid lateral collision at all times, while no parts other than those intended should come into contact while working with the machine. Furthermore, all parts included must be properly assembled to ease access to the tooling required for quick adjustments.

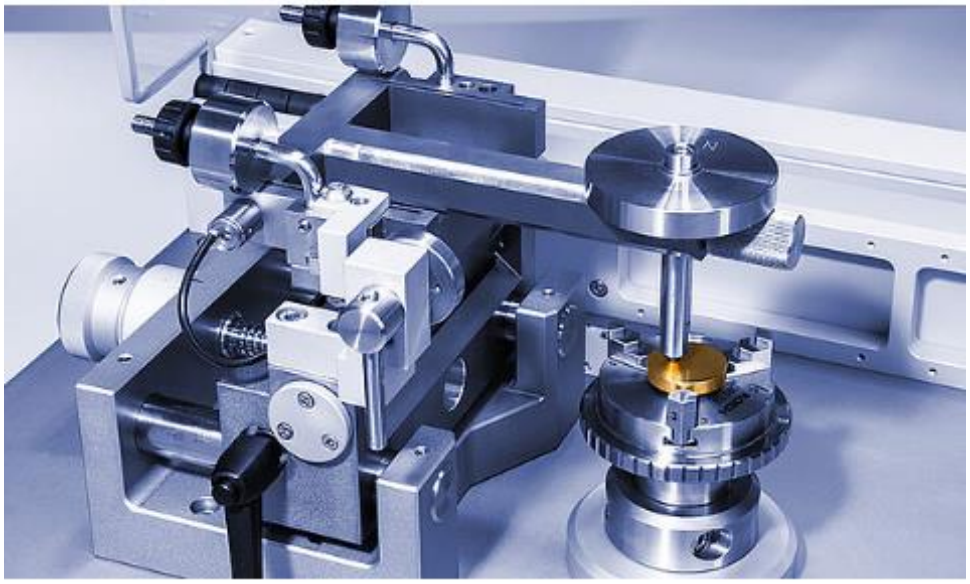

Figure 65 Anton Paar TRB3 Pin-on-Disc Tribometer

The working principles of the experimental rig will be now presented, along with a closer look on the final 3D design. To ensure the best fit of all the aforementioned parameters, the assembly is composed of two main entities: The Input Assembly and the Fixed Assembly.

- The Input Assembly contains the rotating disc specimen, the DC Motor, and the parts that enable the correct positioning of the disc in place, and also the rotation of the disc.
- The Fixed Assembly is composed of a cylindrical assembly that is constrained by a measuring load cell on one side and free to move on the other direction.

Both entities are bolted to the base plate, which can be adjusted to ensure flatness. In contrast to other designs shown in market analysis, this rig is used for disc-on-disc analysis, and the rotating moments are greater than the ones expected on the fixture of the TRB3 pin-on-disc rig. The rig uses 2 discs, one attached to each assembly; The motor-driven disc (RD) and the friction-driven disc (FD) which is fixed. The FD is constrained in XYZ motion by the Fixed Assembly cylinders. It is also constrained relatively to its housing by the preload of the bolts used for attachment, or only by the bolts if they act as pins passing through the disc. The full assembly of the custom design is presented in the figure 66.

The axis of the FD is supported by spherical bearings, and a pin is mounted eccentrically and perpendicularly to the axis of the bearings and can come into contact with the Load Cell (LC). The pin has fixed length; hence the measurement of the LC can be converted into input torque from the Contact of the two discs. The bearings introduce error into the measurements due to friction inside the elements and possible misalignment of the housing pockets but this can be mitigated by correct lubrication and good manufacturing tolerances. A separate bracket mounted on the bottom plate is used to mount the load cell which is parallel to the pin. The mount of the LC is designed so that the measuring device comes in contact only with the pin. This results in the transfer of vertical forces in the direction of the measurement and the LC is subjected only in bending, ensuring the correct measurement through the strain gauge bridge. The bracket and its mounting plate (vertical) have adequate stiffness and they do not influence the data.

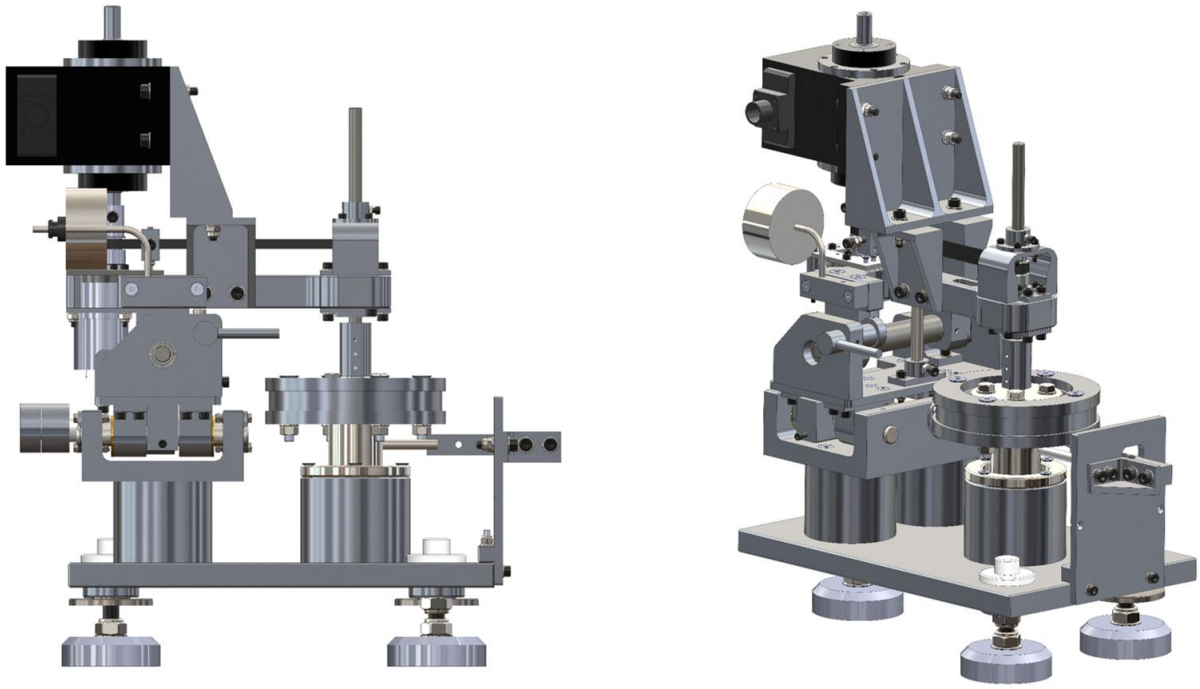

Figure 66 Complete custom tribometer design, Side & Isometric Views

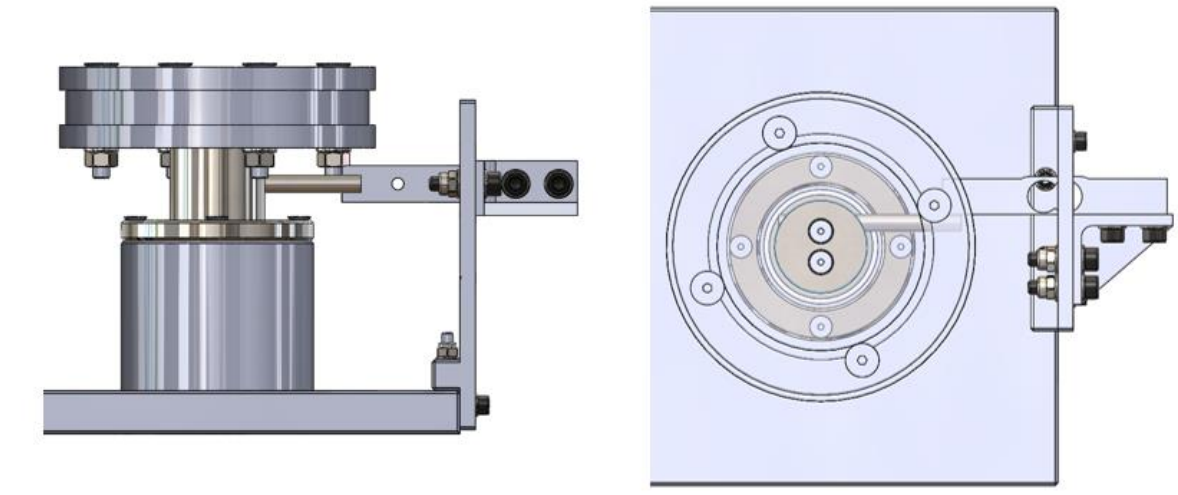

Figure 67 Fixed base and load cell attachment for custom tribometer, Side and Top Views

The Input Assembly consists of two (2) separate subassemblies responsible for the RD mounting, positioning, and driving. Those are the Main Lever (ML) and the Moving Base Assemblies respectively. The RD is connected to the ML assembly using a custom-designed coupler, and be adjusted in height according to disc thickness, to avoid overstressing into the contact. The coupler is fixed in XYZ movement by 2 bearings, which are then mounted on the ML using aluminum brackets. The ML assembly can pivot enabling tool access to the RD for any setup needed. The pivot axle is made of steel and is mounted on the

MB assembly. The latter can move linearly to set the position of the axle of the RD exactly in the center of the FD, or slightly eccentrically, if it is required by the nature of the experiment.

The MB assembly consists of the fixed Pi-shaped base and two (2) linear motion shafts are rigidly mounted on the latter. The shafts are used to support the MB plate and allow for smooth rolling and a trapezoidal threaded shaft is used to control the position of the MB plate. The pivoting shaft mounts are bolted on the plate, which on top of which the following parts are mounted: The positive stop of the linear motion, the positive stops of the ML and the safety stop axle, which is used to prevent damage due to excessive wear in the disc. The linear motion mechanism is based on brass bushings with free tolerance with the shaft, fitted into brackets under the MB plate. To constrain the motion of the ML two aluminum blocks are positioned on the plate, which are designed to contact the back of the lever when it is pivoted excessively.

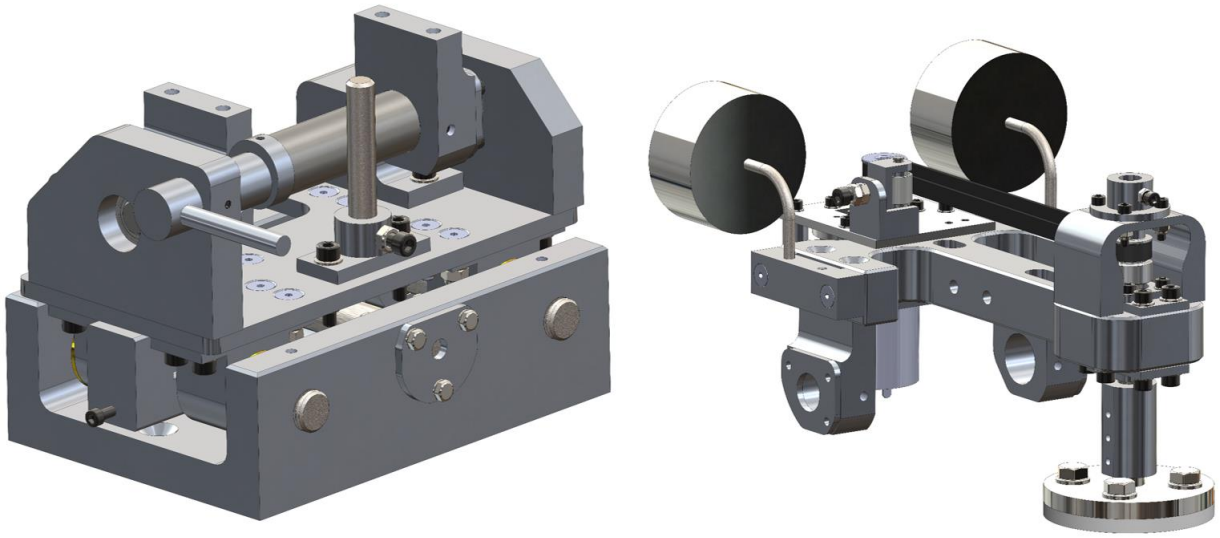

Figure 68 Main Base and Main Lever for custom tribometer, Isometric Views

Apart from the components used for the mounting of the discs and the rotation, the system also contains electrical units responsible for the movement and tracking of the RD. A DC motor is connected to the disc coupler using a belt and pulley system with no slip. This machine element is chosen due to its ability to connect two rotating bodies positioned at remotely from each other (in contrast to gear connections), can be assembled easily, is lightweight and furthermore very reliable. The motor is mounted on the ML to allow for pivoting without stretching the belt. The motor is one of the heaviest components thus it is positioned near the ML axle to reduce bending moments. The belt is pretensioned using an adjustable idler to ensure accurate power transfer at all times. The balancing counterweights are mounted on the ML and also the torque-measuring transducer, mounted on the rear side to provide direct measurements of the motor input torque and speed.

Based on design, the testing rig includes miscellaneous features to further improve its functionality. During the setup phase of the experiments, the user controls a cam lever that set the ML to the off, standby, or on position, equal to the Anton Paar design. The ML is positively stopped from excessive movement due to wear by an adjustable pin positioned between the steel axle and the FB. To restrain the linear movement, a handle is attached to a stopping block actuating on the rail, while a double-cylinder handle is used for the position tuning. Finally, the design of the coupler and the fixed assembly takes into consideration future improvements, all components can easily be replaced with new designs to fit wet friction experiments

involving liquids. For the purposes of this thesis the fluid adjustment is not designed, yet the mounting of the FB housing using bolts allows for design freedom if the rig is updated furthermore. All in all, the rig designed covers the requirements set in the start of this section and accounts for possible problems during function which are eliminated. The detailed design of each element allows smooth movement or steady fixtures when required respectively, and the user can easily understand the working principles and the setup options.

4.4.2 Range of Application – Motor Selection

To enable greater adjustability, the rig allows the use of different disc designs, thicknesses and materials. The application range of the rig is derived from two parameters, the components' DoF and the input load range. Firstly, the movement range both linearly for position and angularly for the rotational velocity of the disc allows the correct positioning and speed specified by the user. The application range is expanded considering the available load range, which is chosen to be greater than the ones met on pin-on-disc designs. Specifically, the Anton Paar holds up to 10N normal, while this design allows up to double of that.

Range of motion and angular velocity: The rig is not intended for pin-on-disc tests, which usually require a wide range of linear motion to position the pin in different radiuses. The range of movement is 5.5mm ambisymmetrical to the center position (11mm total) defined as the point where the coupler and FD axles are coincident. This range enables the user to test eccentric scenarios, useful for smaller RDs. The angular velocity ranges from 0 to 500 rpm, which is chosen to reduce cost and weight, considering the mounting method of the motor. AC motors are not suitable given their excessive size and weight as the rig would be bulkier in size and weight. Voltage is set to 24V and angular velocity is controlled using Pulse Width Modulation (PWM), which is a very reliable and economical method to control DC motors. The motor chosen is able to deliver the maximum expected torque of the friction pair.

Range of measurements: The rig must be able to measure up to 1kg of lateral force reaction at a lever of 50mm. This torque depends on the normal force applied by the user, the Area of the frictional contact, and the friction coefficient under examination. The maximum load of our tribometer is limited to 15 N of vertical force applied under normal conditions and 20 N for materials with low COFs. For reference, the Anton-Paar tribometer can be loaded up to 5 N vertically, regardless of the material of the specimen. The load is applied by premade discs placed on a steel pin that is attached to the ML directly above the coupler. Disc are added using O-rings to reduce vibrations and noise.

Based on the requirements described, the working parameters of the DC motor can be calculated. The required driving moment is calculated based on the surface of friction and the vertical load. Assuming the vertical load F_{load}, the pressure p is uniform across the entire surface, and uniform CoF μ_k, the required moment on the coupler side is calculated as follows:

$$M = \int_A dM = \int_A \mu_k * p * r dA$$

$$M = \mu_k \frac{F_{load}}{\pi(R_o^2 - R_i^2)} * \int_{R_i}^{R_o} r * (2\pi r) dr$$

$$M = \frac{2}{3}\mu_k F_{load}\left(\frac{R_o^3 - R_i^3}{R_o^2 - R_i^2}\right)$$

Where:

- R_o, the outer radius of the friction area
- R_i, the inner radius of the friction area

Assuming a 99% efficiency on the belt assembly, the required moment of the motor is equal to:

$$M_{motor} = \frac{100}{99} * M = \frac{200}{297}\mu_k F_{load}\left(\frac{R_o^3 - R_i^3}{R_o^2 - R_i^2}\right)$$

Given Ro = 30mm, Ri = 5mm, Fload = 15kg, μ_k = 0.6 in the most extreme scenario:

$$M_{motor} = \frac{200}{297} * 0.5 * 15\left(\frac{0.03^3 - 0.005^3}{0.03^2 - 0.03^2}\right)$$

$$M_{motor} = 0.1861\ Nm = 1.861\ kg.cm$$

The motor selected is the JGB37-3530 with a nominal voltage of 12 V at 333 rpm, producing 1.14 kg/cm of torque and a Stall torque of 4.5 kg/cm. The selected gear motor is extremely economic, features an all-metal casing with a metal gearbox and reducing ratio of 30:1. It weighs 180 gr, is relatively small in dimensions, can be mounted using a maximum of 6 M3 bolts, and uses a 15mm 6 axle with 12mm of flat morphing for its connection. It is evident that the angular speed is below par with our goal, yet the motor is an extremely low-cost solution for this prototype phase and can be rotated up to 400 RPM with a small overvoltage. A simple PWM controller can be used, and the size of the motor allows its replacement with similar or more powerful ones from the market without increasing the price. Alternative motors with similar specifications are:

RS PRO Brushed Geared 834-7663 with nominal specs:

- Voltage = 12V
- Maximum Torque = 1.482 kg.cm
- Angular Velocity = 431 RPM (up to 539)

RS PRO Brushed Geared 834-7672 with nominal specs

- Voltage = 12V
- Maximum Torque = 3.024 kg.cm
- Angular Velocity = 537 RPM (up to 671)

Figure 69 Alternative motor selection. Left: JGB37-3530, Middle: RS PRO 834-7663, Right: RS PRO 834-7672

Both motors feature similar dimensions, a 6mm axle, and M3 bolt attachments. To ensure that the motor is easily replaceable, the mounting plate to the main lever is manufactured with SLS 3D printing from ABS, and the motor is bolted from the top side. The plastic plate is reinforced with an aluminum plate and spacers to increase the bending stiffness and minimize stresses on the plastic. Additionally, the M3 bolt pattern on all motors is the same, allowing for quick replacement, if the user wants to increase the capabilities of the rig for bigger loads. The final motor and its mounting of the motor can be seen in figures 69 & 70.

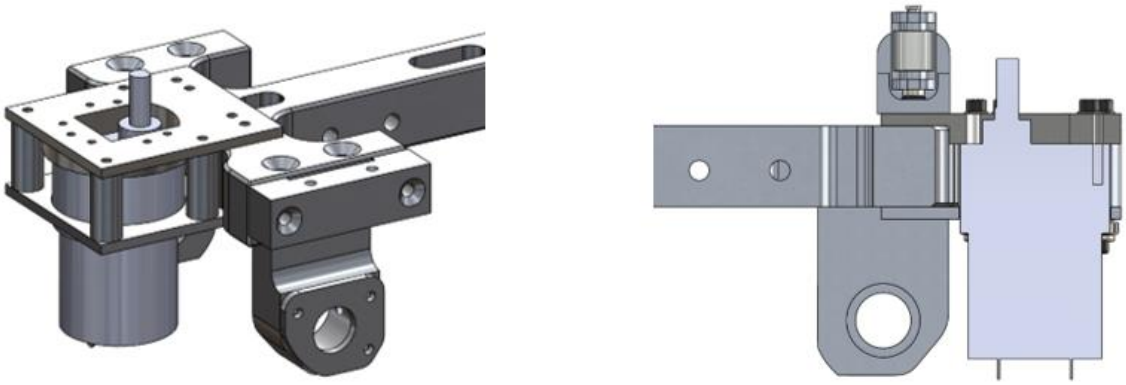

Figure 70 Motor mounting method for custom tribometer, Isometric and Side cross section Views

4.4.3 Measuring Devices

The main goal of each experiment is to measure the lateral force reaction from the friction moment transferred through the pin. To achieve this, an OEM Strain Gauge Load Cell is used with a measuring range of [0, 1] kg. To extract better accuracy, the load cell is positioned in parallel with the pin. The LC is mounted on a separate bracket, which has been simulated using FEA to define geometrical thickness based on the stiffness objective. The LC has a proportional gain to the applied strain, incorporating Wheatstone bridge formation with four strain gauges.

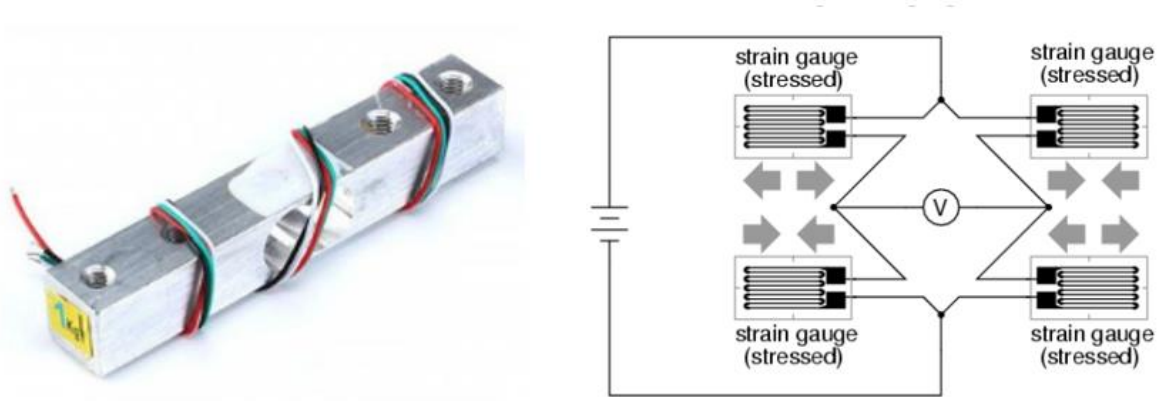

Figure 71 Left: Load Cell used for custom tribometer
Load Cell OEM for custom tribometer, Right: Load Cell electrical working principle (A. Bhattarai).

To improve knowledge of the state of the system at all times, a torque transducer is attached to the motor side using a custom coupler. The selected transducer is the Magtrol 415-304 from the TM Series. With nominal rated torque of 1 Nm, and the maximum speed at 6000 RPM with an error margin of less than 0.1%. The model is selected due to its availability ignoring its big size and heavy weight. This device is used to gain additional information on the rotational speed and torque of our motor, as it is not directly required for the functionality of the rig. The additional information gained can be used for preliminary calculations to compare the theoretical values of CoF with the ones measured by the Load Cell. Regarding its mounting, the device is attached to the ML so that it can pivot along with the main motor. The mounting base of the transducer consists of three brackets, two on either side of the lever, and one bigger on top of them to attach the sensor. The brackets are connected using bolts through slots making the system adjustable for case of using different motors or small off-center alignments.

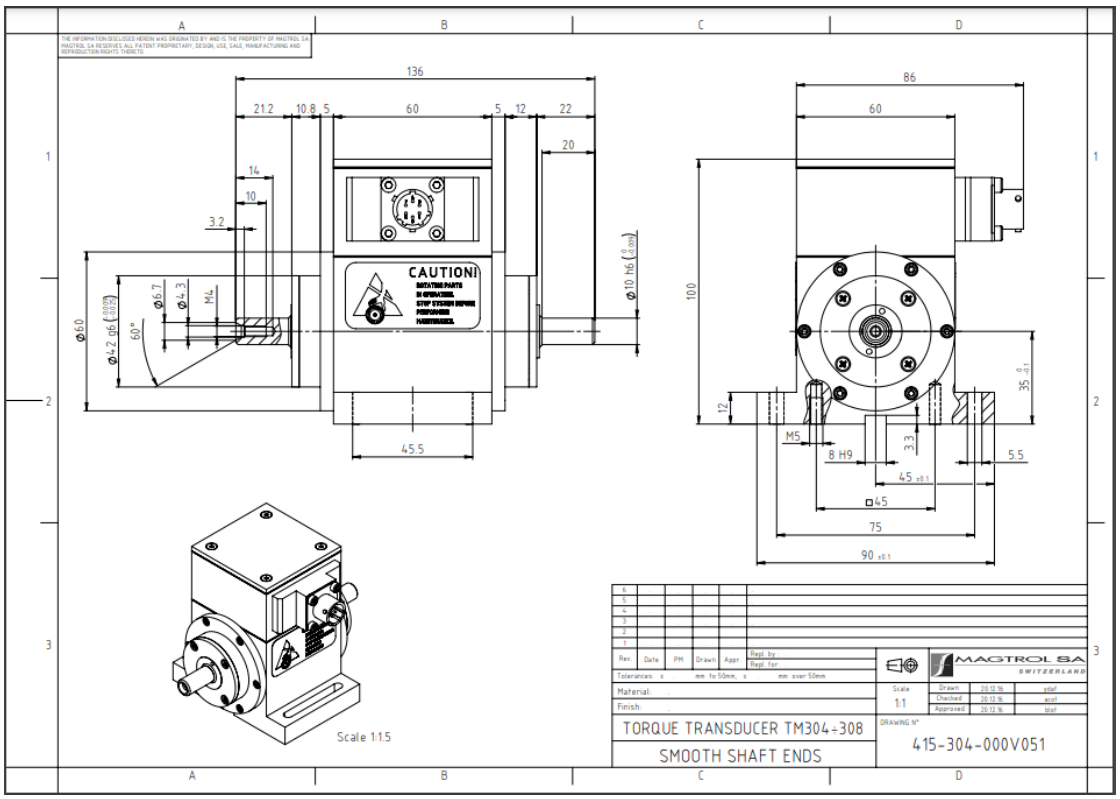

Figure 72 Magtrol transducer TM 304 mechanical drawing

Using those 2 measuring devices, and the PWM control, the state of the rig is known at all times. The difference in input and output torque can be calculated and plotted, and a module can be used to stop the experiment in case of extreme difference in values corresponding to an incident. The transducer also allows for accurate knowledge of the PWM output, and a separate module can indicate deviations from the desired behavior. Finally, given the transducer values, a fail-safe loop can be programmed to avoid overstressing of the motor, making the functionality of the system independent of the user. This is extremely useful, as tribological experiments often endure many hours.

4.4.4 Materials and Cost Reduction

In this entity, the cost reduction actions taken during the design of the experimental rig are presented. The actions are divided into 4 categories: Material selection, Manufacturing method, Bought Items, and Design Concepts. On some occasions, certain needs must be fulfilled making unavoidable a certain action, e.g. the rig requires a load cell, whereas on others the design concept is critical for cost reduction as it determines possible manufacturing methods and material selection, and may lead to unnecessary overspending if not properly thought.

From the design perspective, complex geometries are rejected and existing concepts are utilized. Excessive stress is geometrically prevented by the design, leading to an overall reduction in size and weight. For example, the bracket connecting the pivot shaft and the lever are designed with minimal length to prevent bending stresses without restricting the pivot motion with the motor mounted. The rail concept is manufactured using custom brass inserts to avoid expensive OEM market products. The same applies to

the off-center lever, the motor mount, and the load cell bracket. The entire fixed assembly is the product of a prexisting assembly while the Pi-Base and the Bottom Plate are designed to enable possible future redesigns. To further improve efficiency, many parts are assembled together using the same bolt for 2 brackets, e.g. transducer bottom mounts and bearing mounts.

In terms of purchased items, the motor choice for this prototype phase is based on the findings from 4.4.2. The OEM load cell and the motor are selected to guarantee system operation and can be further upgraded in future versions. The transducer is already available; therefore, a relative flexibility exists for the design and material selection of its mounting brackets. The motor controller makes use of Arduino PWM, which is a low-cost solution with easy customization.

The ultimate cost of the assembly can vary significantly depending on the manufacturing processes used. Since the rig is a prototype, milling and turning was chosen the majority of the parts. The parts' complexity is maintained as low as feasible, and CNC-milled parts are 3-Axis millable at the expense of weight over complicated 5-Axis designs. The pivot axle is connected to the main lever using bolts instead of a complex clamp. The coupler is divided into two simple sections to avoid using a complicated component, and the rail mechanism is based on brass inserts inside simple brackets. A flat 5mm plate is used for the MB, merely drilled and milled to shape. The ML consists of a single solid piece and requires re-attachment in the machine for drilling on flat planes, a rather simple procedure. The motor bracket is produced using FDM or SLA additive manufacturing technology, and it is further supported by low-cost components made by lathing. The adjusting mechanisms incorporate simple milled brackets and jam nut mechanisms, which are reliable under the given maximal working loads.

Materials' selection has an impact on manufacturing. Aluminum 6082 has good mechanical qualities and low density, making it the primary substance used. Low-friction low-cost materials like PTFE and brass are used for particular parts and connections. Due to its characteristics and incredibly low cost, ABS is employed in additive manufacturing in place of steel for important axles and shafts. Finally, the rig features some components that were designed with durability and rigidity requirements in mind. For instance, the Pi-Base needs to be sturdy to enable repeated use with zero plastic deformation allowed, thus expense on material was allowed. Overall the actions taken into the design allow for an assembly that is easy to produce, reliable and of extremely low cost. Expensive materials were avoided and clever concepts were chosen during the design phase to improve the economic and lead time parameters.

4.4.5 Tribometer Compliances and FEA Models

The critical components of the tribometer rig are defined as the ones that carry significant loads and are subjected to increased values of bending and/or shear stress. Starting from the rotating disc, those are the coupler shafts, the bracket carrying the test weights, the ML, the pivot shaft, the pivot shaft mounts, the MB, and the rail shafts. Additionally, the support bracket of the LC is a critical component. Materials used are orthotropic and uniform, with plastic behavior for values of strain greater than 2%. The goal for strain values is less than 0.5% for all components used and specific deformation limits on maximum workable conditions for each component.

The coupler shafts are subjected to torsion from the applied torque. For all components subjected to torsion:

$$\tau = \frac{T * R}{J} = \frac{2T * R}{\pi R^4} = \frac{2T}{\pi R^3}$$

Given an allowable and conservative shear stress value of 100 MPa for steels in any condition and a safety factor of 3, the allowable minimum diameter for every Solid Shaft is equal to 3.06mm. All axles used for the driving of the torque have a minimum diameter of 6mm and are not subject to further examination.

The main lever and all other critical components are subjected to their own weight, which lies near the fixture, thus producing no bending moments, the load applied for the test, and the torque of the motor. Each entity was modeled as a remote load applied to the most relevant surface. The FEA models are simple and are modeled using Solidworks Simulation Static. Iterative design with weight reduction perspective is carried out until the parts reach their targets.

The FEA analysis was carried out until appropriate working conditions for all critical components of the assembly was achieved. Hand calculations were taken into account for bolt attachments, while M3 bolts are not subjected to critical loads. Countersunk bolts are fitted with proper cone attachments to transfer the preload, and torque nuts are used for secure fastening in the majority of the connections. Blind connections are also calculated using hand calculations based on thread material and length. Compliance goals were extremely strict to prevent errors in the measurements. Since the rig is static, reinforcing critical components while keeping in mind compact and efficient design is preferred. The critical goals set are achieved with the exception of the maximum rotational speed, which will be improved in future refinements of the design by upgrading the motor.

Closing this chapter, the following observations are presented. First and most important is the fact that the final designed rig can be used across every lab environment, due to the small dimensions and weight and the design is made as to acquire the most reliable results for any measurement within the working range. Additionally, the structure it is compatible with a wide range of disc designs, varying in diameter and height, material and surface treatment. The final weight, including bolts, is shy of 8kg, with a bounding box of 405x170x425mm with the transducer tilted to the highest position and 350x170x405mm in static position (length x width x height). Therefore, it can be easily carried across different rooms or desks, and the adjustable legs beneath the base plate enable for accurate measurements regardless of the location the machine is put. The final outcome can also be modified in a non-destructive way to fit liquid adaptor for experiments regarding wet clutches or other applications. Materials used can be found easily in the market, and the lead time is extremely low, due to the clever design principles used. The setup can be performed by any individual in a simple way and furthermore the rig offers fail-safe mechanisms both active and passive to prevent excessive damage to the machine. Belts are used for the torque transfer from the motor, with the possibility for additional petitioning if needed. Finally, the pivot mechanism used makes the device small in size, and enables quick replacement of the discs for different sets of experiments.

5. Conclusions and Future Research

This thesis examined a different approach to optimize the braking capabilities for automotive applications. In braking systems, the term optimization bears different meanings depending on the context. Road cars aim for smooth braking to ease passenger experience, while motorsport environment desires hard scratchy braking that immobilize the vehicle. To achieve this, special alloys and composite materials are used in complicated and heavyweight assemblies, often requiring excessive cooling airflow to maintain the designed parameters and material integrity. High level applications such as F1 and WRC even study the pads' paths and pressure variation across surface to further improve the braking time when approaching corners. Additional improvements involve different disc and pad designs to customize the system for specific requirements of each specific race. Material selection is critical while the design of the system can limit the range of improvements as maximum physical properties are not exploited.

The current thesis proposes a different concept to further improve motorsport applications. Initiating from the FS world, the idea proposed involved altering the surface topology of the braking discs using macroscale features to create 3D profiles across the surface of the disc. By doing so the assumption under examination relies on the introduction of bending stresses along with the existing shear. The pad deformation as it is hardly pressed against the 3D surface is now depending on the height distribution across the surface, and bending of the material is mandatory to occur to maintain the desired pressure. This is merely a concept to be proven, and no hard conclusions can be made from assumptions.

After evaluating the nature of standard and sophisticated braking systems in chapter 1, a short familiarizing with similar concepts from literature was made in Chapter 2. Applications on clutches present similar ideas to improve the contact for bigger power transfer.

In order to validate the idea proposed a series of steps were taken, and can be further continued in the future:

- First of all, an equivalent FEA model was created to compare different features and their implications during the frictional contact phenomenon. The model was validated through a series of steps as per chapter 3, until convergence was achieved for any design in a systematic and reliable way. Models with extreme features were proven to either enlarge CoF or Stress as expected from theory, while smoother ones proved to have smaller impact. The model was created in static environment with an approximation of linear bodies and movement. In reality the circular geometry introduces variation of pressure across the radius of the disc, and unequal wear across the points, that varies through time.
  Using FEA, seven (7) different families of features where examined in a wide range of conditions and feature amplitudes, to create universal results regardless pressure or feature amplitude. Material properties proved restrictive as bodies were stiff and could not easily deform to fit every design proposed. Amplitudes of maximum 100μm were tested, meaning the concept requires accurate manufacturing and exceptional surface roughness. The impact of the latter can be further examined in future research along with wear phenomena, to derive conclusions about the efficiency of elegant manufacturing methods. Roughness is changing in microscale, while the feature is in macroscale, therefore even components with lesser surface quality may be suitable to fit the concept requirements.

- After finishing with FEA modeling, the results were assessed to design 2 features for experimental measurements using the pin-on-disc tribometer. A prototype phase was carried out using SLS printed miniatures, followed by the actual set of experiments of DMLS printed discs. Specimens

where printed, then sandblasted to improve surface characteristics, examined using a scientific profilometer, and finally tested using the Anton Paar TRB3 tribometer. Measurements using the profilometer indicated similar roughness values for all features, and also provided useful insights for the printing method. Features using linear elements were captured with bigger accuracy, while blends of edges were completely suffocated. The amplitude of the features is on the same scale as the layer size of the printing, therefore a quantization of the blends took place, leading to a poor feature representation.

Pin-on-disc experiments are usually chosen to validate the CoF of materials in steady state rotating conditions. The method proved to be insufficient to acquire conclusions, as the full contact between pad and disc equivalent bodies was not across the total surface, rather only on a specific point. Additionally, the relative stiffness of the bodies involved was not up to standard, as the experiments were carried out using steel balls for the pin. One other factor influencing negatively the measurements was the inability to secure the discs in place, as the chuck used is suitable for bigger objects with better cylindricity of the outer surface. Discs wobbled in certain experiments, and results may be misleading on some occasions. Future sets of experiments can be carried out after re-evaluating the post processing of the surface quality of produced discs, and even the overall volume of objects.

- In order to facilitate future research, the final step of this thesis was based in improving the available tools to expand available knowledge of the frictional contact. A fully functional disc-on-disc tribometer was designed using low cost elements and innovative solutions. The final model provides a reliable, affordable and lightweight solution that can accommodate wide range of materials and designs, and even offers the possibility for eccentric tests. The rig designed can also fit an assembly containing fluids to test wet friction phenomena. The design is using aluminum as well as steel and brass for the custom made components, and standard OEM parts to reduce total cost.

  The final outcome is similar to its inspiration, the Anton Paar TRB3, and can pivot to enable disc change, offers a set of 3 positions including resting position, and can be used with bigger loads compared to most of the other rigs. PWM is used to control the rotational speed, and a pretentioned belt transfers power from the motor to the disc. This way, the featured disc is connected directly to the motor, and softer materials or even actual pad composites can be placed in the fixed position, closer to the actual physical model.

  Finally, the disc attachment relies on bolts, and the device is no longer extremely sensitive to the chuck clamping, which was often proven catastrophic for the measurements. The device is yet to be used for experiments, yet the design steps from concept to detailed design were carried out with the outmost sincerity, and minimal flaws are expected during the prototype phase. Future research can take full advantage of this custom rig, and captivate frictional phenomena in great detail, as the experiment is closer to reality than any pin-on-disc alternative.

Current research indicates a big chance of proving the concept. It is important to acknowledge that there was a constrain of limited time for the experiments; essential parameter influencing negatively the findings of the current paper, yet future research may validate this assumption using consistent datasets tested in the custom tribometer. Appropriate material selection and variable speed control can be used to simulate the actual braking phenomenon. Alternative manufacturing techniques such as metal EDM or post grinding can be considered to create realistic specimens. Although no conclusions can be drawn, results both from the FEA model as well as the short testing phase indicate a slight variation of CoF using features across the

surface of the disc. Repetition of the same tests with different discs and in different environments can be proven useful to make valuable observations. Finally, research can also be enriched by improving the FEA model to predict expected results during the experiments. Cylindrical geometry, wear and roughness can be introduced to improve the existing one, as well as transient simulation using variable velocity and heat transfer. All in all, the concept is far from being proven, but the first hard steps have been carried out to facilitate future research. If proven positively, motorsport applications will benefit from the outcomes of the research, as more speed will be carried across tracks, and braking zones will be harder and shorter than ever.

6. Literature References

[1] Belhocine, A., & Omar, W. Z. W. (2018). Computational fluid dynamics modeling and computation of convective heat coefficient transfer for automotive disc brake rotors. In Computational Thermal Sciences: An International Journal (Vol. 10, Issue 1, pp. 1–21).

[2] Marques, F., Flores, P., Pimenta Claro, J. C., & Lankarani, H. M. (2016). A survey and comparison of several friction force models for dynamic analysis of multibody mechanical systems. In Nonlinear Dynamics (Vol. 86, Issue 3, pp. 1407–1443).

[3] Berger, E. (2002). Friction modeling for dynamic system simulation. In Applied Mechanics Reviews (Vol. 55, Issue 6, pp. 535–577). ASME International.

[4] Wang, Q. J., & Chung, Y.-W. (Eds.). (2013). Encyclopedia of Tribology. Springer US.

[5] Szeri, A. Z. (2003). Tribology. In Encyclopedia of Physical Science and Technology (pp. 127–152).

[6] Johnson, K. L. (1985). Contact Mechanics. Cambridge University Press.

[7] Goryacheva, I. G. (1998). Contact Mechanics in Tribology. In Solid Mechanics and Its Applications.

[8] Popov, V. L. (2010). Contact Mechanics and Friction.

[9] Karnopp, D.: Computer simulation of stick-slip friction in mechanical dynamic systems. J. Dyn. Syst., Measurement, Control 107, 100–103 (1985)

[10] Wriggers P. (2008). Nonlinear Finite Element Methods.

[11] Bengisu, M.T., Akay, A.: Stability of friction-induced vibrations in multi-degree-of-freedom systems. J. Sound Vibr. 171, 557–570 (1994)

[12] Dahl, P.R.: A solid friction model, Technical Report, The Aerospace Corporation, El Segundo, California (1968)

[13] Haessig, D.A., Friedland, B.: On the modeling and simulation of friction. J. Dyn. Syst. Measurement Control 113, 354–362 (1991)

[14] de Wit, Canudas, Canudas de Wit, C., Olsson, H., Åström, K.J., Lischinsky, P.: A new model for control of systems with friction. IEEETrans. Autom. Control 40, 419–425 (1995)

[15] Swevers, J., Al-Bender, F., Ganseman, C.G., Projogo, T.: An integrated friction model structure with improved presliding behavior for accurate friction compensation. IEEE Trans. Autom. Control 45, 675–686 (2000)

[16] De Moerlooze, K., Al-Bender, F., & Van Brussel, H. (2010). A Generalised Asperity-Based Friction Model. In Tribology Letters (Vol. 40, Issue 1, pp. 113–130).

[17] Eriksson, M., Bergman, F., & Jacobson, S. (2002). On the nature of tribological contact in automotive brakes. In Wear (Vol. 252, Issues 1–2, pp. 26–36).

[18] Ogilvy, J. A. (1991). Numerical simulation of friction between contacting rough surfaces. In Journal of Physics D: Applied Physics (Vol. 24, Issue 11, pp. 2098–2109).

[19] Goryacheva, I.G. (1998). Wear Models. In: Contact Mechanics in Tribology. Solid Mechanics and Its Applications, vol 61.

[20] Sheng Chen, G., & Liu, X. (2016). Friction Dynamics of Vehicle Brake Systems. In Friction Dynamics (pp. 161–210).

[21] Kinkaid, N. M., O'Reilly, O. M., & Papadopoulos, P. (2003). Automotive disc brake squeal. In Journal of Sound and Vibration (Vol. 267, Issue 1, pp. 105–166).

[22] Krbata, M., Eckert, M., Majerik, J., & Barenyi, I. (2020). Wear Behaviour of High Strength Tool Steel 90MnCrV8 in Contact with Si3N4. In Metals (Vol. 10, Issue 6, p. 756).

[23] Neys, A. (2012). In-Vehicle Brake System Temperature Model

[24] Travaglia, C. A. P., & Lopes, L. C. R. (2014). Friction Material Temperature Distribution and Thermal and Mechanical Contact Stress Analysis. In Engineering (Vol. 06, Issue 13, pp. 1017–1036).

[25] Belhocine, A., & Bouchetara, M. (2014). Structural and Thermal Analysis of Automotive Disc Brake Rotor. In Archive of Mechanical Engineering (Vol. 61, Issue 1, pp. 89–113).

[26] Bena, W., & Sirata, G. (2022). Coupled Thermal Stress Analysis of Volvo Truck Disc Brake. In D. G. Mohan (Ed.), Advances in Materials Science and Engineering (Vol. 2022, pp. 1–10).

[27] Jaenudin, Jamari, J., & Tauviqirrahman, M. (2017). Thermal analysis of disc brakes using finite element method.

[28] Belhocine, A., & Abdullah, O. I. (2020). Finite element analysis (FEA) of frictional contact phenomenon on vehicle braking system. In Mechanics Based Design of Structures and Machines (Vol. 50, Issue 9, pp. 2961–2996).

[29] Valvano, T., & Lee, K. (2000). An Analytical Method to Predict Thermal Distortion of a Brake Rotor. In SAE Technical Paper Series. SAE 2000 World Congress.

[30] Yildiz, Y., & Duzgun, M. (2010). Stress analysis of ventilated brake discs using the finite element method. In International Journal of Automotive Technology (Vol. 11, Issue 1, pp. 133–138).

[31] Yin, J., Hao, Q., Liu, Y., Zhang, S., & Sha, Z. (2022). Multiobjective optimization of internal and surface structure of high-speed and heavy-duty brake disc. In Advances in Mechanical Engineering (Vol. 14, Issue 1, p. 168781402110704).

[32] Afzal, A., & Abdul Mujeebu, M. (2018). Thermo-Mechanical and Structural Performances of Automobile Disc Brakes: A Review of Numerical and Experimental Studies. In Archives of Computational Methods in Engineering (Vol. 26, Issue 5, pp. 1489–1513).

[33] Preda, C., Bleotu, R. M., & Pinca-Bretotean, C. (2022). Study and thermal analysis of vanes shape design for brake disc in automotive industry. In Journal of Physics: Conference Series (Vol. 2212, Issue 1, p. 012025).

[34] Lindgren, A. (2016). Development of Brake Cooling

[35] Vdovin, A., & Le Gigan, G. (2020). Aerodynamic and Thermal Modelling of Disc Brakes—Challenges and Limitations. In Energies (Vol. 13, Issue 1, p. 203).

[36] Cravero, C.; Marsano, D. (2022). Computational Investigation on the Aerodynamics of a Wheel Installed on a Race Car with Multi-Element Front Wing. In Fluids (Vol. 7, Issue 6, p. 182).

[37] Cravero, C., & Marsano, D. (2022). Flow and Thermal Analysis of a Racing Car Braking System. In Energies (Vol. 15, Issue 8, p. 2934).

[38] Campbell-Brennan, J. (2020). Cooling Vanes and the Heat Rejection of an Automotive Brake Rotor; a CFD Study

[39] Vdovin, A., Gustafsson, M., & Sebben, S. (2018). A coupled approach for vehicle brake cooling performance simulations. In International Journal of Thermal Sciences (Vol. 132, pp. 257–266).

[40] Belhocine, A., & Bouchetara, M. (2013). Thermomechanical Stress Analysis of Vehicles Gray Cast Brake. In SAE International Journal of Passenger Cars - Mechanical Systems (Vol. 6, Issue 2, pp. 1371–1382).

[41] Belhocine, A., & Abdullah, O. I. (2020). Finite element analysis (FEA) of frictional contact phenomenon on vehicle braking system. In Mechanics Based Design of Structures and Machines (Vol. 50, Issue 9, pp. 2961–2996).

[42] Guleryuz, I.C. & Yilmaz B. (2020). Investigation of Heavy-duty Vehicle Brake Disc Cooling Behavior

[43] Tirovic, M., & Stevens, K. (2017). Heat dissipation from a stationary brake disc, Part 2: CFD modelling and experimental validations. In Proceedings of the Institution of Mechanical Engineers, Part C: Journal of Mechanical Engineering Science (Vol. 232, Issue 10, pp. 1898–1924).

[44] AbuBakar, A. R., & Ouyang, H. (2008). Wear prediction of friction material and brake squeal using the finite element method. In Wear (Vol. 264, Issues 11–12, pp. 1069–1076).

[45] H. Jang, K. Ko, S.J. Kim, R. Basch, J.W. Fash, The effect of metal fibers on the friction performance of automotive brake friction materials, Wear 256 (2004) 406–414

[46] S.K. Rhee, Wear equation for polymers sliding against metal surfaces, Wear 16 (1970) 431–445

[47] S.M. Hsu, M.C. Shen, A.W. Ruff, Wear prediction for metals, Tribol. Int. 30

[48] Söderberg, A., & Andersson, S. (2009). Simulation of wear and contact pressure distribution at the pad-to-rotor interface in a disc brake using general purpose finite element analysis software. In Wear (Vol. 267, Issue 12, pp. 2243–2251).

[49] Ostermeyer, G. P., & Müller, M. (2005). New Developments of Friction Models in Brake Systems. In SAE Technical Paper Series. 23rd Annual Brake Colloquium and Exhibition.

[50] Liu, W., Ni, H., Chen, H., & Wang, P. (2019). Numerical simulation and experimental investigation on tribological performance of micro-dimples textured surface under hydrodynamic lubrication. In International Journal of Mechanical Sciences (Vol. 163, p. 105095).

[51] Greiner, C., & Schäfer, M. (2015). Bio-inspired scale-like surface textures and their tribological properties. In Bioinspiration & amp; Biomimetics (Vol. 10, Issue 4, p. 044001).

[52] Chen, L., Li, R., Xie, F., & Wang, Y. (2019). Load-bearing capacity research in wet clutches with surface texture. In Measurement (Vol. 142, pp. 96–104).

[53] Kinkaid, N. M., O'Reilly, O. M., & Papadopoulos, P. (2003). Automotive disc brake squeal. In Journal of Sound and Vibration (Vol. 267, Issue 1, pp. 105–166).

[54] Kussuma H S, M. F., & Sutikno. (2019). Testing of mechanical characteristics of coconut fiber reinforced for composite brake pads for two-wheeled vehicles. In IOP Conference Series: Materials Science and Engineering (Vol. 546, Issue 4, p. 042018). IOP Publishing.

[55] VIDERŠČAK, D., SCHAUPERL, Z., ORMUŽ, K., ŠOLIĆ, S., NIKŠIĆ, M., MILČIĆ, D., & ORMUŽ, P. (2022). Influence of Brake Pad Properties to Braking Characteristics. In Promet - Traffic&Transportation (Vol. 34, Issue 1, pp. 91–102). Faculty of Transport and Traffic Sciences.

[56] Sasthi CHARAN Hens. (2020). Evolution of automotive brake material. UNIVERSITY OF ENGINEERING & MANAGEMENT.

[57] Sheng Chen, G., & Liu, X. (2016). Friction Dynamics of Vehicle Brake Systems. In Friction Dynamics

[58] Mulani, S. M., Kumar, A., Shaikh, H. N. E. A., Saurabh, A., Singh, P. K., & Verma, P. C. (2022). A review on recent development and challenges in automotive brake pad-disc system. In Materials Today: Proceedings